Universität Augsburg University

Application of Thermal Analysis – Single Photon Ionization Time-of-Flight Mass Spectrometry for Studies of Inorganic Clusters and Ionic Liquids

Dissertation
zur Erlangung des akademischen Grades

Dr. rer. nat.

eingereicht an der

Mathematisch-Naturwissenschaftlich-Technischen Fakultät

der Universität Augsburg

von

János Varga

Augsburg, März 2017

Die vorliegende Arbeit entstand in der Zeit von 1. 6. 2013 bis 31. Dezember 2016 in der Arbeitsgruppe Comprehensive Molecular Analytics (CMA) des Helmholtz Zentrums München im gemeinsamen Massenspektrometrie-Zentrum der Universität Rostock und des Helmholtz Zentrums München im Rahmen des sonderfinanzierten Forschungsprojektes „Mehrdimensionale Analyse thermischer Prozesse“ der Bayerischen Forschungsstiftung.

Dissertation eingereicht am 24. 03. 2017

Tag der mündlichen Prüfung: 05. 05. 2017

Erstgutachter: Prof. Dr. Armin Reller, Universität Augsburg

Zweitgutachter: Prof. Dr. Ralf Zimmermann, Universität Rostock

Danksagung

Ich möchte mich bei Prof. Dr. Armin Reller bedanken, dass er mir als externer Doktorand die Möglichkeit und Unterstützung geboten hat, an seinem Lehrstuhl für Ressourcenstrategie der Universität Augsburg zu promovieren.

Mein besonderer Dank gilt Herrn Prof. Dr. Ralf Zimmermann für sein Vertrauen, die vielseitige Unterstützung des Projektes, und den gewährten Freiraum während der Durchführung dieser Arbeit.

Ich bedanke mich bei meinen Betreuern und Kollegen Herrn Dr. Georg Matuschek und Herrn Dr. Mohammad Reza Saraji-Bozorgzad für konstruktive Diskussionen, wertvolle Ideen und Hilfe. Mein besonderer Dank gilt an meinen sensationellen Kollegen und Freunden Herrn Sebastian Wohlfahrt und Herrn Dr. Michael Fischer.

Ich bedanke mich bei der Bayerischen Forschungsstiftung für die Finanzierung des Projektes, sowie unseren industriellen Projektpartnern Netzsch-Gerätebau GmbH und Photonion GmbH.

An aktuellen und ehemaligen Mitgliedern der Arbeitsgruppe danke ich für die gute Zusammenarbeit.

Vielen Dank an Frau Renate Diessenbacher an dem Lehrstuhl für Ressourcenstrategie für die stets freundliche Betreuung des Projektes an der Universität Augsburg.

An Frau Dr. Anastasia Efimova und Herrn Prof. Dr. Peer Schmidt (Brandenburgische Technische Universität, Cottbus-Senftenberg) danke ich für die Kooperation zum Thema Ionische Flüssigkeiten und für die Proben.

Ich bedanke mich bei Herrn Dr. Sergey Bokarev, Herrn Tobias Möhle und Herrn Prof. Oliver Kühn (Universität Rostock) für die quantenchemischen Berechnungen.

Ich bedanke mich bei Joachim Nagler für seine Unterstützung.

Darüber hinaus gilt mein Dank allen Freunden. Ihr könnt euch nicht vorstellen, wie wichtig euer Rückhalt für mich war.

Zudem bedanke ich mich bei meiner Familie aus ganzem Herzen für alles.

Mein besonderer Dank gebührt meiner Verlobten, Teodóra Bán, die immer auf meiner Seite stand.

Herzlichen Dank

Abstract

In this study, Thermal Analysis – Skimmer – Single-Photon Ionization Time-of-Flight Mass Spectrometry technology (TA–Skimmer–SPI-TOFMS) was used for the elucidation of the gas phase behavior of inorganic elemental clusters and ionic liquids. Thermal analysis coupled with mass spectrometry is an often-used tool in material sciences. However, it is seldom used for the characterization of inorganic vapors with less volatility nor the investigation of clusters.

The skimmer coupling enables the online transfer of compounds even with low volatility from the thermal analyzer into the mass spectrometer. The ionization energies of sulfur and selenium clusters are between 8 and 10 eV. For characterization, the fragmentation of the individual species must be avoided. Therefore, conventional electron ionization (EI), with kinetic energies of 70 eV, is not suitable. Single photon ionization (SPI) is a soft ionization method where VUV (vacuum ultraviolet) photons are generated by a deuterium lamp (Hamamatsu Photonics, Hamamatsu City, Japan). The non-fragmenting character of the ionization was tested and verified by gas chromatography (GC) separation of the GC-measurable species with subsequent mass spectrometric investigation, using the same deuterium photon source for the ionization as in the aforementioned TA–Skimmer–SPI-TOFMS. We detected different molecular species with 2 to 8 atoms in temperature-dependent equilibria in the vapor phase. The relative concentrations of the individual species could be calculated from their individual mass traces.

Ionic liquids are often referred to as green alternatives of volatile organic solvents. Their thermal behavior is relevant due to the emerging number of high-temperature, larger-scale applications. Also, knowledge regarding the decomposition products is necessary for the treatment and recycling of used ionic liquids. The objective of this study was the stability of several 1-alkyl-3-methylimidazolium halides, the determination of the degradation products, and the elucidation of their decomposition patterns and structure-stability relations. The applied technology provided real-time monitoring of the evolving species. Therein, the almost fragment-free soft ionization with VUV photons, generated by a deuterium lamp (Hamamatsu Photonics), played a crucial role. The main decomposition products were alkylimidazoles, alkyl halides, alkenes, and hydrogen halides. We detected unfragmented molecules whose formation was previously only assumed by electron ionization mass spectrometry. From the decomposition products, we deduced the fragmentation patterns and discussed their dependence from the alkyl chain length and the halide anion. Generally, the decomposition occurred via the reversed Menshutkin reaction, elimination, and bond cleavages. Our results did not suggest the formation of clusters from the investigated ionic liquids nor the evaporation prior to their decomposition.

Publications

PUBLICATIONS IN PEER-REVIEWED JOURNALS

2016 **Varga J**, Wohlfahrt S, Fischer M, et al. *An Evolved Gas Analysis Method for the Characterization of Sulfur Vapor*, Journal of Thermal Analysis and Calorimetry, 2017;127:955-960. DOI: 10.1007/s10973-016-5651-z

Fischer M, Wohlfahrt S, **Varga J**, et al. *Evolution of Volatile Flavor Compounds During Roasting of Nut Seeds by Thermogravimetry Coupled to Fast-Cycling Optical Heating Gas Chromatography-Mass Spectrometry with Electron and Photoionization*, Food Analytical Methods, 2017;10:49-62 DOI: 10.1007/s12161-016-0549-8

2015 Wohlfahrt S, Fischer M, **Varga J**, et al. *A dual-stage consumable-free thermal modulator for the hyphenation of thermal analysis, gas chromatography and mass spectrometry (TA-GC-MS)*. Analytical Chemistry, 2016;88:640-644. DOI: 10.1021/acs.analchem.5b04183.

Fischer M, Wohlfahrt S, **Varga J**, et al. *Optically Heated Ultra-Fast-Cycling Gas Chromatography Module for Separation of Direct Sampling and Online Monitoring Applications*. Analytical Chemistry, 2015;87(17):8834-9. DOI: 10.1021/acs.analchem.5b01879.

2014 Fischer M, Wohlfahrt S, **Varga J**, et al. *Evolved gas analysis by single photon ionization-mass spectrometry*. Journal of Thermal Analysis and Calorimetry, 2014;116(3):1461-9. DOI: 10.1007/s10973-014-3830-3.

PRESENTATIONS ON INTERNATIONAL CONFERENCES (ONLY FIRST-AUTHORSHIPS)

08/2016 2016 International Confederation for Thermal Analysis and Calorimetry, August 14-19, 2016, Orlando, Florida, USA

08/2015 43rd Annual Conference of the North American Thermal Analysis Society, August 10-13, 2015, Montreal, Quebec, Canada

09/2014 Conference of the German Thermal Analysis Society (GEFTA), September 16-19, 2014, Berlin, Germany

POSTERS (ONLY FIRST-AUTHORSHIPS)

03/2015 6th Coupling Days on Hyphenated Techniques „Thermal Analysis to Evolved Gas Analysis, April 14-16, 2015, Selb, Germany

08/2014 International Mass Spectrometry Conference (IMSC), August 24-29, 2014, Genf, Switzerland

Table of contents

Motivation

One emphasis of the Comprehensive Molecular Analytics group at the Helmholtz Zentrum München is to construct innovative thermal analysis – mass spectrometry systems. Different coupling and ionization techniques are in the foreground here.

In this study, Thermal Analysis – Skimmer- Single-Photon Ionization Time-of-Flight Mass Spectrometry technology was used for elucidation of the gas phase behavior inorganic elemental clusters and ionic liquids. Thermal analysis coupled with mass spectrometry is an often-used tool in material sciences. However, it is seldom used for the characterization of inorganic vapors with less volatility and the investigation of clusters.

The elements of the group 16 of the periodic table require special instrumentation as they have high boiling points (sulfur: 445 °C, selenium: 685 °C) which makes usual capillary coupling unsuitable for those speciation. These elements build elemental clusters in the gas phase; soft ionization is needed for the speciation of these vapors to avoid strong fragmentation that usually occurs with electron ionization. The applicability on these matrices of the homebuilt thermal analysis – single photon ionization time-of-flight mass spectrometry with skimmer coupling (TA - Skimmer -SPI-TOFMS) represents the first part of this work.

A second application of TA - Skimmer -SPI-TOFMS is presented in this study. Therein, the question was how chosen ionic liquids behave at elevated temperatures: Do they evaporate? Are there intact ion pairs in the gas phase? Do they build clusters? If not, what are the decomposition pathways? The thermal behavior 1-alkyl-3-methylimidazolium salts are now a frequently researched field as a consequence of their rising larger scale utilization. The softness of single photon ionization (SPI) is also necessary for the characterization of complex mixtures and reaction monitoring. The aim was also to elucidate which additional benefits the TA - Skimmer -SPI-TOFMS could provide compared to other analytical techniques and conventional TA-MS measurements in reaction monitoring.

Fundamentals of the employed techniques

Thermal analysis

Materials usually undergo changes on heating. Humans were always interested in the effect of heat on these changes during history (early attempts to produce pottery, extracting metals, or making glass). However, more controlled and more quantitative experiments started only in the late 19th century which was enabled by the invention of thermocouple by Le Chatelier [1]. According to the recent IUPAC definition, thermal analysis is the study of the relationship between a sample property and its temperature as the sample is heated or cooled in a controlled manner [2]. Several techniques belong to this collective term, depending on which property or physical quantity is measured during the temperature program. *Table 1* summarizes the thermoanalytical techniques.

Property or physical quantity	Technique	Technique acronym
Heat	Scanning calorimetry	
Temperature	Thermometry	
Temperature difference	Differential thermal analysis	DTA
Heat flow difference	Differential scanning calorimetry	DSC
Mass	Thermogravimetry or Thermogravimetric analysis	TG TGA
Dimensional and mechanical properties	Dynamic mechanical analysis Thermomechanical analysis Thermodilatometry	DMA TMA TD
Electrical properties	Dielectric thermal analysis Thermally stimulated current	DEA TSC
Magnetic properties	Thermomagnetometry	
Gas flow	Evolved gas analysis Emanation thermal analysis	EGA ETA
Pressure	Thermomanometry Thermobarometry	
Optical properties	Thermoptometry Thermoluminescence	 TL
Acoustic properties	Thermosonometry or Thermoacoustimetry	
Structure	Thermodiffractometry Thermospectrometry	

Table 1: Summary of the thermoanalytical techniques [2]

The technique where the weight of the sample is measured is called thermogravimetry (TG) or thermogravimetric analysis (TGA). TGA is usually allied with another thermoanalytical technique as differential thermal analysis (DTA) or differential scanning calorimetry (DSC). While DTA measures the temperature difference between the sample and an (inert) reference material, DSC measures either the difference in heat flow or the difference in electrical power to the sample and the reference material (heat flow vs. power compensation DSC) [2]. Modern devices can record the DSC signal at the same time as the actual thermogravimetric measurement. This technique is called simultaneous thermal analysis (STA).

Briefly, the general setup of a TG/DSC device contains the following parts: balance, furnace, atmosphere control, crucible, thermocouples, temperature control, and data collection. The system of a balance plus furnace is called thermobalance.

Modern balances work on the principle of magnetic force restoration: the force exerted by the object being weighed is lifted by an electromagnet. A detector measures the current required to oppose the downward motion of the weight in the magnetic field. The typical mechanism consists of a coil of wire suspended in a magnetic field. Because the magnetic field is radially oriented relative to the coil, the direction of current flow and the direction of the magnetic field are perpendicular at all points. The force exerted is therefore in the direction of the axis of the coil. The coil is supported by precision springs, which allow it to move in the direction of its axis. An optical sensor detects the position of the coil, and provides a feedback signal to an electronic amplifier. The amplifier automatically adjusts the current to maintain the position of the coil at a reference position (the “null” point). The amount of force exerted by the coil is directly proportional to the amount of current flowing in it. So, by measuring that current, the force can be calculated [3].

The furnace can usually work up to 1600 °C, and use a wire of metals (platinum) or alloys (Kanthal, Nichrome, and platinum/rhodium) to heat up. Systems are desired to perform also cooling at a controlled rate as heating. For cooling, liquid nitrogen is used generally. The atmospheres can be inert (nitrogen, argon etc.), oxidizing (synthetic air), reducing (hydrogen) or reactive (other gases). Thermobalances can also be operated under vacuum conditions. The crucibles are usually made of metals (usually platinum), fused alumina, silica or ceramics. For the measurement of the sample temperature, thermocouples are used. These consist of two different conductors forming an electrical junction so as it produces a temperature-dependent voltage. A second, entirely separate thermocouple system is used for control the furnace temperature. Therefore, it is positioned as near as possible to the source of the resistively heated wire. The analogue signals (mass and temperature) are digitized and collected by a computer. A typical commercial thermobalance in vertical setup is illustrated in *Fig. 1*. If more information is needed on the sample composition, evolved gas analysis can be applied. Volatiles can be released by physical (evaporation) or chemical process (decomposition or other reactions) [1].

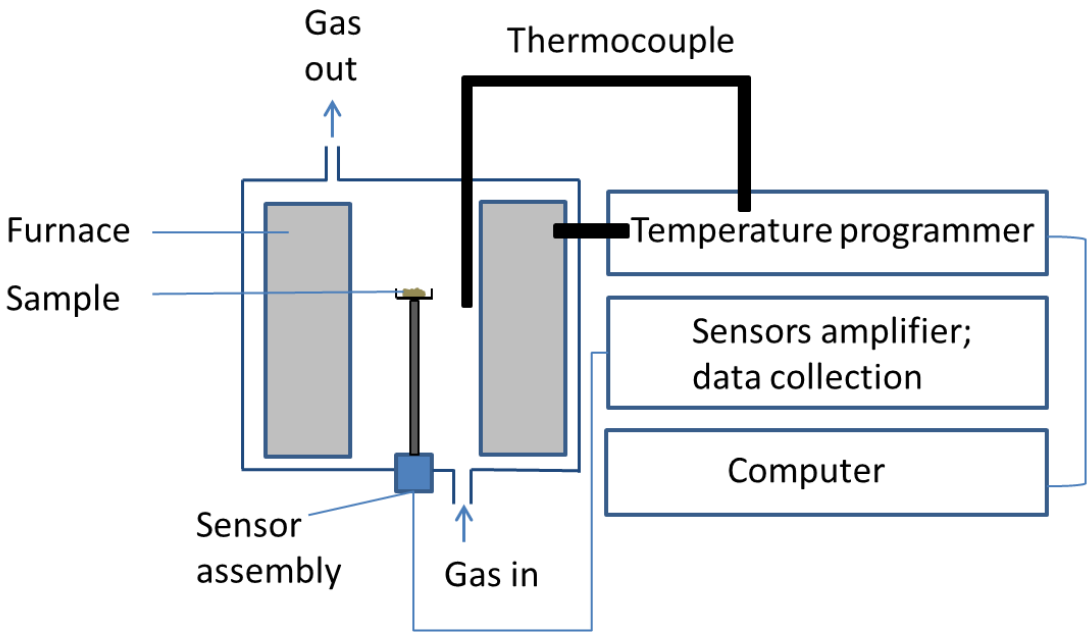

Fig. 1: Schematic diagram of thermal analysis system (reproduced after [4])

Time-of-flight mass spectrometry

Mass spectrometry is an analytical technique where species will be ionized and sorted based on their mass-to-charge ratio (m/z). Results are displayed as spectra of the relative abundance of detected ions as a function of the mass-to-charge ratio [5].

Time-of-flight mass spectrometry (TOFMS) separates ions by their m/z values in a field-free region after acceleration through a fixed accelerating potential. Ions of the same initial translational energy and different m/z require different times to traverse a given distance in the field-free region [6].

The physical background of TOF mass spectrometry is described by the basic TOFMS equations:

Mass – energy relationship:

$$qV = \frac{1}{2}mu^2 \quad \textbf{(1)}$$

Force on a charge in an electric field:

$$F = Eq \quad \textbf{(2)}$$

Newton's second law:

$$F = ma \quad \textbf{(3)}$$

As a consequence, the acceleration in a constant electric field is:

$$a = \frac{Eq}{m} \quad \textbf{(4)}$$

where q = charge; V = electrical potential through which an ion having charge q 'falls'; m = ion mass; u = ion velocity; F = force experienced by charge; E = electric field strength; a = acceleration [7].

The ions produced in the ion source will fly into the direction of the detector due to an accelerating potential (V); their kinetic energy will be proportional to their charge (q), shown in Eq. 1.

Ions with the same kinetic energy but different mass will fly with different velocities. This will lead to their separation in the flight tube and therefore they will reach the detector at different times. Ions with bigger masses will be slower and the smaller ones will be faster. The time of flight (t) depends only on the mass to charge rations of the ions besides a certain ion source – detector distance (L) and accelerating potential.

Basically, there are two geometries of acceleration of incoming ions into TOF mass spectrometers. In the linear geometry, the accelerated ions fly in the consistent direction coming from the ion source. Another possibility is the orthogonal acceleration (oa) or orthogonal extraction where the pulsed acceleration of ions is perpendicular to their original direction of travel into a mass spectrometer [6].

The drawback of linear TOFs is that they proved to be difficult to interface with continuous ion sources due to limitations of ion sampling efficiency imposed by the need to pulse the source or gate the ion beam [8] . Matrix assisted laser desorption/ionization (MALDI) is a pulsed ionization method, therefore it is well suited for the linear geometry.

As evolving gases leave continuously the thermal analysis cell and ions are produced in the gas phase, the oa geometry is inevitable in TA-MS. The first attempt for the orthogonal acceleration is from 1964 by O´Halloran et al. but the rediscovery and breakthrough is dated 1989 when Dawson et al. announced the construction of a prototype instrument. Orthogonal accelerator alternates between fill-up and push-out mode [9].

Nowadays, oaTOFs are widely used in the mass spectrometric community. In this study, an oaTOFMS (CTOF, Tofwerk, Thun, Switzerland) was coupled with the STA device. The schematic setup of an oaTOFMS is depicted in *Fig. 2.*

An important feature of TOFs is a reflectron introduced by Mamyrin et al. [10]. It provides non-mass-dependent kinetic energy focusing [11] by reversing the direction of the flight of the ions. Reflectrons consist of a series of lenses with linearly increasing voltages. The development of reflectrons contributed significantly to the increase of resolution of TOFs [12].

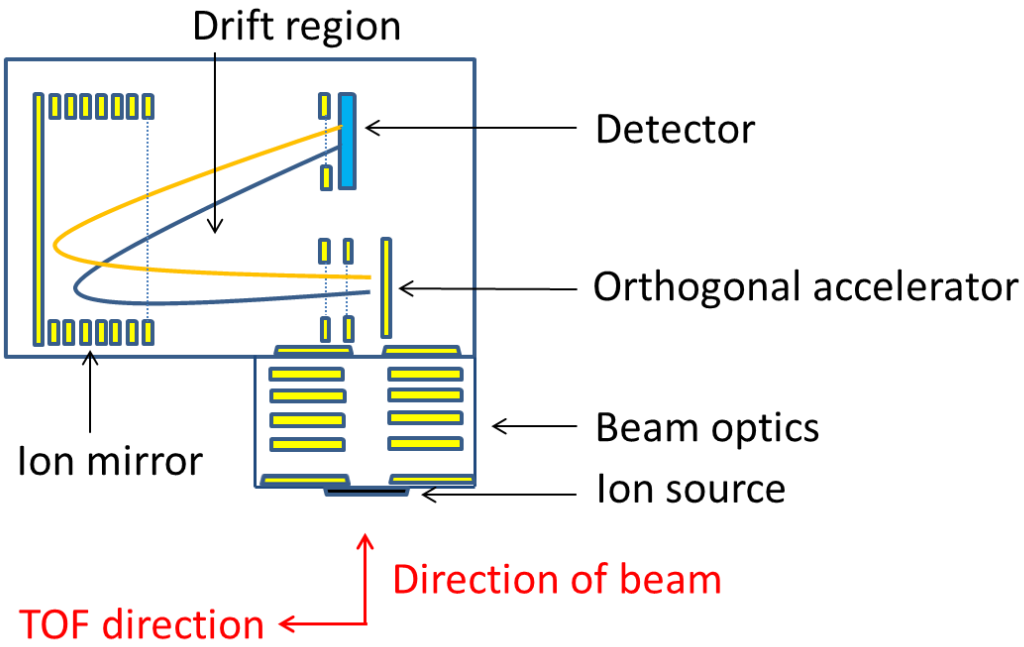

Fig. 2: Schematic setup of an oa - single stage reflectron-TOFMS (after [8,11]**)**

Ionization methods

A hard ionization method: electron ionization

Electron ionization (EI) was introduced by Dempster, Bleakney and Nier. The former term electron impact is deprecated, since electrons do not impact molecules [6]. It is often applied in organic mass spectrometry and works well for the most gas-phase molecules but causes extensive fragmentation that leads to the loss of molecular ion (or low molecular ion intensity). This fact makes EI spectra interpretation often difficult or even impossible for very complex mixtures.

A basic element of an EI source is a heated filament (cathode) emitting electrons. These are then accelerated towards to the anode and collide with the gaseous molecules of the analyte.

The wavelength energy of the electron is:

$$I = \frac{h}{mu} \qquad \textbf{(5)}$$

where m is its mass, u its velocity and h Planck´s constant ($6.63*10^{-34}$ m^2kg/s). When the wavelength is close to the bond lengths, the wave is disturbed and becomes complex. If one

of the frequencies corresponds to an energy level of a transition in the molecule, an energy transfer can occur which leads to a certain excited state and an electron can be expelled.

The kinetic energy of the ionizing electrons (the acceleration potential) plays an important role in electron ionization. The approximate ionization energy of most organic molecules is 10 eV; the excess of this energy leads to fragmentation. This fragmentation can provide structural information on the molecules. Standard electron ionization uses 70 eV acceleration potential of the electrons, which leads to the highest yield in a wide maximum in the number of ions produced. At higher potentials, the wavelength becomes too small and molecules become "transparent" to the electrons. At lower potentials, the yield drops also.

The pressure in the ion source is important; hence it is directly correlated with the ion yielded during EI. The number of ions produced per unit time in a volume V can be described by the following coefficient:

$$I = NplV \tag{6}$$

where p is the pressure, I electron current, and N the constant proportionality coefficient.

Soft ionization methods

To overcome the boundaries of strong fragmentation, soft ionization methods can be used.

Chemical ionization (CI), field ionization (FI), fast atom bombardment (FAB), field desorption, plasma desorption, matrix assisted laser desorption ionization (MALDI), electrospray (ESI), atmospheric pressure chemical ionization (APCI), atmospheric pressure photoionization (APPI), atmospheric pressure secondary ion mass spectrometry and photoionization (PI) [13]. In the following, some background of photoionization provided.

Photoionization (PI) is a general term, where ionization of an atom or molecule occurs by one or more photons:

$$M + h\nu = M^+ + e^- \tag{7}$$

Where h is the Planck´s constant and ν the frequency.

In the case of multiphoton (MPI) ionization two or more photons are absorbed [2]. Laser-based resonance-enhanced multiphoton ionization (REMPI) involves a multiphoton resonance where the intermediate is a Rydberg state and the final state is an ion. The initial state of the system, photon energy, angular momentum and other selection rules can help in determining the nature of the intermediate state. Robert N. Compton and Philip M. Johnson pioneered the development of REMPI. The technique was named by Johnson [14].

In practice, a tunable laser is used for the REMPI. Multiphoton absorption by molecules can lead to fragmentation. The molecule can absorb several photons resonantly or non-resonantly to reach a dissociative state below the ionization level. If the laser pulse is very much shorter than the lifetime of the dissociative state, the molecule fragments to form neutral moieties. These fragments may absorb further photons to ionize or further fragment (this process is known as ladder switching). If the pulse is shorter than the lifetime of the dissociative state then the up-pumping rate may be so high that the ionization level is reached (ladder climbing). Ladder switching is more appropriate to ns irradiation while ladder climbing is more characteristic of fs/ps irradiation [15].

REMPI is often used for the analysis of certain compound classes, such as aromatic hydrocarbons using UV wavelengths that are readily accessible with standard pulsed lasers. REMPI exhibits a high selectivity for these compounds [16]. For other compounds, REMPI is usually not suitable, since the energy supplied by the ionization process doesn´t exceed the ionization energy of many compounds. Typical REMPI ionization energies are in the range of 4.1 to 5.2 eV [17]. The principle of REMPI is showed in *Fig. 3.*

Single-photon ionization (SPI) with vacuum-ultraviolet photons (wavelength range of the ionizing photon is 100 nm and 200 nm) is a much more universal PI method and it allows the soft ionization of almost all organic compounds with some exceptions (methane PI= 12.61 eV, ethane 11.52 eV, ethene 10.51 eV - data from NIST database). The IE of most organic molecules is <~10 eV [18]. The universality of SPI is a great advantage since it covers both nonpolar and polar small molecules without matrix effects as well as higher mass, nonpolar analytes [16].

The SPI ionization process (*Fig. 3*) is induced by the absorption of only one photon and is performed with sources and optics for VUV radiation in the photon energy range of 7.5 eV – 11.8 eV, which corresponds to wavelengths of ~165-105 nm. 7.5 – 8.0 eV radiation requires the use of calcium fluoride optics; higher energy photons require the use of magnesium or lithium fluoride optics. Note that photon ionization must be performed in vacuum or nitrogen or noble gas atmosphere since water or oxygen absorbs VUV photons.

There are several options for the generation of VUV photons. Basically, it can be distinguished between techniques that produce continuous wave (CW) or pulsed output beam. Various discharge lamps and the electron-beam –pumped excimer light source (EBEL) belong to the CW sources. Pulsed output beam is performed with lasers.

Gas-discharge lamps generate photons by sending an electrical discharge through an ionized gas, a plasma. For SPI, typical discharge lamps are filled with various noble gases (argon, krypton, xenon). In microwave discharge lamps, for example, a He/H_2 filling to generate hydrogen Lyman-α atomic radiation (121.5 nm) and made of gold [16]. Modern deuterium discharged lamps are also used in applied mass spectrometry for the ionization; they provide higher photon densities which lead to enhanced intensities.

In the EBEL, the excimer process generating VUV photons and the energetic electrons are separated with a silicon nitride foil in space. A dc electron beam at 20 keV is used for the excitation of pure gases at pressures up to 1.7 bar. Argon, krypton, and xenon and their mixtures were used as second excimer continua providing an efficient light source in the VUV spectral region. The foil separating the two chambers is thin (300 nm) [19]. The emission spectrum of the EBEL exhibits a Gaussian distribution and intensity. The emission spectrum is more stable in time than in the discharge lamps.

Several advantages (relative small size and compactness, easy handling, affordable price) of single photon ionization by deuterium lamps make them an ideal choice for modern, benchtop analytical devices. For this reason, we used a commercially available deuterium lamp with air cooling for the soft ionization of the evolving compounds.

Pulsed lasers can also emit VUV radiation for SPI. Van Bramer et al. produced coherent 10.5 eV VUV photons by frequency tripling the third harmonic of an Nd:YAG (355 nm) in a mixture of xenon and argon. Another study used a nitrogen laser, Nd:YAG laser, or an ArF excimer laser for desorption of biotinylated self-assembled monolayers with SPI [20].

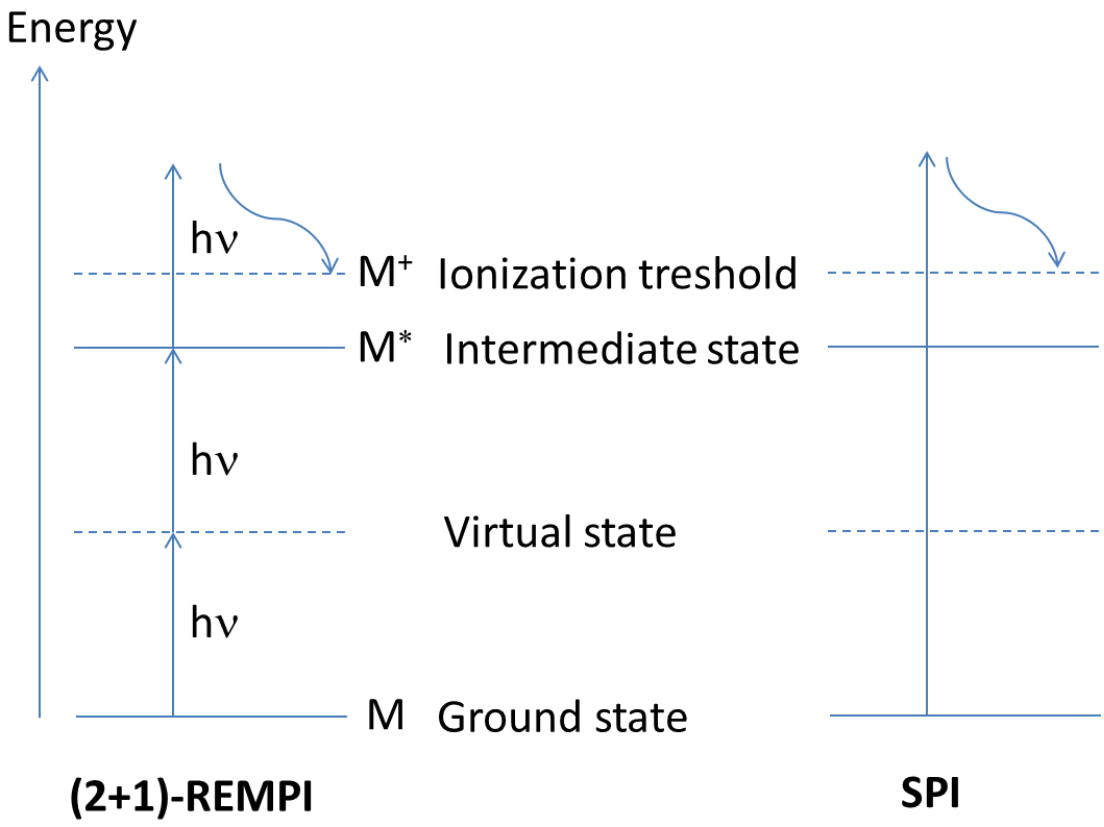

Fig. 3: Principle of REMPI and SPI

Photoionization cross sections

For quantification purposes, relative or absolute photoionization cross sections are needed. Photoionization cross sections can be measured or calculated with quantum chemical methods.

The photoionization cross section is a probability per unit area, per unit time that a photon of a given energy can be absorbed by an atom or molecule to excite the photoelectrons. It is a fictitious area which is usually given in barns (10^{-24} cm^2) or megabarns (10^{-18} cm^2) and can be expressed as a quotient of the absorbed photons (P) and the total number of photons (I):

$$\delta(h\nu) = \frac{P(h\nu)}{I(h\nu)} \quad \textbf{(8)}$$

However, the atom/molecule that has received energy exceeding its ionization threshold does not necessarily ionize. In general, there are other decay channels, such as superexcitation, and the following autoionization or dissociation into neutral fragments. Various pathways are possible for a molecule AB as follows [21]: direct ionization (9), superexcitation (10), autoionization (11), and dissociation (12), schematically represented as:

$$AB + energy \rightarrow AB^+ + e^- \quad \textbf{(9)}$$

$$AB + energy \rightarrow AB' \quad \textbf{(10)}$$

$$AB' \rightarrow AB^+ + e^- \quad \textbf{(11)}$$

$$AB' \rightarrow A + B \quad \textbf{(12)}$$

The transition probability that the absorption of a photon by a molecule in the ground state will get into an excited or an ionized state can be expressed in terms of the optical oscillator strength f_j as

$$f_j(E_j) = (E_j/R)M_j^2 \quad \textbf{(13)}$$

where E_j is the excitation energy to form the state j, R the Rydberg energy, M_j^2 the dipole matrix element in atomic units squared for the state j formation. The total sum of the oscillator strength including discrete and continuous spectra can be expressed as the total number of electrons (Z) in the molecule:

$$\sum_j fj(Ej) = \int_I^\infty \left(\frac{df}{dE}\right) dE = Z \quad \textbf{(14)}$$

where I is the first ionization potential, and df/dE is the oscillator-strength distribution. Eq. 14 is called the Thomas-Kuhn-Reiche sum rule. The oscillator-strength distribution is proportional to the cross section for the absorption of a photon energy E [22].

The probability of photoabsorption and photoionization is dependent on the molecule´s nature and the photon energy. The absorption cross section (σ_a) is a probability that a photon with certain energy will be absorbed. The photoionization cross section (σ_i) describes the probability for ionization through a photon on an analogous way to the absorption cross sections. The quotient of the cross sections for photoionization and photoabsorption is called photoionization quantum yield η, which describes the ratio of formed ions and absorbed photons. Although the excitation energy is sufficient for ionization at close range to the IE, the ionization quantum yield is much smaller than 1. Typical molecular photoionization cross sections are in region of 10 Mb. In EI, organic compounds have similar cross sections at 70 eV ionization energies. In SPI, the cross section differences are bigger, often one order of magnitude. However, the photoionization cross sections with the same compound class are similar [23].

Cool et al. [24] determined the total photoionization cross sections of hydrocarbons with photoionization mass spectrometry using VUV radiation using photon energies for 9.7 eV to 11.75 eV.

Adam et al. [23] presented a method for the determination of photoionization cross sections of 22 substances (alkanes, alkenes, alkynes, dienes, monoaromatic species). They state as the photoionization properties of compounds belonging to one compound class are rather similar the scheme applied can be used for an approximate quantification of compound classes. The used VUV light was produced by the harmonic generation of Nd:YAG laser light.

Eschner et al. [25] described a GC-MS method for the determination of cross sections. They found that photon energies of about 10 eV are a good compromise between when considering universal ionization, maximum ion signal, and ionization with too extensive ionization. This requirement was achievable with the EBEL lamp according to the authors.

Photoelectron spectra and thus photoionization cross sections can be calculated with quantum chemical methods. The agreement between the calculated and experimental photoelectron spectra is recently quite satisfactory.

In cooperation, photoelectron spectra were calculated connected to this PhD work, for sulfur clusters by the Institute of Physics of the University of Rostock (18051 Rostock, Germany). Data will be published in a separate study.

Gas chromatography

Gas chromatography (GC) is a separation science and has its roots in the 40´s of the last century and was invented by James, Martin, and Synge [26,27]. Since that, however the technique improved significantly, the basic components of the system are the same: the heart of a GC is the column which is a separation tube. The sample solution is injected into a heated injector. After volatilization, it is transported via a carrier gas (helium or nitrogen is used usually as carrier gas) to the column where the various components will be separated due to the

different interactions of the molecules with the stationary phase. Qualitative information is gained based on the retention time (RT). Following that, the detector determines the quantity of the components that exit the column. *Fig. 4* shows the basic scheme of a GC.

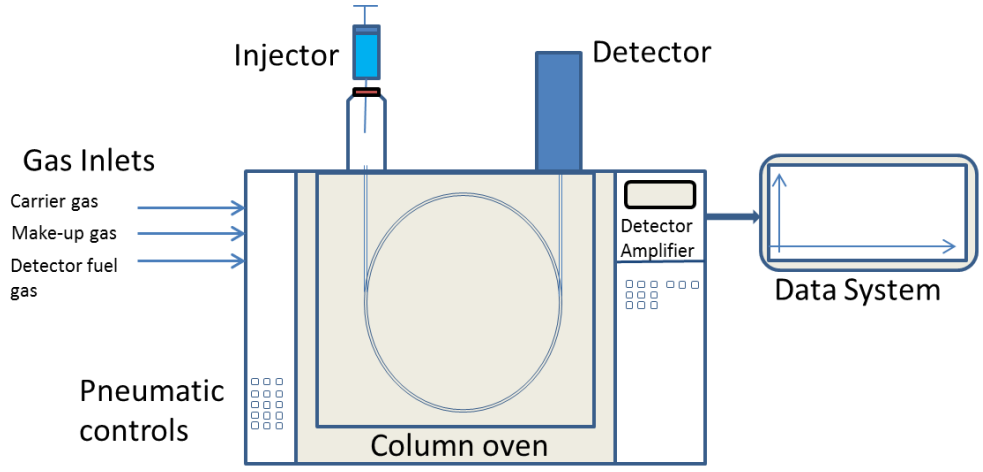

Fig. 4: Scheme of one dimensional gas chromatography system

The GC column is rarely a packed column like in liquid chromatography. In the capillary column, the stationary phase can be either coated on the inner wall as a thin film (wall-coated open tubular, WCOT) or impregnated into a porous layer on the inner (porous layer or support coated open tubular, PLOT and SCOT). Most common column material is fused silica which is highly flexible, durable and chemically inert and based on fiber-optic technology [26].

The most common detector types are the flame ionization detector (FID), thermal conductivity detector (TCD), electron capture detector (ECD), nitrogen phosphorous detector (NPD).

Gas chromatography – mass spectrometry

The major challenge to couple gas chromatography with mass spectrometry is the pressure difference; the pressure of the exiting carrier gas is about 10^5 Pa while the low vacuum of the MS is lower by 8 to 9 orders of magnitude. In practice, coupling is performed by simply inserting the capillary column into the ion source. For most GC runs, the gas flow is 1 to 2 mL/min, usual pumping speed for mass spectrometers at least 300 L/sec [28].

Evolved gas analysis

Evolved gas analysis (EGA) is a collective term for techniques where the evolving gas or vapor is qualitatively or quantitatively determined [2]. Online EGA is usually performed by coupling the TA with Fourier transform infrared spectroscopy (FTIR spectroscopy) or mass spectrometry. It is possible to use a gas chromatograph between TA and the hyphenated technique, when the main advantage is its ability to separate complex mixtures and distinguish between isomeric compounds.

EGA by TA coupled with Fourier transform infrared spectroscopy

The FTIR spectroscope records the IR absorption spectra of the effluent by performing rapid scans. However, FTIR spectroscopy is less sensitive than MS and responds only to polar molecules. Difficulties occur when the effluent is a complex mixture, as the superimposed FTIR spectra could be impossible to interpret. FTIR can be also critical for the detection of inorganic molecules.

The coupling interface between TA and FTIR usually consists of a flexible transfer line which must be heated to avoid condensation of the evolved gases. This coupling has two potential disadvantages: the transfer line causes a slight delay between the release and the detection of evolved gases and condensation or interaction effects are possible. It is possible also to couple the FTIR to the TA via a short connection tube between the furnace and the gas cell [29].

EGA by TA coupled with mass spectrometry

MS is considerably more sensitive than FTIR spectroscopy and can detect all gases. Conventional mass spectrometer type in TA-MS couplings is a quadrupole mass analyzer (QMS). The used mass spectrometer was an orthogonally accelerated time-of-flight mass spectrometer (oa-TOFMS) in this study. The use of time-of-flight mass spectrometers is relatively rare and new in this field.

In principle, there are two main options to couple mass spectrometry with thermal analysis devices. In most cases, transfer of the evolving gases from the thermal process is performed via a heated capillary. This method is usually performed with a deactivated fused silica capillary, where transfer times can lead to a delay in the detection of the evolving gases. The usual transfer line temperature is below 300 °C which does not allow the transfer of low volatile compounds. The TA-capillary-MS coupling is generally applied for the investigation of organic compounds, often applying photoionization to gain fingerprint mass spectra [30][31] or with an additional GC step (TA-GC-MS) [32][33] for the better separation of highly complex matrices. A further disadvantage of the capillary coupling is that the evolving molecules often undergo decomposition or interactions take place in the capillary. Thus, it is obvious that another approach is necessary for the characterization of less volatile compounds such as inorganic compounds of the group 16. An online sampling of these compounds is possible by the skimmer inlet technology, which contains a second pressure reduction step [34][35]. Transfer times are much shorter than with capillary coupling and condensation is prevented. The skimmer coupling is usually achieved through a divergent nozzle and a conically distended aperture (skimmer) with an orifice positioned into the central part of the expanding gases. Nozzle and skimmer are either made of heat resistant metals for application temperatures up to 800 °C or alumina up to 1450 °C or glass carbon up to 2000 °C. Schematic diagram of a TA-MS coupling with skimmer interface is depicted in *Fig. 5*.

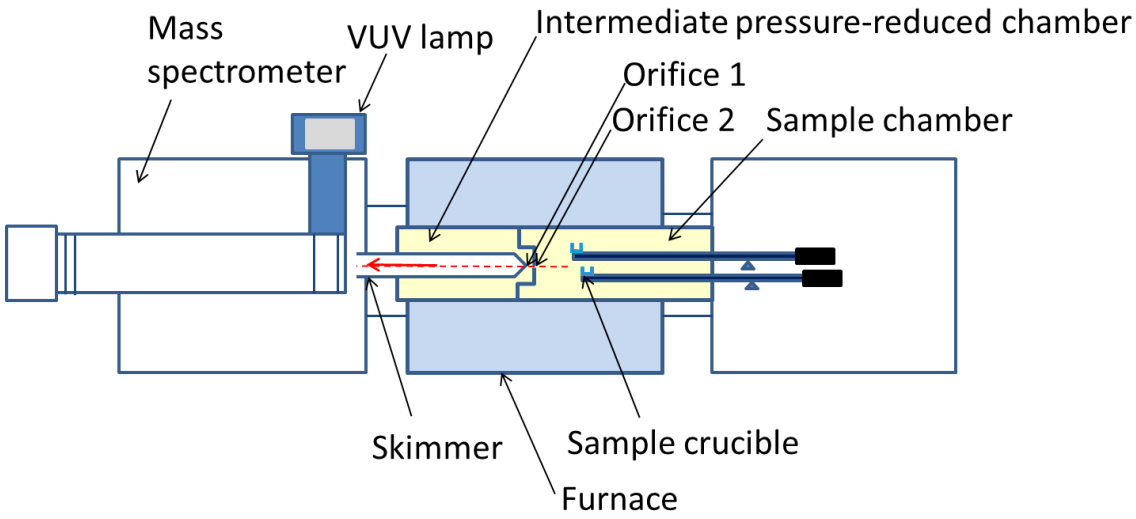

Fig. 5: Schematic diagram of a TGA-MS system using a skimmer type interface (horizontal setup)

EGA by TA coupled with gas chromatography – mass spectrometry

For the better separation of highly complex mixtures, an additional GC step can be used between TA and MS. TA-GC-MS is a modulated technique which means that the effluent from the TA is trapped and reinjected to the GC column through a modulator. The gas chromatographic step is a fast one with a short column in order not to compromise the online character of the coupling. Fischer et al. described a new ultrafast-cycling gas chromatography module which can be adapted to TA-MS easily. The continuously evolving gases of the TA was modulated in 30 s cycles [33].

Background on the composition of sulfur and selenium vapors

The vapors of elemental sulfur and selenium exhibit a complex molecular composition; the characterization of these vapors is still challenging. The vapor phase above a melt sulfur or selenium sample contains different ratios of allotropic modifications in temperature and pressure dependent equilibria. Due to the lack of data gained with modern analytical techniques, ”it is obvious that more work and new approaches” are necessary [36]. The computational evaluation of these vapors also triggers the need for reliable thermodynamic data on the vapor compositions.

There are some publications available on the speciation of vapor generated by heating elemental sulfur. The used analytical techniques are pressure and density measurements, different spectroscopic methods such as vibrational (Raman), UV-Vis spectroscopy or recently near edge structure (XANES) spectroscopy [37][38][39] and mass spectrometric methods. In the following, we detail the results on sulfur and selenium vapor achieved with mass spectrometric methods.

Sulfur vapor contains measurable quantities of several species S_n (n=1,2, …, 10) [40], although the mass spectrometric evidence for S_9 and S_{10} in the equilibrium sulfur vapor is weak. The standard method for the mass spectrometric investigation of vapors is based on Knudsen-cell source whose effusing gases are ionized in the ion source of the mass spectrometer (Knudsen effusion mass spectrometry, KEMS). Berkowitz et al. [41] studied with KEMS elemental sulfur and sulfides (HgS, CdS, ZnS, FeS, SrS, CaS) those decomposition upon heating produces sulfur vapor. Evolving species from the Knudsen cell were ionized by electron ionization; the appearance potential of the evolving species was also established by reducing the ionization energy. They found that saturated vapor contains the molecules of S_2-S_8 and detectable but insignificant amounts of S_9 and S_{10}. Mass spectrometers coupled with Knudsen cells use usually electron ionization, which makes impossible to distinguish between parent ions and fragment ions of the different sulfur species. To overcome this issue, mass spectrometers with photoionization can be used. Berkowitz et al. described a 60°-sector mass spectrometer coupled with Knudsen cell made of nickel [42]. Photons for ionization were generated using a 1 m vacuum-ultraviolet monochromator. The experimental apparatus was rather complicated and no publications are available with a modern benchtop mass spectrometer.

In selenium vapor, the species Se_n (n=2-8) are present similarly to sulfur, the major species is Se_6 following by Se_2-Se_5; Se_7 and Se_8 are in the order of 10 % according to Goldfinger et al. They evaluated the temperature range 450-510 K. Fujisaki et al. observed also Se_9 investigating the temperature range 375-460 K, the ionization energy was 40 eV [43]. Berkowitz et al. conducted measurements on elemental selenium as well as on HgSe, SrSe and CdSe with KEMS, however the used ionization technique was electron ionization [44]. They reduced ionization energies from 75 eV, and established the appearance potential of the species, which were in the range of 8.3 eV and 10.4 eV. They assumed also, that the ion intensities for Se_8^+,

Se_7^+, Se_6^+, Se_5^+ and Se_2^+ were all due to parent ions. After making corrections for isotopic abundance, secondary-electron yield, and estimated ionization cross sections they deduced the partial pressures of 5 gaseous species at T=469 K, the result is Se_8<Se_2<Se_7<Se_5≤Se_6. Later on, the same group conducted photoionization studies on Se_2 evolving from CdSe, the ionization potential obtained from this study is 8.88±0.03 eV [45]. According to Grimley et al. [46], the contributing species in equilibrium vapor phase are Se_2, Se_4, Se_5, Se_6, Se_7, and Se_8; data were gained with angular distribution mass spectrometry. The mole fractions of the species are Se_8 (0.01) < Se_4 (0.02) < Se_2 (0.03) < Se_7 (0.06) < Se_6 (0.40) < Se_5 (0.46) at 483 K. The conclusion of Yamdagni et al´s study [47] is that selenium vapor phase contains the species Se_n (n=2, 5-8), however they do not give mole fractions. In recent study with Knudsen cell electron impact mass spectrometry of Viswanathan et al. [48] observe the selenium species Se_n (n=2-9) in the temperature range of 380-480 K, they concluded, that the ratios follow in the following order: Se_4≤Se_3<<Se_2≈Se_8<Se_5≈Se_7<Se_6 at 480 K.

Investigation of sulfur species with gas chromatography

It is possible to separate sulfur species with gas chromatography (GC). However, it applies only for the sulfur molecules that can be evaporated under normal GC-conditions. It is also to consider that there is always a dynamic equilibrium between the different sulfur species presumably taking place also during the chromatographic separation. Part of this PhD work was the separation of sulfur species with GC and their ionization with EI and SPI. However, the GC separation of S_8, S_7 and S_6 can be found in the literature, the photoionization of the separated species is not described yet.

Injecting a sulfur solution into the injector of the gas chromatograph, S_8, S_7 and S_6 species will be formed in different ratios depending on the gas chromatograph (mainly injector) temperature. The evolving species can be separated on a nonpolar stationary phase which enables the investigation of the ionization behavior with different ionization techniques.

Richard et al. [49] used GC with electron capture ionization for the positive identifications of the elemental sulfur extracted from various environmental (coal, particulate, soil, and water) samples. Elemental sulfur as standard for quantification was solved in cyclohexane. They detected a major peak assigned to S_8, however, the freshly prepared sulfur solution exhibited two early eluting minor peaks. MS data suggested that they are lower subspecies of sulfur. The minor peaks were not present in the chromatograms from sulfur solutions stored for an extended period.

Chen et al [50] investigated sediment samples. Sulfur was extracted with CCl_4. The MS was operated in EI mode at an ionization potential of 70 eV. the manifold temperature and mass transfer line were maintained at 220 and 280 °C, respectively. However, the study focused on the quantitative determination of S_8, also smaller subspecies can be seen on the chromatogram.

Toniazzo et al. [51] assumed the formation S_6 in the chromatograms of the sulfur standard solved in hexane. The influence of the injection temperature was evaluated.

Gryglewicz et al. [52] found that an optimum of GC-MS when both the injection and column temperatures are the same, 180 °C.

Similarly, Burger et al. [53] observed S_8 and smaller quantities of S_6 during the GC-MS analysis of cheetah urine. The extraction media was dichloromethane.

Kornprobst et al. [54] introduced a GC-EI-MS method where the injector temperature was 230 °C and a temperature gradient was used. They observed the formation of S_6, S_7 and S_8.

Zhao [55] developed a method for the for the determination of elemental sulfur in naphtha and gasoline by GC-EI-MS.

Yin et al. [56] described the investigation the elemental sulfur content in gas oil with GC-PFPD (pulsed photometric detector). They evaluated the effect of the injection temperature on the formation of the respective species. they conclude when injection temperature was higher than 180 °C, elemental sulfur mainly pyrolyzed to S_6, S_7 and S_8. A too high injection temperature might lead to the pyrolytic decomposition of compounds in gas oil. Therefore, as a compromise, the injection temperature was chosen as 300 °C.

A summary of the GC parameters in the abovementioned articles is provided (*Table 2*). Unfortunately, the description of the methods is not always complete. Missing details are marked as n.a. (=not available).

Authors	**Observed species**	**Injection**	**Column**	**Carrier Gas**	**Temp. Program**
Richard et al.	S_6, S_7, S_8	220 - 240 °C	Chromosorb W HP 2 m X 4 mm i.d., Gas Chrom Q	n.a.	120, 180, 200 °C, isothermal
Chen et al.	S_8	300 °C	Supelco SPB 30 m X 25 mm	n.a.	40-200 °C
Toniazzo et al.	S_6, S_8	25 °C	DB5 30 m X 0.25 mm	n.a.	70-150 °C 10 °C /min, 150-300 °C 6 °C/min
Gryglewicz et al.	S_6, S_7, S_8	180 - 270 °C	HP-5 30 m X 0.25 mm, 0.25 μm	0.6 ML/min He	n.a.

Burger et al.	S_6, S_8	Desorption from PDMS rubber for 5 min at 220 °c	PS-089 (equiv-alent DB-5) 40 m X 0.3 mm	n.a.	2 °C/min from 40 °C to 280 °C
Kornprobst et al.	S_6, S_7, S_8	Split 5/100, Temperature of injector: 230 °C	DB-5 30m X 0.2 mm, 25 µm	Helium	140-170 °C 5°C/min; 170-250 °C 3 °C/min; 250 °C 6 min
Zhao	S_8	270 °C	Nonpolar 30m X 0.2 mm	Helium 100 kPa	60 °C for 2 min; 60-200 °C 40 °C/min; 200-230 °C 6 °C/min, 230-260 °C 40 °C/min
Yin et al.	S_6, S_7, S_8	120 - 320 °C	Fused silica cap. column (no further details)	n.a.	80 °C for 2 min; 80-280 °C 6 °C/min

Table 2: Summary of GC methods applied for elemental sulfur

Background on 1-alkyl-3-methylimidazolium halide ionic liquids

Introduction to ionic liquids (ILs)

Ionic liquids (ILs) are organic salts that have a melting point below 100 °C. However, they have been first described already in the 1910s they got into the focus of research and industry only in the last 20 years due to their interesting characteristics. The terms room-temperature ionic liquids (RTIL), nonaqeous ionic liquid, molten salt, liquid organic salt, and fused salt are also used.

They are considered as environmental friendly, green alternatives for traditional volatile organic solvents (VOCs) due to their insignificant vapor pressures. They have also other interesting properties such as their high conductivity, variable range of density and viscosity values, tunable polarity and solubility as well as their high thermal and chemical stability [57,58].

This fine tuning of properties is possible due to the large number of organic cations and anions that can be combined to from different ionic liquids [59]. This enables the design of ILs to optimize yield, selectivity, substrate solubility, product separation, and even enantioselectivity. At least, a million binary ionic liquids and 10^{18} ternary ionic liquids are possible [60].

Their ever-increasing relevance is also mirrored by the growing number of publications [61,62]. ILs are recently an intensively researched area due to their huge potential in industrial applications.

Usage as solvents is maybe the most widespread application. They can be used as solvents in organic and inorganic reactions [63–67]. Also, unusual combinations of reagents can be brought into the same phase. An advantage, they are often composed of poorly coordinating ions which makes them highly polar yet non-coordinating solvents. They can be a nonaqueos, polar alternative for two-phase systems as they are immiscible with many of organic solvents. But there are also hydrophobic ionic liquids that can also be used as immiscible polar phases with water. They also can be used in high-vacuum systems [57].

There are numerous other fields of applications, lubricants [68–71], propellants [72,73], engineering and electrochemistry [74]). In analytical chemistry, they can be used as e.g. extraction medium for liquid-liquid extraction [75–78], stationary or mobile phases in separation sciences [79–82] or matrices in matrix assisted laser desorption/ionization time of flight mass spectrometry (MALDI-TOF) [83].

Fig. 6-7 show some commonly used cations and anions for ionic liquids.

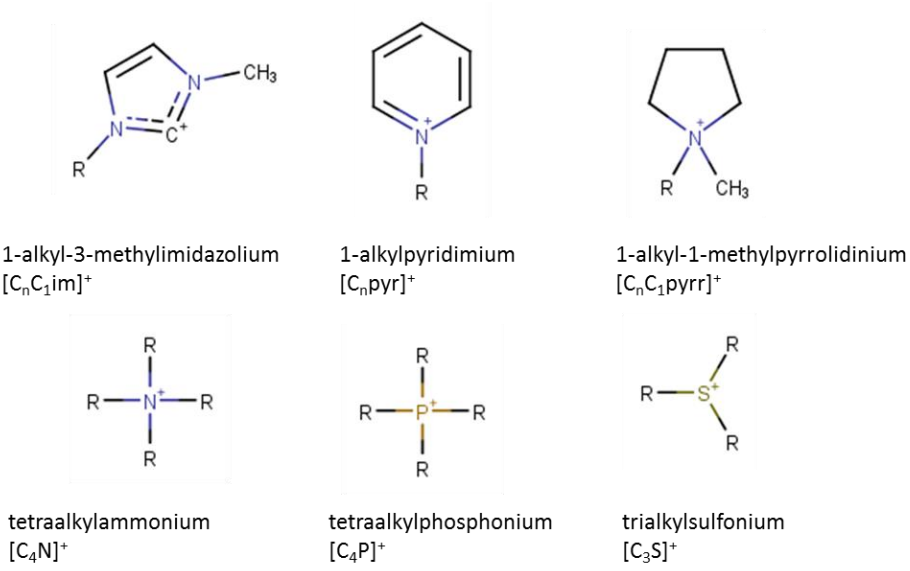

Fig. 6: Commonly used cations in ionic liquids

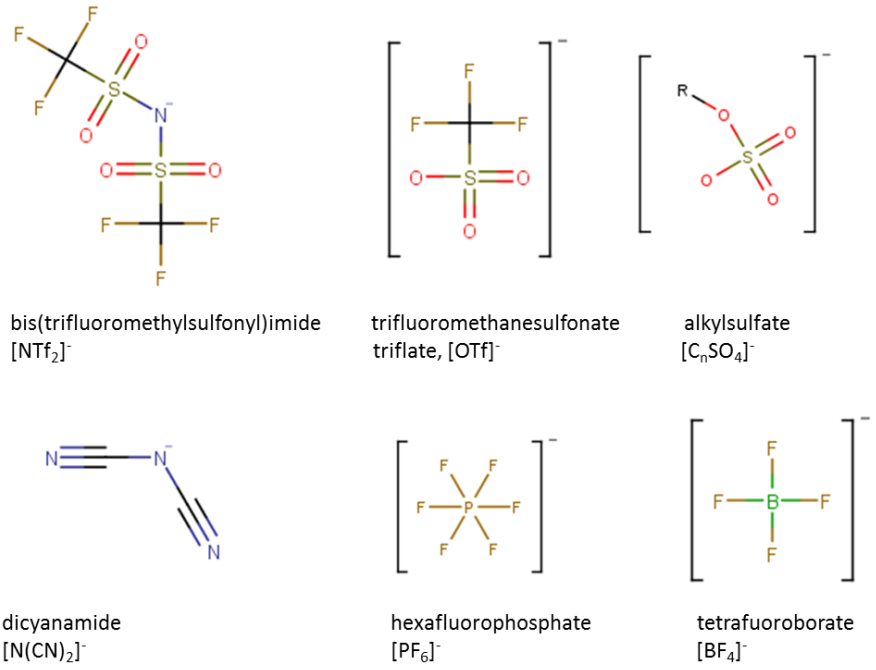

Fig. 7: Commonly used anions in ionic liquids

Due to the possible complex structures of both the cations and anions, and the resulting systematic names, there are various approaches to systematically abbreviate ionic liquids. E.g. $[bmim]^+$ and $[BMIM]^+$ refer to the 1-butyl-3-methylimidazolium cation. To circumvent ambiguities (e.g. between propyl- and pentyl-groups), also an alphanumeric system is used such as $[C_4C_1im]^+$ for 1-butyl-3-methylimidazolium cation. It also can be noted if the alkyl chain is not linear, e.g. $[^tC_4C_1im]^+$ for tert-butyl. If the side chain is functionalized, then the type and position of the functional group are noted: $[(OH)^4C_4C_1im]^+$ when there is an alcohol group on

the terminal carbon of the butyl chain. In-chain inclusion of non-carbon atoms can also be shown [(C_1OC_2)C_1im]+ shows the presence of an ethereal oxygen between the second and terminal carbon atoms. Alkyl chains are saturated unless noted otherwise; [(C_1=C_2)C_1im]$^+$ represents the 1-allyl-3methylimidazolim cation. For cyclic cations, alkylation is assumed to be on the heteroatom(s) unless otherwise indicated by giving the numerical position of the alkylation on the ring such that 1-butyl-2,3-dimethylmidazoliumm becomes [$C_4C_1C_1^2$im]$^+$. The same system can be used for alkyl chains in anions; e.g. [C_4OSO_3]$^-$ for butyl sulfate [58].

Handling of ionic liquids

During handling of the ionic liquid, the reactivity with the air should be considered. Oxygen is usually not critical, the solubility of O_2 in most ionic liquids is relatively low [84].

Regarding moisture, hygroscopic behavior and hydrolysis should be considered. Ionic liquids with anions [PF_6]$^-$, [SbF_6]$^-$, [BF_4]$^-$, and [C_nSO_4]$^-$ undergo hydrolysis. Regarding the fluoro-salts, even the toxic and corrosive HF will be formed [85]. The hydrophilicity of the ionic liquid is mainly determined by the basicity of the anion. The hygroscopic behavior should be taken into account as it can strongly influence their performance [86].

The insignificant vapor pressures of ILs doesn´t mean that they are nontoxic, it just means less likely accidental exposure compared to volatile organic solvents. In general, the increasing length of alkyl substituents leads to increasing toxicity due to the enhanced lipophilicity. Transdermal exposure is the main risk factor of ionic liquids. ILs, that are liquid when in contact with skin and are lipophilic (more ability to interfere with biological membranes), are most critical regarding to transdermal toxicity.

High-temperature applications of ionic liquids

Since the high-temperature applications represent a sizeable share, it is of great importance to study the thermal behavior and collect information about the correct and safe operation temperatures. The most relevant applications are high-temperature solvents, heat transfer and storage medium [87], and high-temperature lubricants.

Molten salts were proposed as heat transfer fluids for high temperatures such as 250 to 1000 C already in the 60s. Wu et al. published a study about the applicability of alkyl-methylimidazolium hexafluorophosphate and tetrafluoroborate as thermal storage in solar thermal electric power systems. They found that decomposition temperatures were up to 420 °C and the storage density was six times higher than that of the thermal oil (59MJ/m^3 vs. 378 MJ/m^3). ILs are excellent media for liquid thermal storage and heat transfer fluids due to their high heat capacity, wide liquid temperature range, high density, high chemical stability, non-volatility, and high storage density. Low viscosity and high thermal conductivity makes them excellent candidates as heat transfer fluids for solar thermal power plant systems. However, the economic feasibility as liquid thermal storage media and heat transfer fluids needs to be further investigated [88].

A generally known example for the application of ILs as high-temperature reaction media is the BASIL process developed and operated by BASF. The use of 1-methylimidazole as an acid scavenger and nucleophilic catalyst increased the productivity of the alkoxyphenylphosphine formation process by a factor of 80000. The reaction temperature is approx. 80 °C, the plant went on stream in Q3/2004 at BASF´s Ludwigshafen site [60]. Degussa also presented an ionic liquid based process for the synthesis of organosilicon compounds. The use of an ionic liquid solvent enabled the catalyst to be easily recycled and reused without further treatment after separation form the product at the end of the reaction; reaction temperature was 90 °C [89].

Jiménez et al. tested 1-methyl-3-octylimidazolium tetrafluoroborate and 1-methyl-3-hexylimidazolium hexafluorophosphate for high-temperature steel lubrication up to 300 °C [90]. Philips et al. tested 1-n-ethyl-3-methylimidazolium tetrafluoroborate, 1,2-di-methyl-3-butylimidazolium bis(trifluoromethylsulfonyl)imide, and 1,2-di-methyl-3-butylimidazolium hexafluorophosphate as high-temperature lubricants also until 300 °C. They concluded that ILs have a great promise as lubricants up to moderate temperatures because the investigated ILs broke down at higher temperatures in reaction with the iron/steel surface to form several reaction products (mainly FeF_2) [91]. Polyethylene glycol functionalized dicationic ionic liquids with alkyl or polyfluoroalkyl substituents showed outstanding tribological properties at 300 °C; the imidazolium based dicationic ILs showed decomposition temperatures even higher than 415 °C [92,93].

1-alkyl-3-methylimidazolium halide ILs

Imidazolium ionic liquids have been the most widely studied family of ionic liquids. The main advantages of the 1-alkyl-3-methylimidazolium halide ILs studied in the current study are their low melting temperatures and the simplicity of their handling and preparation. They are frequently used as reaction media, among them applications at increased temperatures [94].

Many imidazolium halides are commercially available or can be prepared simply by the reaction of the appropriate halogenoalkane. Most halide salts are solid at room temperature, allowing purification of the intermediate salts by recrystallization, most often from acetonitrile; ethyl acetate can be added to aid precipitation of the salt and removal of unreacted starting materials. Finally the salt is dried in vacuum [57,58].

Thermal behavior

In general, the following techniques can be used for the determination of thermodynamic properties of ionic liquids [95]:

1. Activity coefficient measurements using GC technique
2. Thermodynamic properties determined by adiabatic calorimetry and thermal analysis (DSC, TG-DTG)
3. Estimation and prediction of physicochemical properties of ILs based on experimental density and surface tension data

The vapor pressure of ILs is a relevant question as their green character is based on the assumption that they do not evaporate unlike volatile organic compounds. This non-volatility implies less exposure risk and less risk for ignition.

However, the non-volatile and non-flammable character of ILs is outpaced [96–100].

Deyko et al. successfully evaporated 8 common dialkylimidazolium-based ionic liquids in ultra-high vacuum and analyzed their vapors by electron ionization mass spectrometry. The pressure of the vacuum chamber was $5*10^{-10}$ mbar. They found that the studied 1-butyl-3-methylimidazolium and 1-octyl-3-methylimidazolium as cation containing ILs evaporated as neutral ion pairs [101].

Eagle et al. presented experimental data to demonstrate that several ionic liquids can be vaporized and recondensed without significant decomposition. They concluded that the only possible mechanism for volatilization of the studied ILs is as intact ions, either alone or aggregated [99].

However, ILs usually have a negligible vapor pressure, they shouldn´t be necessarily considered safe when working with or near a heat or ignition source. All necessary precautions must be maintained and the usage of particular ILs near a source of heat, flame, or ignition must be reconsidered [97].

It is well known that ionic liquids can be thermally decomposed. As the evaporation under atmospheric conditions is usually negligible, the mass loss upon heating is due to decomposition. Thermoanalytical (TA) methods such as thermogravimetric analysis (TGA) and differential scanning calorimetry (DSC) are applied for the investigation of thermal stability. For the detection of breakdown products hyphenated analytical techniques such as pyrolysis-gas chromatography-mass spectrometry (Py-GC/MS) [102,103], simultaneous thermal analysis (STA) coupled with either Fourier transform infrared spectroscopy (TA-FTIR)[104,105] or mass spectrometry (TA-MS) [87,106–109], thermal desorption mass spectrometry (TDMS) [105] are necessary. Of course, not only online analytical techniques are possible to investigate the decomposition and the end products; the literature contains offline methods such as gas chromatography [110] ESI-MS, potentiometric titration [111] as well as UV-Vis and fluorescence spectroscopy [112]. An interesting aspect is the comparison of the quantum chemical aided prediction [104,107–109,113] of possible ways of thermal decomposition and its temperatures of ionic liquids with experimental data.

In the following, the results on 1-alkyl-3-methylimidazolium halides gained with TA-MS are detailed. Efimova et al. [106,114] investigated the decomposition of 1-ethyl- and 1-butyl-3-methylimidazolium halides by means of TA-MS with the capillary coupling. Two main decomposition patterns were suggested: the formation of the ethyl halide and 1-methylimidazole is more preferred over the formation of the methyl halide and 1-ethylimidazole. However, the

unambiguous identification of these species is not evident due to the applied electron ionization (EI) where the applied ionization energy was 70 eV.

The drawback of the capillary coupling is that it doesn´t enable the *in-situ* detection of the evolving compounds. Evolving molecules often undergo decomposition or interactions can take place during the transfer from the TA to the MS. As the usual transfer line temperatures are up to 300 °C the transfer of low volatile compounds is beyond possibility. Hao et al. [107] used TA-Skimmer-MS for the investigation of 1-allyl-3-methylimidazolium chloride and 1-butyl-3-methylimidazolium chloride ([bmim][Cl]). The high ionization energy (70 eV) may have caused that the expected decomposition products butyl chloride and 1-butylimidazole were not detected upon decomposition of [bmim][Cl].

In this study, "soft" photoionization was used overcome the boundaries of electron ionization. Chambreau et al. [108] applied tunable synchrotron photoionization at the Chemical Dynamics beamline 9.0.2.3 at the Advanced Light Source facility at the Lawrence Berkeley National Laboratory, Berkeley, CA for the investigation of the decomposition products of 1-ethyl-3-methylimidazolium bromide ([emim][Br]) at 457 K. Briefly, photoionization mass spectra were measured from 8.0 to 15 eV in 0.1 eV steps. They concluded from the absence of m/z=111 ($emim^+$ cation) that [emim][Br] as intact ion pairs is not a significant pathway leading to mass loss.

Decomposition of alkylimidazolium ionic liquids

It should be noted that only the volatile breakdown products can be detected with the above named online analytical methods. For the detection of non-volatile breakdown products, off-line analytical methods are necessary such as HPLC-MS.

A short overview is provided about the possible decomposition reactions in the investigated ILs. Alkyl scrambling (transalkylation) is a considerable decomposition pathway (*Fig. 8*, reaction a). These cations can be formed either due to a re-alkylation of a previously dealkylated cation with an anion, which carries an alkyl chain of the same type, or by a direct exchange of the alkyl chains of two cations. The resulting components are charged and together with the initial anion, again ILs. Of course, these decomposition species are non-volatile. The deprotonation of the C2-atom of the fused ring by strong nucleophiles results in carbenes (*Fig. 8*, reaction b) that can react with other IL cations or any dissolved decomposition products present in the liquid phase [115].

The reverse Menshutkin reaction leads to a tertiary amine and an alkyl halide by the reaction of the quaternary ammonium cation with the halide anion (*Fig. 8*, reaction c) [96].

The possible mechanisms of the reverse Menshutkin reaction are S_N1 (unimolecular nucleophilic substitution) and S_N2 (bimolecular nucleophilic substitution). For allyl and benzylimidazolium halides, an S_N1 mechanism could be proposed. In other cases, steric factors are more

important and S_N2 kinetics is dominant [96]. Hofmann elimination must be considered as a possible competing process in cases where the alkyl substituent can form an alkene; especially with more basic anions than iodide [110].

Furthermore, the hydrolysis of the investigated ILs is mentionable as they are humidity sensitive.

To summarize it, the decomposition products can be volatile or not, charged or uncharged, fragments or higher structures compared to the original molecules.

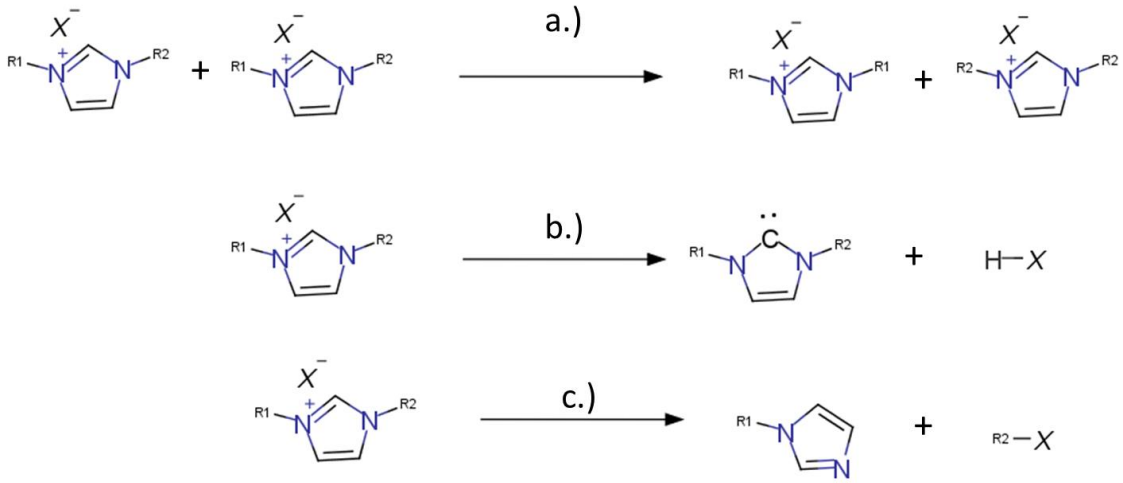

Fig. 8: Decomposition mechanisms of dialkylimidazolium cations [115]

Short- and long-term stability

Usage experience shows that short and long term stabilities of ILs differ significantly from each other. For instance, degradation temperatures ranging from 235 to 450 °C for 1-methyl-3-butylimidazolium bis(trifluormethylsulfonyl)imide are reported [116].

There are various ways to evaluate the decomposition temperature from thermogravimetric data: (1) the (extrapolated) onset temperature of a thermogravimetric (TG) curve, (2) the peak temperature of the differentiation of a TG curve (DTG), or (3) the (extrapolated) onset temperature of a DTG curve [106]. None of these temperatures describes the “real” decomposition temperature. They correspond to the mass loss of at least 10% for all classic evaluation methods.

To deduce the thermal stability from thermogravimetric data is obviously an overestimation and therefore cannot be used for e.g. synthesis design.

Complex (mathematic) characterization and/or data gained with other analytical techniques are required for the evaluation of long-term stability and safe operation temperatures.

To demonstrate that ILs degrades already at lower temperatures indicated by TG analysis, [bmim][Cl] samples were treated at different temperatures between 100 and 200 °C for 24 hours by Meine et al. [111]. To identify possible decomposition products, they analyzed the aged products by ESI-MS. They also introduced a potentiometric titration of alkylimidazoles, one of the most important degradation products of alkylimidazolium based ILs, as identified before with ESI-MS. They concluded that titrating imidazoles is a precise, low-cost and quick analytical method to assess thermal stability. They found that [emim][Cl] and [bmim][Cl] start to degrade when heated above 120 °C.

Del Sesto et al. [112] observed the formation of impurities in pyrrolidinium and imidazolium ILs starting above 150 °C by an increase in fluorescence. The colored impurities were formed well below the TGA onset decomposition of 400 °C.

There are also thermoanalytical approaches combined with calculations to provide information of long-term stability. It is possible to apply a kinetic model. Seenberg et al. [117] to estimate the so-called maximum operating temperature (MOT) that corresponds to the mass loss of 1 % for a certain period of time. This kinetic model has been applied for the calculation of MOT for some ILs [118,119].

Efimova [106] et al. determined the activation energies with integral isoconversional methods using non-isothermal thermogravimetric measurements. They suggest time-dependent application temperature: 1-ethyl-3-methylimidazolium halides (Cl, Br, and I) can be used up to 130 °C for 24 hours, 100 °C, and 75 °C for one year.

TG measurements for the determination of MOTs were done in cooperation with Prof. Dr. Peer Schmidt and Dr. Anastasia Efimova (Brandenburg University of Technology Cottbus-Senftenberg, Chair of Inorganic Chemistry, 01968 Senftenberg, Germany). Detailed data and consequences will be published in a separate study.

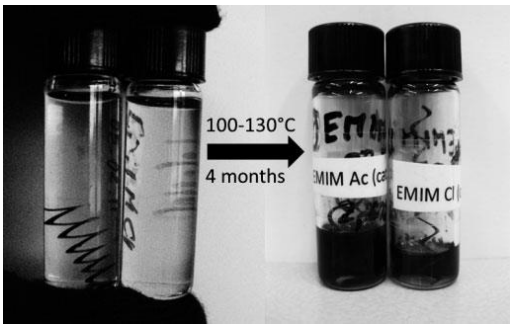

Fig. 9: Samples of [emim][Ac] and [emim][Cl] before and after long-term thermal stress at 100-130 °C for four months [115]

Experimental part

Experimental setup

A commercially available thermal analysis – mass spectrometer system (STA 409 CD with QMS 403/5 Skimmer®-Coupling, Netzsch-Geraetebau GmbH, Selb, Germany) was modified. The quadrupole analyzer was replaced by an orthogonal acceleration time-of-flight mass spectrometer (CTOF, Tofwerk, Thun, Switzerland). The scheme of the system is depicted in *Fig. 10*. The instrument described by Saraji-Bozorgzad et al. [120] was further modified with a mirror module and a deuterium lamp.

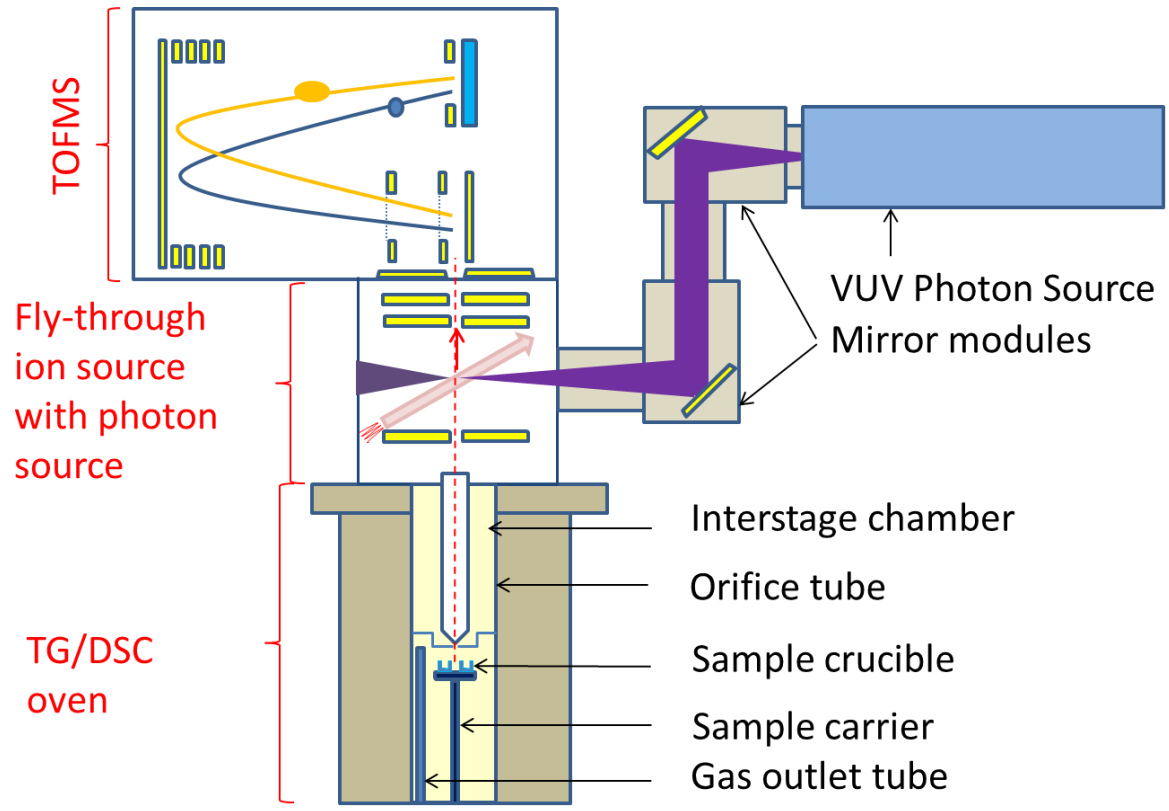

Fig. 10: Scheme of the modified QMS 403/5 Skimmer® device hyphenated with an orthogonal acceleration time-of-flight mass spectrometer and VUV photon source for the soft ionization of evolved gases [121]

VUV light was focused with a mirror module containing two parabolic MgF_2 coated mirrors to enhance the performance of photo ionization. The applied lamp for photoionization was an easy to handle, air-cooled deuterium lamp (Hamamatsu Photonics K. K., Hamamatsu City, Japan). In discharge lamps, in contrast to the EBEL, energetic electrons are generated in the gas

cell. Local maximum of the wavelength–irradiance function is at 122 nm which corresponds to 10.16 eV photon energy (*Fig. 11*). The mass spectrometer can be operated also with standard electron ionization, where the applied ionization energy is usually 70 eV.

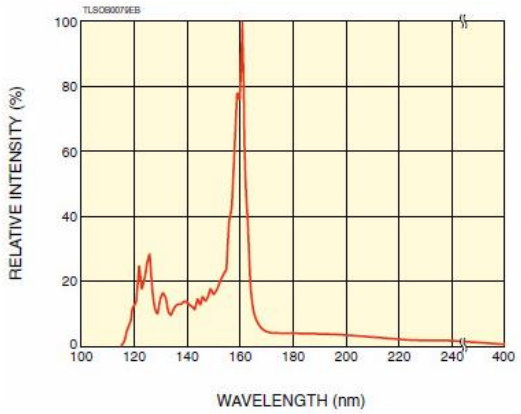

Fig. 11: Spectral distribution of the applied deuterium lamp (Vendor information)

Gas chromatography – mass spectrometry (GC-MS) with different ionization techniques was used for the investigation of the fragmentation patterns of the sulfur species. Therein, it was especially interesting to investigate whether the applied SPI ionization enables the fragment-free ionization of sulfur.

A commercial GC (Thermo, Waltham, Massachussets, USA) was coupled via a heated capillary to a time-of-flight mass spectrometer (CTOF, Tofwerk, Thun, Switzerland). Vacuum ultraviolet photons for SPI were generated by a deuterium lamp (Hamamatsu Photonics K. K., Hamamatsu City, Japan). VUV light was focused with a mirror module containing two parabolic MgF_2 coated mirrors to enhance the performance of photo ionization, similarly to the TA-MS setup described above. The photo of the system is depicted in *Fig. 12*.

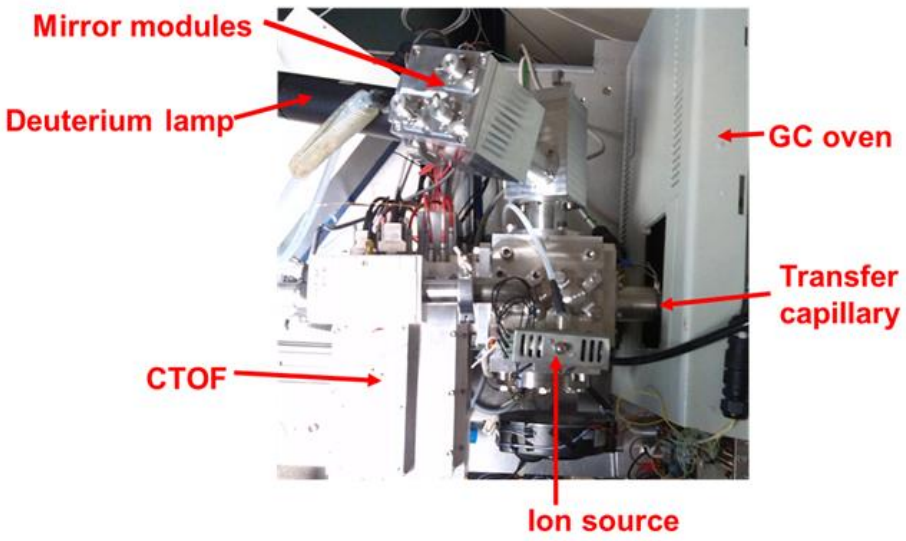

Fig. 12: Photo of the used homebuilt GC-SPI-MS device

Results

Characterization of sulfur and selenium vapors with TG/DSC-Skimmer-SPI-TOFMS

The applicability of the developed system was first tested for the comprehensive investigation of sulfur and selenium, especially for the molecular composition of the vapor phase. In the following, TG/DSC-Skimmer-SPI-TOFMS data are presented.

Measurement conditions

Measurement conditions for the sulfur and selenium samples were: heating rate: 10 °C/min 25-600 °C, purge gas: 30 mL/min N_2, protective gas: 30 mL/min N_2, weighing: 8-23 mg. Samples were placed in aluminum oxide crucibles, with a lid and a small pinhole in the lid. Furthermore, the suitability of the instrumental setup for the investigation of the equilibrium composition of vapors was tested. For this reason, measurements with an isothermal temperature program were performed. Measurement conditions were: heating rate: 10 °C/min until 300 °C, followed by a 30-min isothermal segment, purge gas: 30 mL/min N_2, protective gas: 30 mL/min N_2. Sulfur and selenium was purchased from Sigma-Aldrich (99.5 %, Steinheim, Germany).

Sulfur

Soft ionization plays a crucial role in the characterization of sulfur vapor. The necessity for the usage of soft ionization is showed on *Fig. 13* by comparing mass spectra gained during the TG/DSC measurements with different ionization energies. It depicts the combined mass spectra of elemental sulfur gained during a TA run and thereby demonstrates the differences between EI and SPI techniques. The SPI mass spectrum is depicted in *Fig. 13 a*. The most intense peaks are S_6 and S_8, followed by S_7, S_5, S_2 even S_4 and S_3 can be detected in trace levels (not visible in the spectrum). In *Fig. 13 b*, the EI mass spectrum shows the increased fragmentation due to the higher ionization energy. The main fragment in this case is S_2, the other molecules S_3-S_8 can be hardly seen in the mass spectra. This comparison between the ionization techniques shows that conventional EI is not suitable for the characterization of sulfur vapor, since the assignment of the EI fragments to the respective species is not possible.

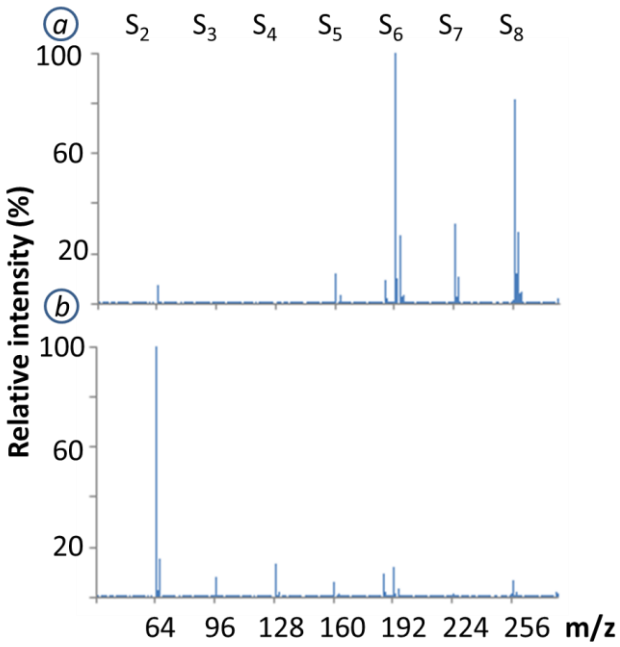

Fig. 13: Mass spectra of sulfur vapor with different ionization techniques: soft ionization performed by deuterium light source (a) 70 eV standard electron ionization (b) [121]

Fig. 14 shows the TG/DSC curves with the corresponding mass traces. The TG curve shows a typical evaporating behavior, on the DSC curve, besides melting and evaporation, allotropic transitions can be followed as well. The first two partly resolved endothermic peaks (extrapolated onsets 103.5 °C, 119.4 °C) belong to the reversible transition into ß-sulfur and the melting, the third peak is the endothermic polymerization peak, belonging to the so called λ-transition (onset 167.3 °C) where viscosity is dramatically increasing due to the formation of polymers, the fourth peak beginning at about 300 °C belongs to the evaporation of the sample [122]. In the 3D plot, on the axes, the m/z value, temperature and signal intensity can be seen. The most intense species are S_6 and S_8, followed by S_7, S_5, S_2, and S_4, S_3 can be detected in trace levels.

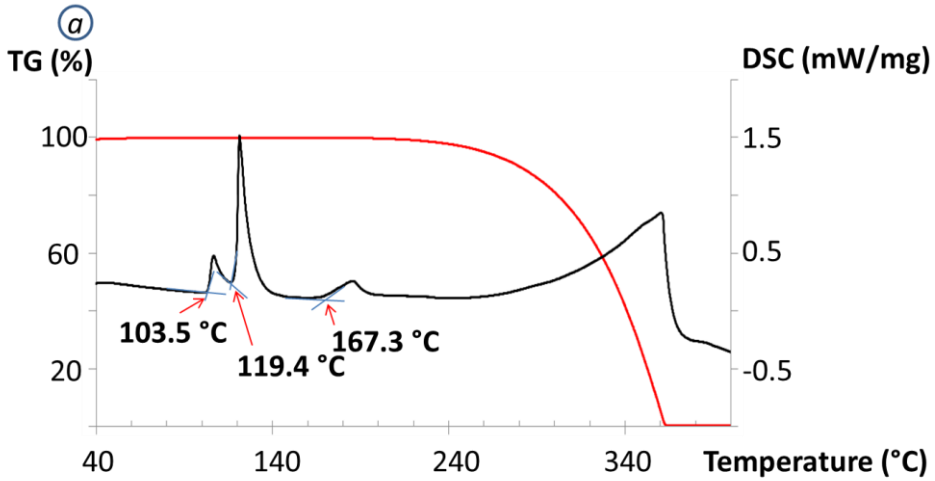

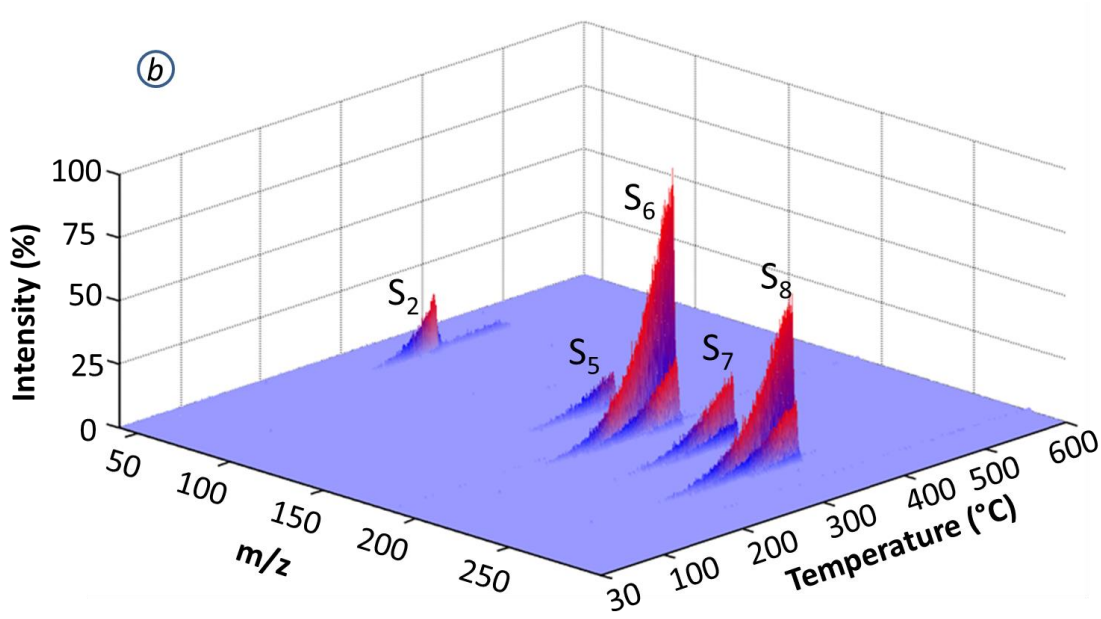

Fig. 14: TA-Skimmer-EI/SPI-TOFMS results for elemental sulfur: TG/DSC curves (a) m/z – temperature – intensity plot (b) [121]

The composition of the vapor phase above the sulfur melt can be calculated from the mass spectrometric traces. During the calculation, also isotopes must be considered. *Fig. 15* shows the molar percentages of the different allotropic modifications of sulfur vapor between 200 °C and 350 °C. The main species are S_8>S_6, however there is an increasing ratio of S_6 at higher temperatures. The amount of S_2 starts to increase fast at ~280 °C and reaches ~1 mol% until 350 °C.

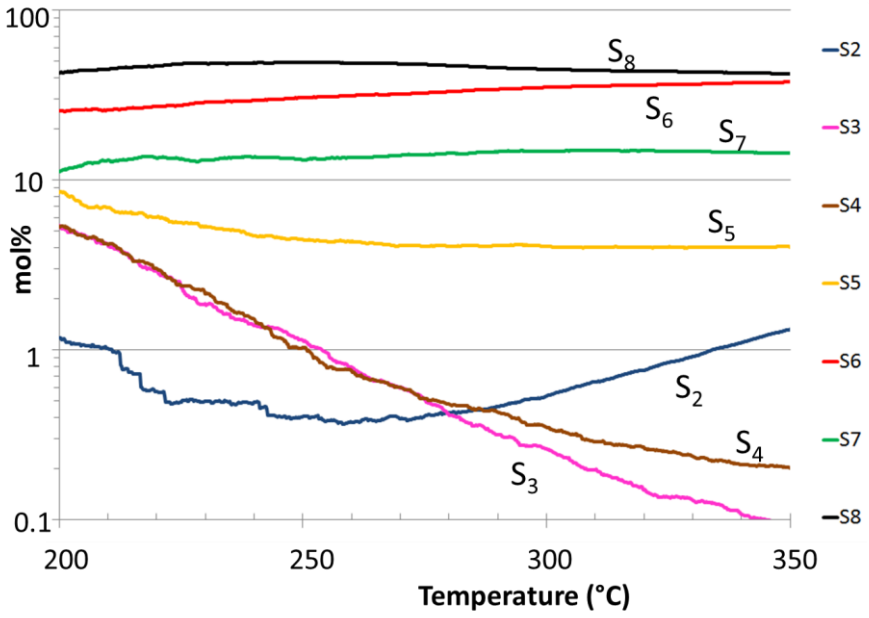

Fig. 15: Composition of vapor above a heated sulfur sample (without cross section correction) [121]

Measurements with an isothermal segment were done to inspect the applicability of the system for equilibrium sulfur vapor. The mol%-temperature diagram and the total ion count (TIC) are depicted in *Fig. 16 a; Fig. 16 b* shows the TG/DSC curves of the investigated sulfur sample. Mass spectrometric data show that the sulfur species S_2-S_8 are detectable effusing through the pinhole from the sample crucible and the equilibrium composition occurs fast after reaching 300 °C and this state is stable during the isothermal segment of the measurement. Comparing the calculated mol% values with literature data (*Table 3*), they are in good agreement for all species. We observed the biggest difference for S_2, but literature [41,123] is also inconsistent for this molecule. Photoelectrons can also cause this discrepancy. The equilibrium state is also proven on the corresponding TG and DSC curves, according to *Fig. 16 b*, mass loss and enthalpy is constant during the 300 °C segment.

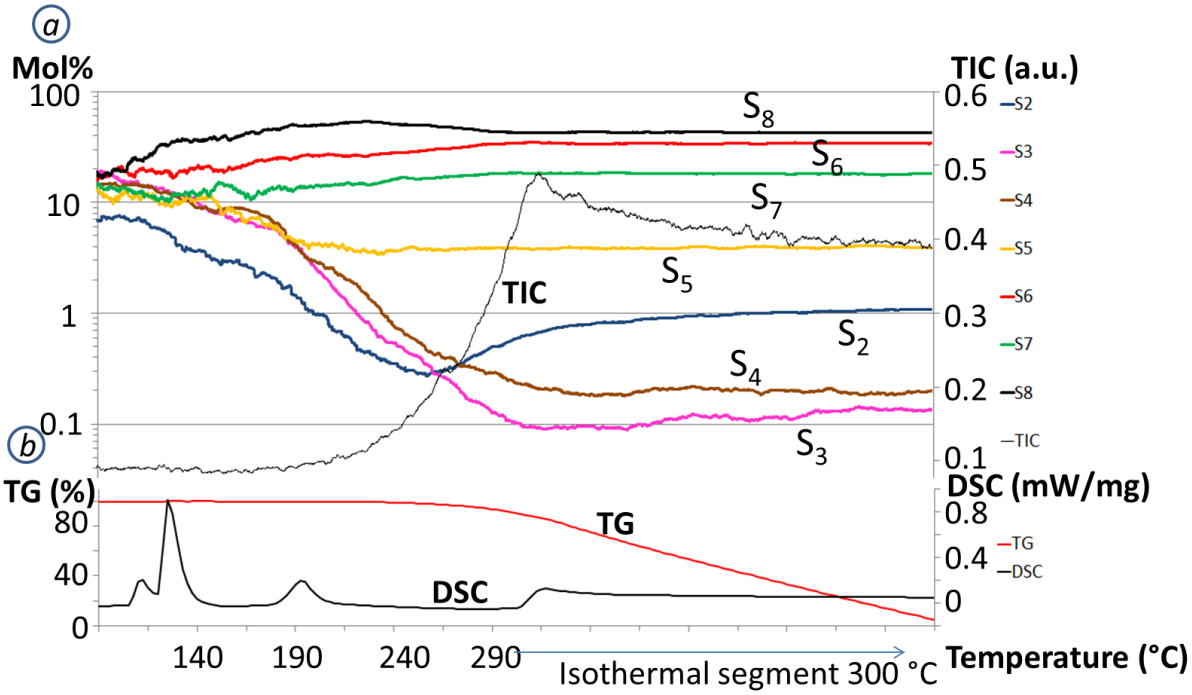

Fig. 16: Equilibrium sulfur measurement: mol% (without cross section correction) and total ion current (TIC) (a) TG and DSC curves (b) [121]

Species	**mol% at 300 °C**	**Literature 1** [41]	**Literature 2** [123]
S_8	45.5±4.1	45	45
S_7	18.5±1.7	20	30
S_6	30.8±3.9	30	20
S_5	4.0±0.7	3	2
S_4	0.2±0.1	0.4	0
S_3	0.1±0.1	0	0
S_2	1.0±0.1	0.4	0.2

Table 3: Molar percentages of sulfur species determined during the isothermal segment calculated by four independent measurements [121]

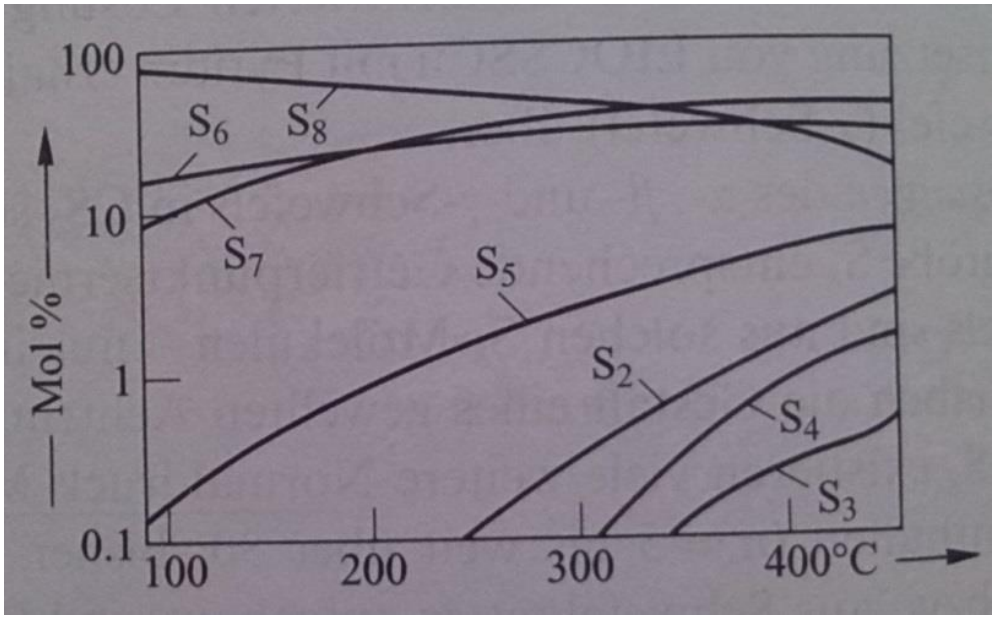

Fig. 17: Composition of saturated sulfur vapor [123]

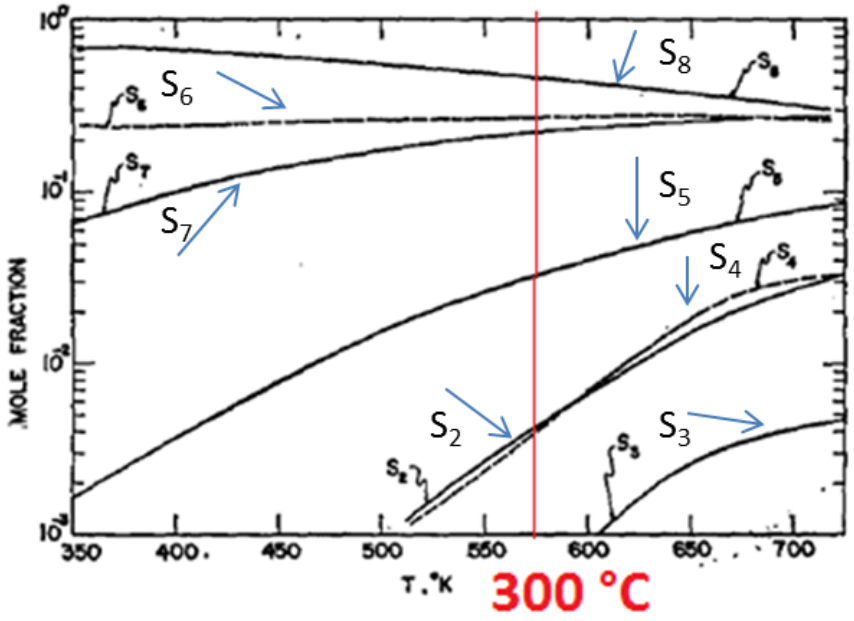

Fig. 18: Composition of saturated sulfur vapor [41]

The probability of photoionization is related to the photoionization cross sections, which must be considered for the more exact relative quantification of the sulfur species. No experimental data are available in the literature for the cross sections of S_2-S_8, Guthrie et al. [124] assumed that the effective ratio of the ionization cross sections is about $\sigma(S8)/\sigma(S2)=2$ and the intermediate species can be interpolated. The only way to have a better estimation of relative cross sections are quantum chemical calculations. During the calculations, the lamp spectra must be considered as well, since the different wavelengths of the ionizing photons lead to different cross section of the same molecule with different lamps.

In cooperation, photoelectron spectra for sulfur clusters were calculated connected to this PhD work by the Institute of Physics of the University of Rostock (18051 Rostock, Germany). Data will be published in a separate study.

Selenium

We followed the same approach for the investigation of selenium vapor. TG and DSC data show mass loss during evaporation and the energetic changes during phase transitions (endothermic peak of melting, endothermic peak of boiling). In the vapor phase, we observed the presence of Se_2 and Se_5-Se_8 in the studied temperature ranges. Isothermal measurements at 500 °C show that the equilibrium state occurs fast after the temperature is set and it is stable during the isothermal segment (*Fig. 21*) There are differences between our results and literature data, although we both excluded the presence of Se_4 in the vapor at 500 °C *(Fig. 19-20, Table 4).* Note that data are not yet cross section corrected.

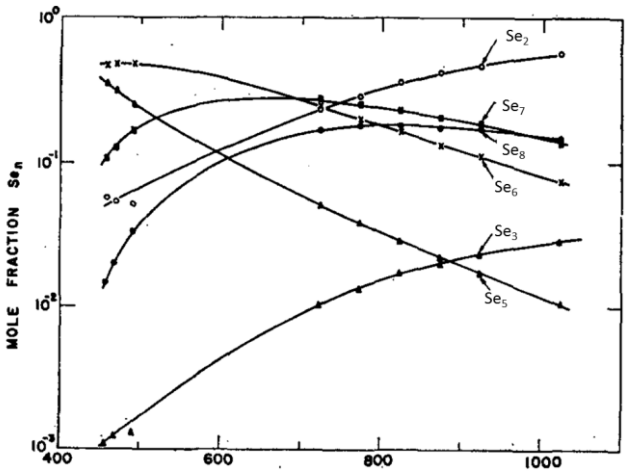

Fig. 19: Composition of saturated selenium vapor [44]

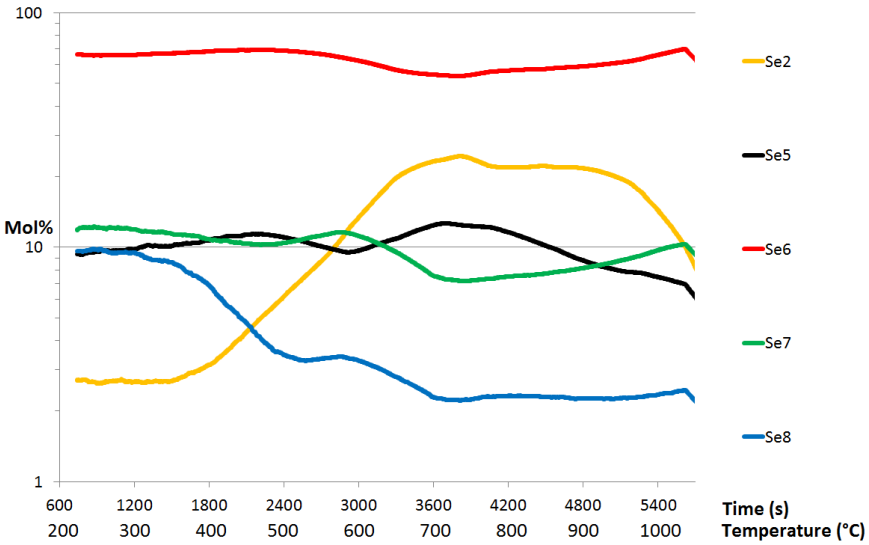

Fig. 20: Composition of vapor above a heated selenium sample

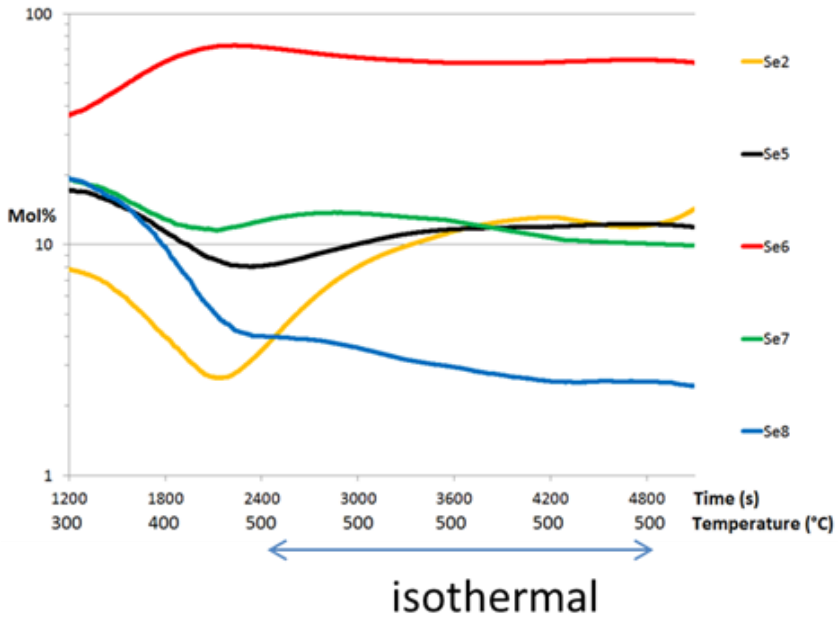

Fig. 21: Equilibrium sulfur measurement with isothermal segment at 500 °C

Spe-cies	**Mol% at 500 °C**	**Litera-ture**[44]
Se_8	3	17
Se_7	10	25
Se_6	60	23
Se_5	15	7
Se_4	0	0
Se_3	0.1	1.5
Se_2	15	26.5

Table 4: Molar percentages of selenium species determined during the isothermal segment at 500 °C

Verification of the non-fragmenting character of SPI for sulfur clusters

Method development

As described before, it is possible to separate the S_8, S_7 and S_6 allotropic modifications of sulfur in the vapor phase with gas chromatography. If a sulfur solution is injected into a GC inlet at higher temperatures, these modifications will be formed. *Fig. 22-24* show the SPI vs. EI mass spectra of S_6, S_7 and S_8. Interestingly, also higher mass modifications (S_7, S_8 for S_6; S_8 for S_7) can be observed in the mass spectra of the respective peaks. This shows that there is a dynamic equilibrium of the species also on the column, during the GC separation.

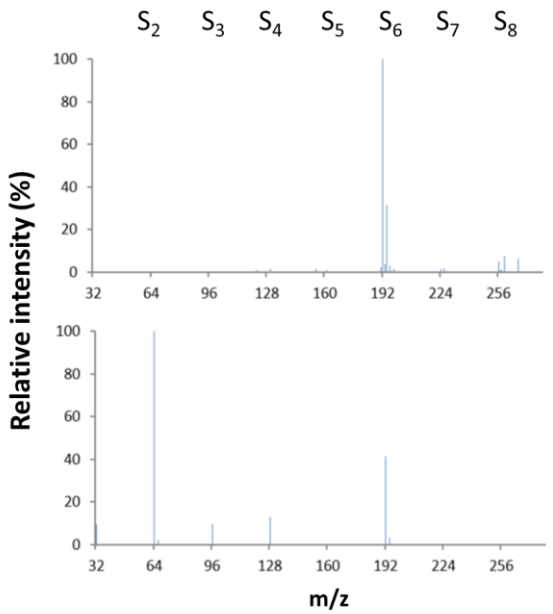

Fig. 22: SPI and EI mass spectrum of S_6

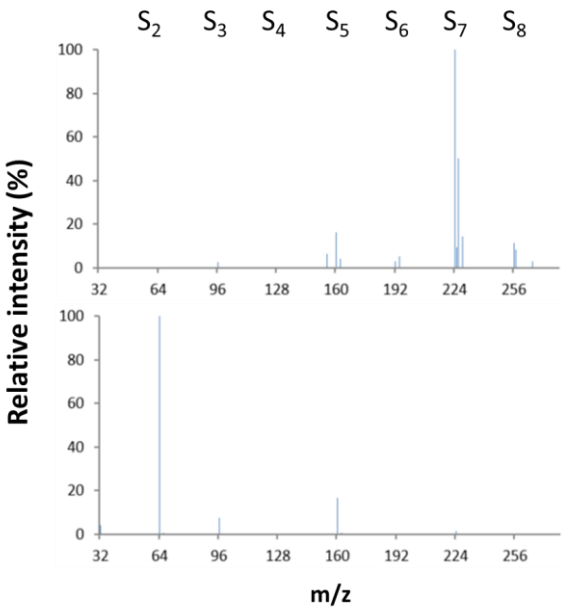

Fig. 23: SPI and EI mass spectrum of S_7

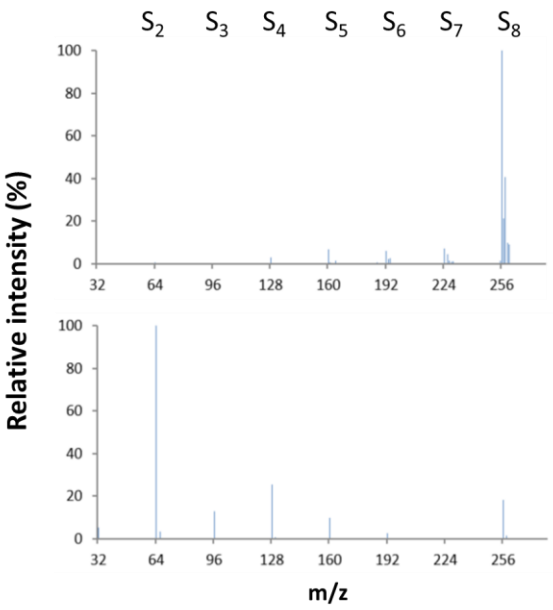

Fig. 24: SPI and EI mass spectrum of S_8

The GC parameters influence the distribution of the allotropic modifications. GC parameters were optimized to separate and gain mass spectra of all species. Besides concentration and solvent of the sample, the influences of the following parameters were evaluated:

- injection temperature
- column temperature and
- transfer capillary temperature.

Fig. 25 shows the influence of the injection temperature. The modifications S_6 and S_7 were formed poorly under 300 °C. To further determination of the relative photoionization cross sections for all three allotropic modifications, the inlet temperature was set to 300 °C.

Increasing column temperature results in an increasing fragmentation of the sulfur modifications S_8, S_7 and S_6. The increasing baseline of m/z=64 can be seen in *Fig. 26*. The influence of transfer capillary temperature is also significant: the S_2 fragment appears at 300 °C. The mass spectrum of S_8 is depicted in *Fig. 27* at different temperatures.

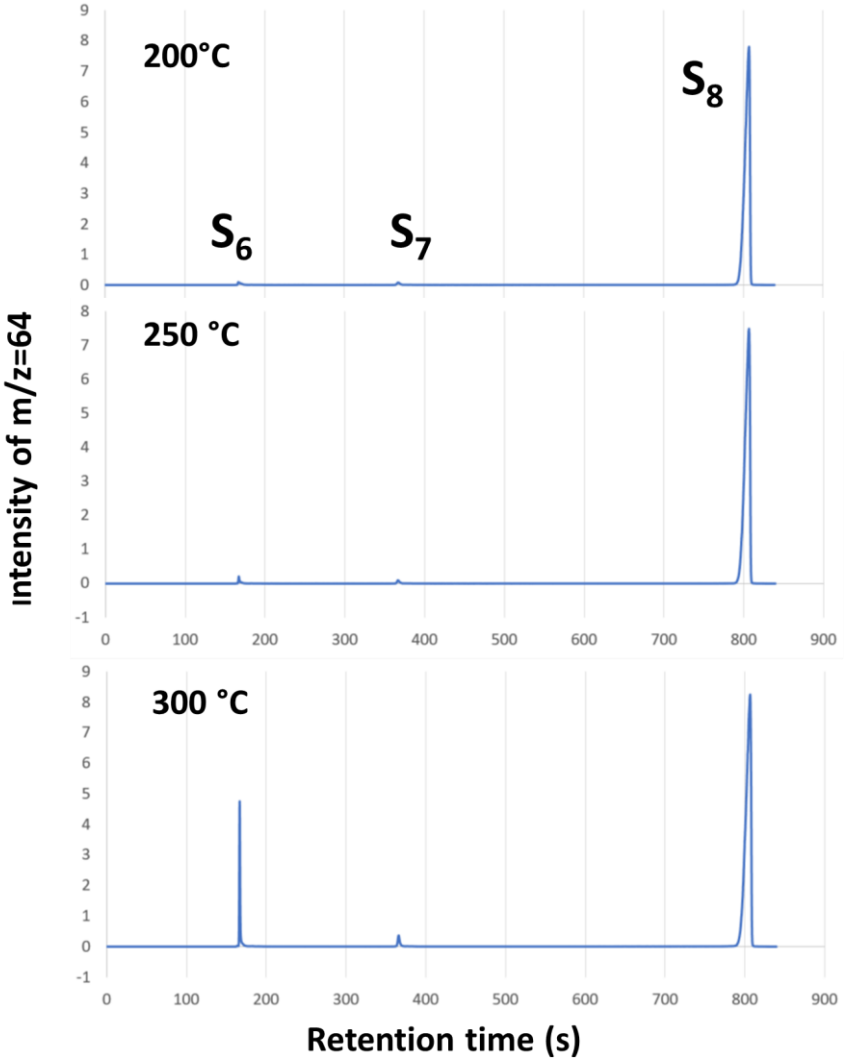

Fig. 25: Influence of the injector temperature on the distribution of S_8, S_7 and S_6

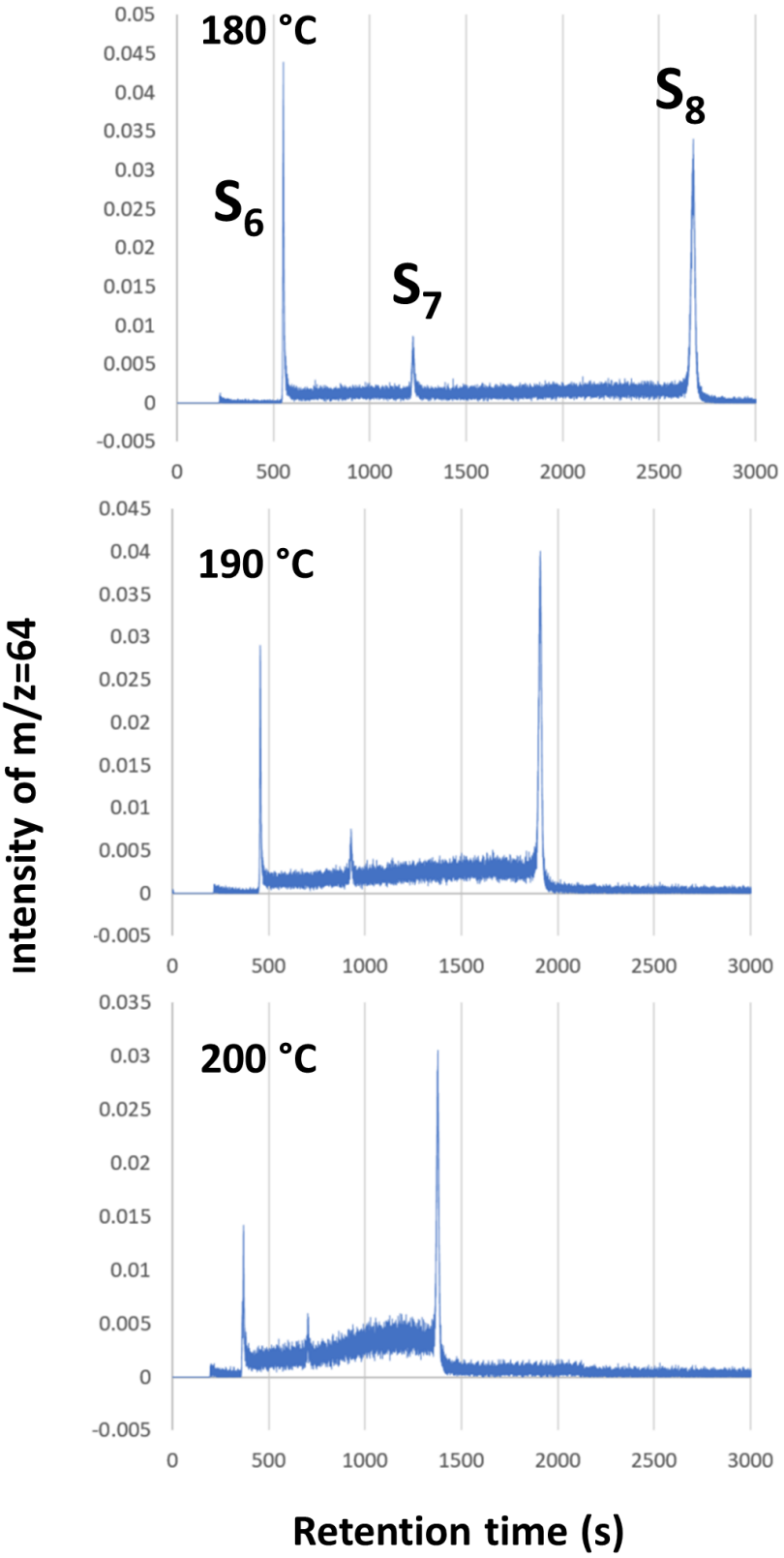

Fig. 26: Influence of the column temperature

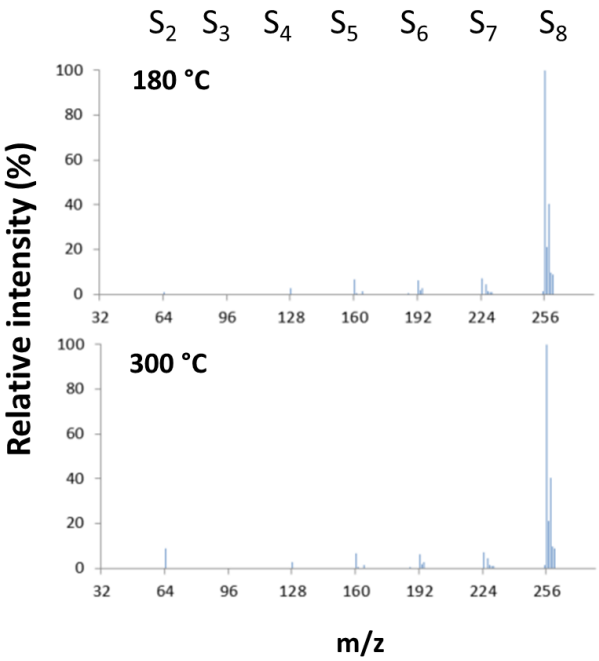

Fig. 27: Influence of the transfer capillary temperature on the attained mass spectra

After evaluations of the parameters influencing the separation, the final GC program is: Column: Factor Four, VF-5ms, 30 m X 0.25 mm X 0.25 mm, mobile phase: Helium 2 mL/min, column temperature: 180 °C for 6 minutes, followed by a 10 K/min ramp until 220 °C, finally an isothermal hold for 5 minutes. Injection volume: 2 µL, Split flow: 100 mL/min, injector temperature: 300 °C, concentration of sulfur solved in cyclohexane: 1 mg/mL).

Characterization of 1-alkyl-3-methylimidazolium halide ionic liquids with TG/DSC-Skimmer-SPI-TOFMS

Measurement conditions and samples

The following measurement conditions were used for the TG/DSC-Skimmer-SPI-TOFMS samples: 1) heating rate of 10 K/min in the 25-500 °C range, 2) purge and protective gas: 30 mL/min nitrogen, helium, argon, synthetic air (only for purge), 3) sample weight: 5 mg in aluminum oxide crucibles with a lid and a pinhole in the lid. Pressures were ca. 40 mbar, 5 * 10^{-5} mbar, and 1.2 * 10^{-6} mbar in the interstage chamber, ion source, and mass spectrometer. Prior to the measurements, the furnace was 3 times evacuated and consequently purged with the measurement gases. However, contact with humidity from air cannot be excluded while placing the sample into the furnace and letting it into the downward position. Note, that the measured ionic liquids are hygroscopic; that can change their physicochemical properties.

1-Ethyl-3-methylimidazolium halides, [emim]*X*: [emim]Cl with purity over 98 % from Sigma-Aldrich (Steinheim, Germany); [emim]Br (> 98 %) and [emim]I (> 97 %) purchased from Alfa Aesar (Ward Hill, Massachusetts, USA). 1-Butyl-3-methylimidazolium halides [bmim]*X*: all three halides (*X* = Cl, Br, I) supplied by Sigma-Aldrich with purity over 99 %. 1-Hexyl-3-methylimidazolium halides, [hmim]*X*: [hmim]Cl supplied by abcr (Karlsruhe, Germany) (purity > 99 %); [hmim]Br and [hmim]I with purity over 98 %, purchased from TCI (Zwijndrecht, Belgium) and Sigma-Aldrich, respectively. The substances were used without any further purification. They were opened, handled and sampled in an argon-filled glove box [$c(O_2, H_2O) \leq 0.1$ ppm, M. Braun LAB 130]. Other chemicals: imidazole (VWR, Radnor, USA), 1-methylimidazole and 1-ethylimidazole (Santa Cruz Biotech, Dallas, USA). Data evaluation was performed with Proteus 5.1.0 (Netzsch, Germany), Tofdaq 1.2.93 (TofWerk, Switzerland) and Origin2016 (OriginLab, USA).

Results and interpretation

The TG/DSC-Skimmer-SPI-TOFMS technique was used for the investigation of thermal behavior, short-term stability, mapping structure-stability relations, as well as the decomposition products and patterns of 1-alkyl-3-methylimidazolium halides under inert gases (nitrogen, helium, argon) and synthetic air flow.

Multidimensional measurement data can be visualized like in *Fig. 28*. In the contour plot, on the axes, the m/z value, temperature, and signal intensity are shown. It can be followed simultaneously which compounds (m/z) evolve, which mass loss and enthalpy changes occur. Data were evaluated also separated (TG, DSC, and MS) and it was also evaluated to what extent TG/DSC data can be used as complementary information to MS data.

The mass spectrometer enables the detection of volatile compounds providing additional information. It is possible that several overlapping processes belong to one TG step; that can be recognized by MS. On the other hand, there are processes where no mass loss occurs (no

volatile compounds); in this case, DSC data are useful to detect changes in the sample. DSC data also help to characterize the process from which the detected compounds evolve and characterize it whether it is an endothermal or an exothermal process.

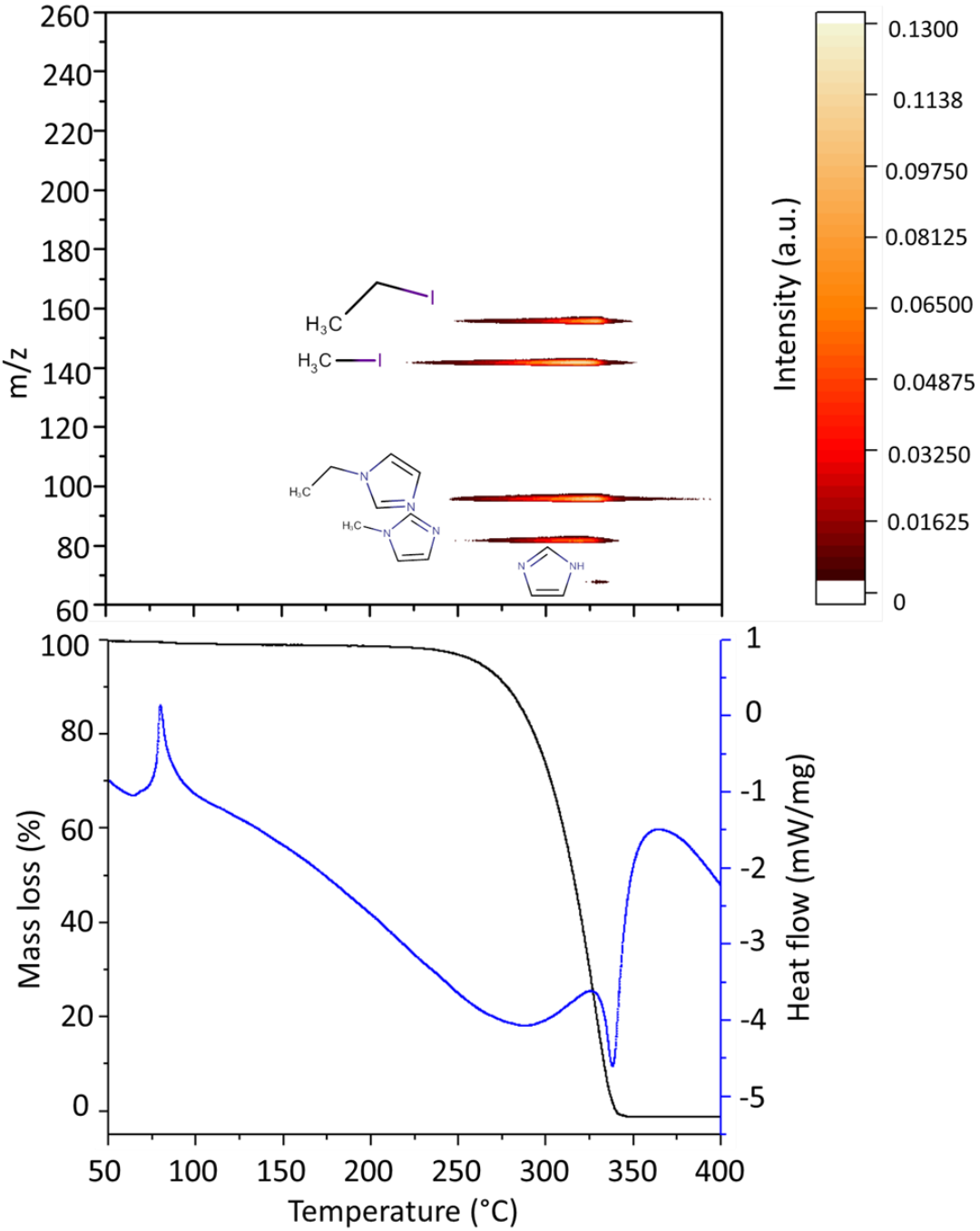

Fig. 28: Multidimensional data gained upon heating [emim][I] in nitrogen atmosphere

TG and DSC data

Upon heating, I observed for all samples a dominant mass loss step of about 100 % at about 250 °C that can be assigned to the decomposition of the substance. Insignificant mass losses (up to 1 %), were detected before the decomposition started. These mass losses could be

identified later (by EI-MS, *Fig. 35*) as the evaporation of moisture. This indicates that the examined compounds do not evaporate until they decompose.

An endothermal melting peak is observed at about 75 °C (onset) on the DSC curve. (In the cases where the investigated ILs were solid at room temperature. Some butyl and hexyl salts are liquids at room temperature.

Decomposition temperatures were determined using the extrapolated onset temperatures of the derived TG (DTG) curves. DSC curves show an endothermal decomposition in inert gas while it occurs in air exothermically and results also in different decomposition products as detected by mass spectrometry (see below). The DSC curves suggest that decomposition occurs by multiple possibly overlapping processes. *Table 5* summarizes the measured decomposition temperatures. It is well known that the experimental conditions, such as heating rate, sample crucible materials, sample weight and atmosphere can influence the thermal analysis results.

The thermal stability increased in order from [emim][Cl] < [emim][I] < [emim][Br] (*Fig. 29*) in nitrogen, argon, and [emim][Cl] < [emim][Br]< [emim][I] in air, helium. The stabilities of the butyl and hexyl salts increased in order from Cl^- < Br^- < I^-. Enhancement of the alkyl chain length leads to decline in thermal stabilities in the certain halide series comparing the ethyl and buthyl salts. It seems, the elongation of alkyl chain from butyl to hexyl has less effect on stability (maybe due to the similar steric effects of butyl and hexyl chains).

The stabilities are determined by multiple factors such as basicity and nucleophilicity of the halide anion and steric effects. The stability temperatures should be accessed carefully as the measured ionic liquids are hygroscopic and that can change their physicochemical properties. However, it can be clearly seen that the chloride salts are less stable than the bromine and iodine salts that have approximately similar decomposition temperatures.

Regarding the atmosphere influence, it can be expected that stability is decreased in synthetic air atmosphere. Based on my measurements, it cannot be confirmed completely. This is caused by the fact that air humidity also affects properties of the ILs.

The extrapolated onset temperature (T_e) of the TG curve of *Fig. 28* is 295.5 °C, whereas the extrapolated onset of the DTG is 276.4 °C. The first evolving compounds were detected already at ~210 °C. That clearly shows that decomposition begins far earlier than the extrapolated onset temperatures and it is complicated to judge of the starting point of the decomposition by thermogravimetric data. It is also possible that decomposition starts with reactions without volatile products, of course, that cannot be detected with this technology. Mass loss between 50 and 210 °C is ~1.15 %, between 210 and 276.4 °C (DTG T_e) is ~10 %. Description of the evolving compounds follows.

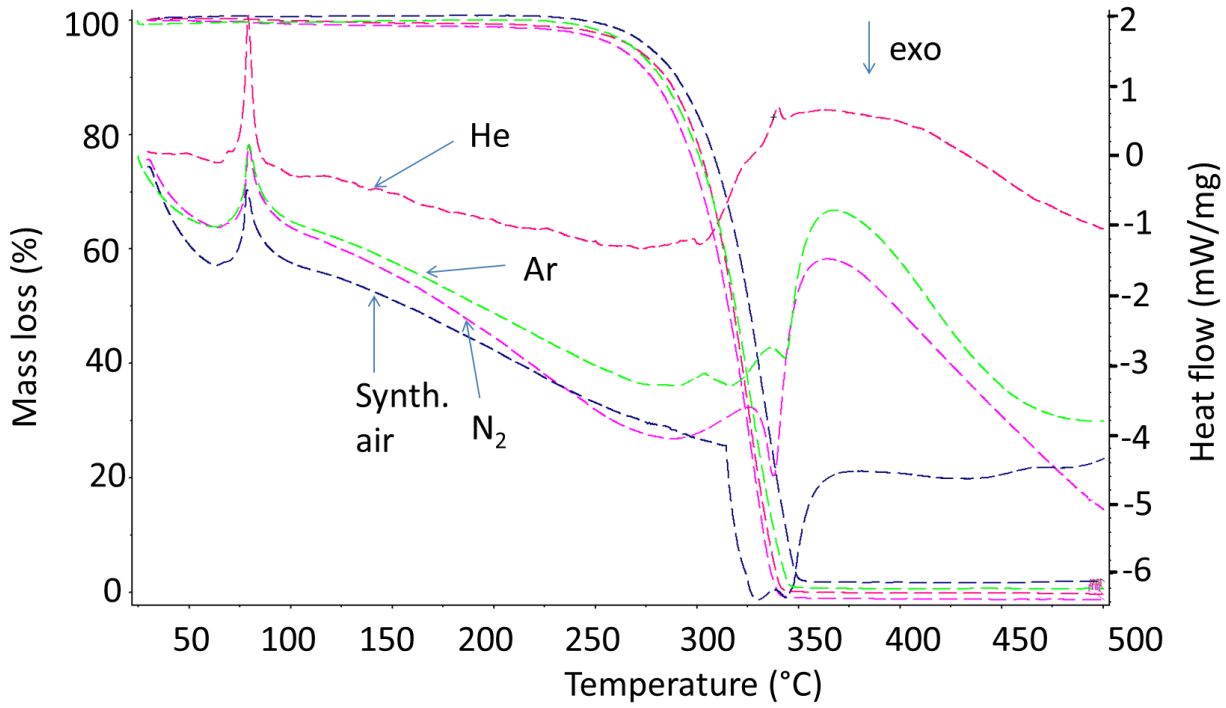

Fig. 29: TG/DSC curves of [emim]I in different gases (helium, argon, nitrogen, synthetic air)

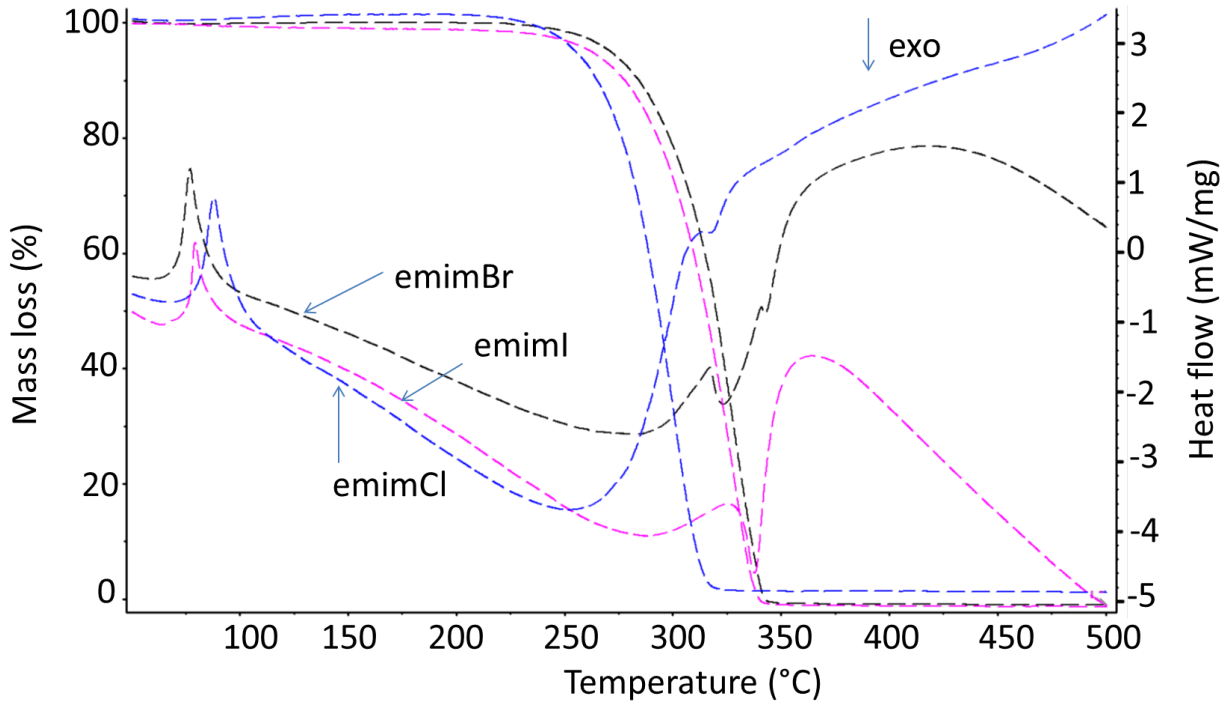

Fig. 30: TG/DSC curves of [emim][Cl], [emim][Br], and [emim][I] in nitrogen

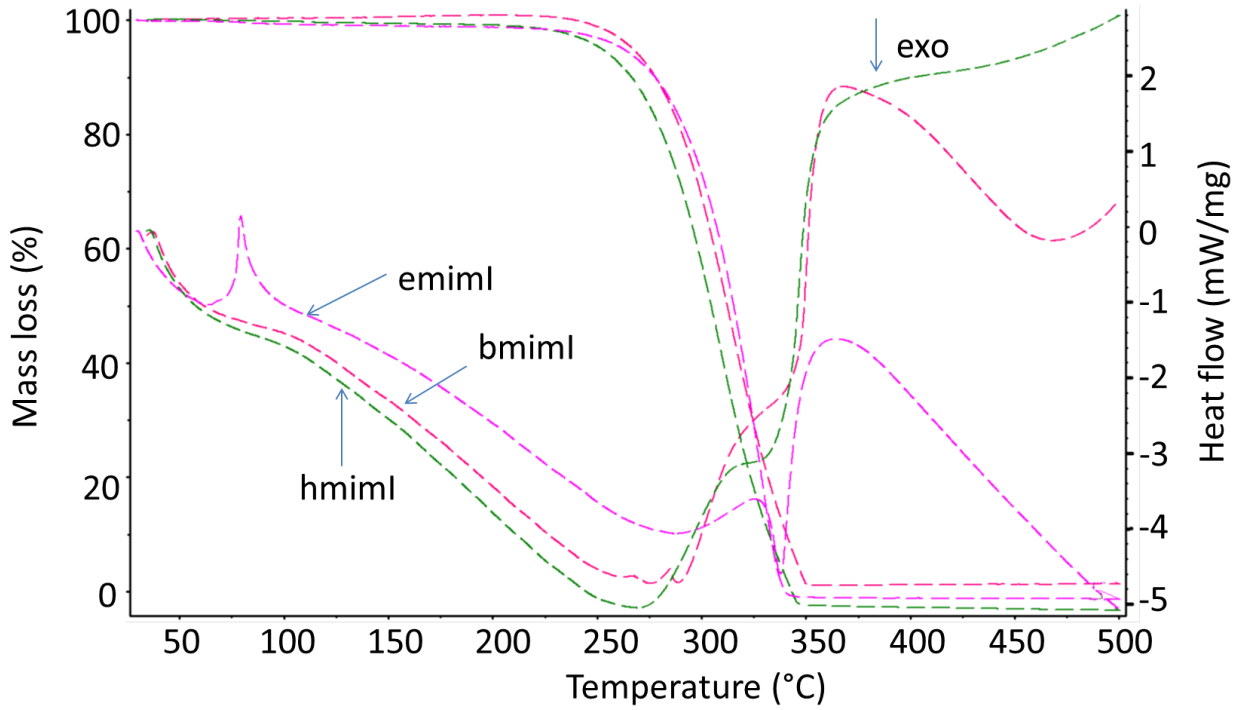

Fig. 31: TG/DSC curves of [emim][Cl], [emim][Br], and [emim][I] in nitrogen

gas flow	T_{onset}-DTG*, °C								
	[emim]*X*			[bmim]*X*			[hmim]*X*		
	Cl	Br	I	Cl	Br	I	Cl	Br	I
N_2	260.4	289.4	276.4	253.6	255.0	261.8	241.2	257.4	262.1
synth. air	268.7	267.9	261.8	243.6	257.9	276.5	-	-	-
He	270.5	274.0	281.2	-	-	-	-	-	-
Ar	266.3	284.6	284.5	-	-	-	-	-	-

Table 5 Onset temperatures of the DTG curves

In the following, mass spectrometric results are presented for the investigation of degradation products. Using soft ionization mass spectrometric data, we discuss the decomposition pathways and possible mechanisms of the investigated ionic liquids.

Fig. 28 depicts the mass traces obtained during the TA-Skimmer-SPI-TOFMS measurement of 1-ethyl-3-methylimidazolium iodide (nitrogen atmosphere). The detected mass traces suggest the formation of ethyl iodide (m/z=156), methyl iodide (m/z=127), 1-ethylimidazole (m/z=96), 1-methylimidazole (m/z=82) and imidazole (m/z=68). *Fig. 32 a* represents the mass traces of the evolving molecules upon heating 1-ethyl-methylimidazolium bromide: ethyl bromide (m/z=108, 110), ethylimidazole (m/z=96), methyl bromide (m/z=94, 96), methylimidazole (m/z=82), and imidazole (m/z= 68). *Fig. 32 b* shows the detected mass traces upon heating

1-ethyl-3-methylimidazolium chloride: 1-ethylimidazole (m/z=96), methylimidazole (m/z=82) and imidazole (m/z=68, very small amount, not shown in the figure).

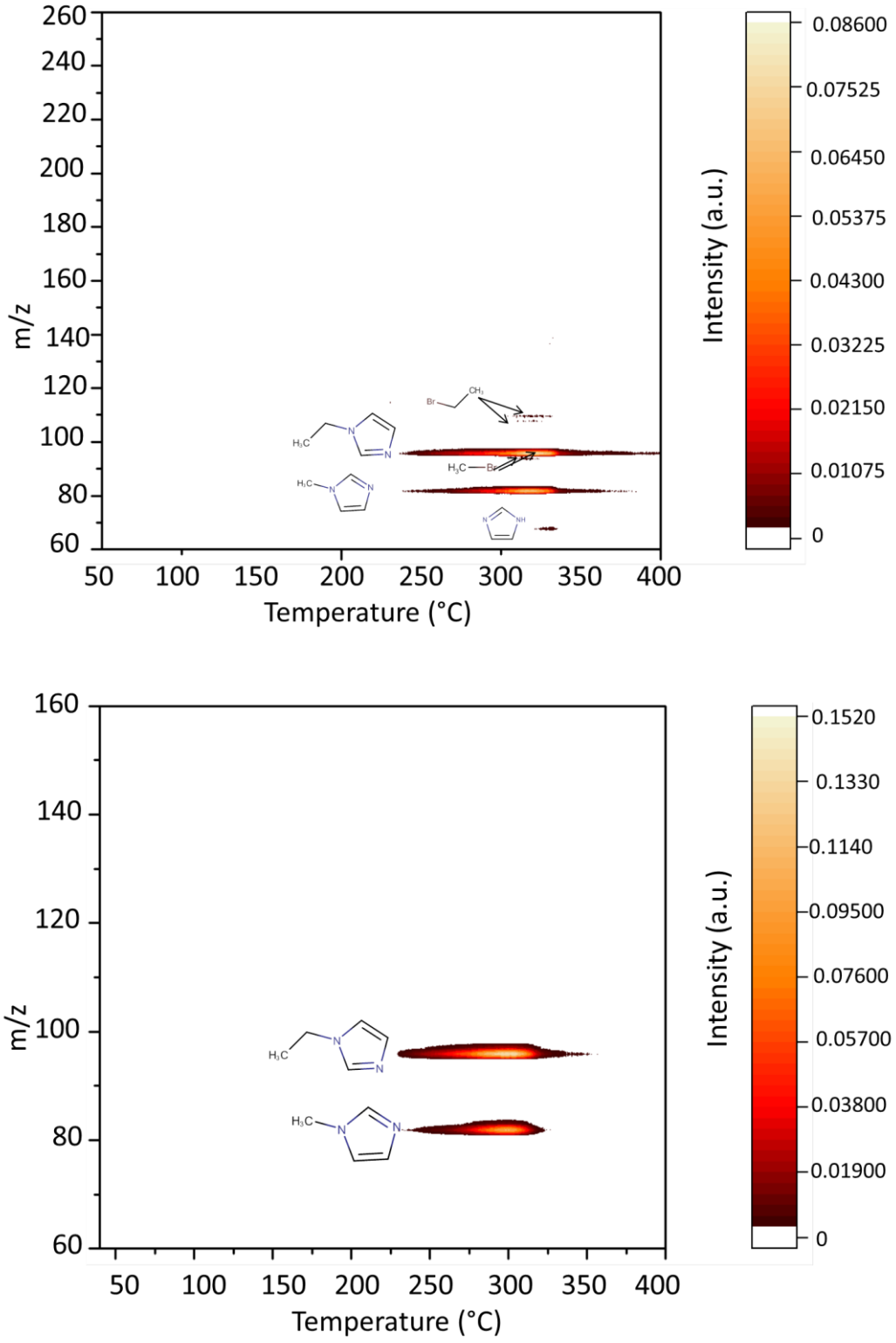

Fig. 32: TA-Skimmer-SPI-TOFMS results of a.) 1-ethyl-3-methylimidazolium bromide b.) 1-ethyl-3-methylimidazolium chloride in nitrogen atmosphere

Applicability of photoionization for the detection of the evolving compounds

Photoionization with VUV photons (10.16 eV) enables the detection of molecular ions with no or less fragments in the case of the aforementioned molecules which is suggested by the photoionization energies of the species (imidazole 8.81 eV, ethyl iodide 9.33 eV, methyl iodide 9.53 eV, no literature data were found for 1-methylimidazole and 1-ethylimidazole). The detection of the alkyl halides evolving from 1-ethyl-3-methylimidazolium chloride or bromide is critical as their ionization energies are higher than the applied ionization energy (ethyl bromide 10.29 eV, methyl bromide 10.53 eV, ethyl chloride 10.98 eV, methyl chloride 11.265 eV). The alkyl bromides can be ionized only to a smaller extent; the applied ionization energy is not suitable for the ionization of alkyl chlorides. Alternatively, it is possible to operate the device in EI mode for the detection of compounds with higher ionization energy that can be obtained with the deuterium lamp. It is especially helpful also for the detection of hydrogen halides (hydrogen iodide 10.38 eV, hydrogen bromide 11.68 eV, hydrogen chloride 12.74 eV) and ethane (10.50 eV) (Ionization energies are taken from the NIST database, the suitability of the used lamp is illustrated in *Table 6*).

Molecule	Ionization energy (eV)
Imidazole	8.81
Methylimidazole	?
Ethylimidazole	?
Hydrogen iodide	10.38
Hydrogen bromide	11.68
Hydrogen chloride	12.74

Molecule	Ionization energy (eV)
Methyl iodide	9.53
Ethyl iodide	9.33
Methyl bromide	10.53
Ethyl bromide	10.29
Methyl chloride	11.27
Ethyl chloride	10.98

Molecule	Ionization energy (eV)
Ethene	10.50
Propene	9.73
Buthene	9.57
Hexene	9.46

Table 6: Summary of photoionization energies of potential decomposition products

To demonstrate the non-fragmenting character of the applied photoionization, we recorded the mass spectra of the pure substances for imidazole, 1-methylimidazole, and 1-ethylimidazole (*Fig. 33 a-c*).

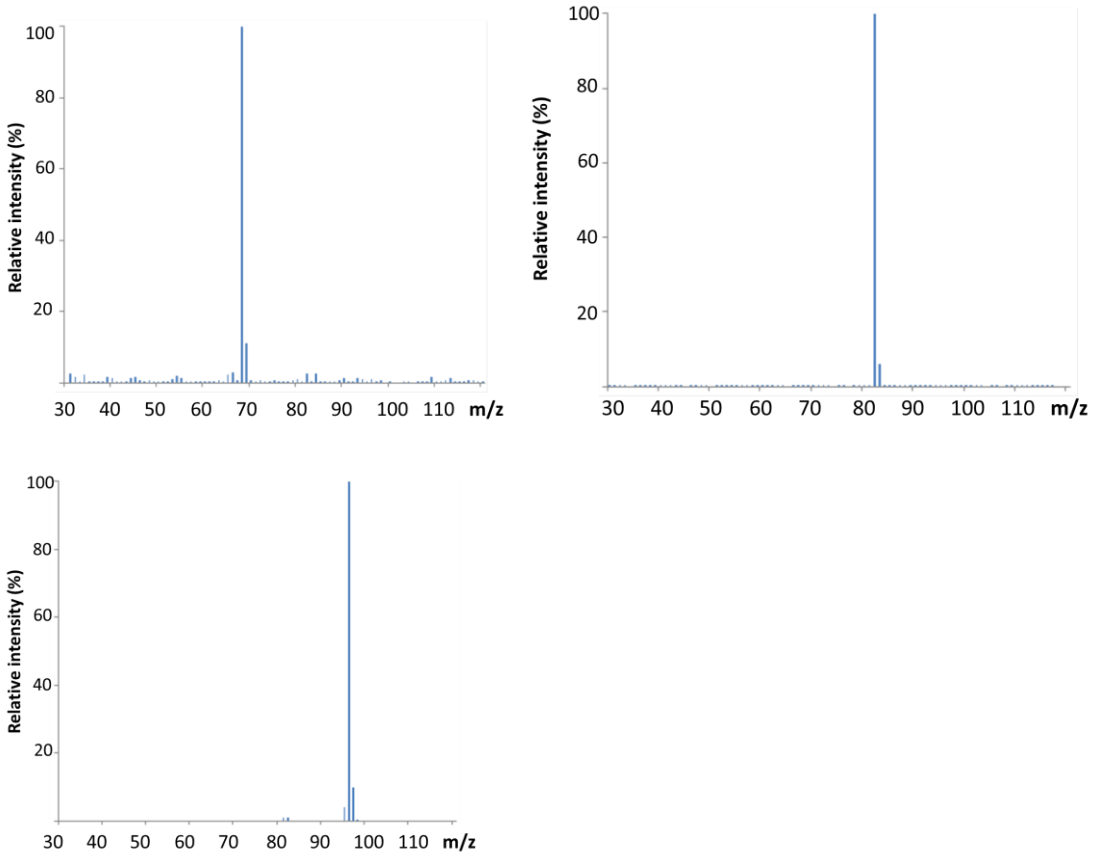

Fig. 33: SPI-MS spectra of a.) imidazole (m/z=68) b.) 1-methylimidazole (m/z=82) c.) 1-ethylimidazole (m/z=96)

Due to the almost fragment-free detection of the decomposition products, it is possible to deduce the decomposition pathways. *Fig. 34 a* and *b* illustrate the formation of ethyl halide, methyl halide, 1-ethylimidazole, 1-methylimidazole which occurs via the reverse Menshutkin reaction. It leads to a tertiary amine and an alkyl halide by the reaction of the quaternary ammonium cation with the halide anion [96]. The detected mass traces affirm that reverse Menshutkin reaction takes place on both alkyl chains. For the iodine salt, the methyl group is slightly more preferred than the ethyl chain, which is suggested by the formation of methyl iodide and 1-ethylimidazole at lower temperatures than ethyl iodide and 1-methylimidazole. For the bromide and chloride salts, this preference is less strong. The reverse Menshutkin reaction starts with the nucleophilic attack of the iodide anion at an alkyl group and followed by a C-N cleavage. According to Chan [110] et al., the mechanism of nucleophilic substitution is S_N2 in the case of dialkyl imidazolium halide salts (and S_N1 for allyl and benzyl substituted salts). I compared the decomposition products and their appearance from [emim][Cl], [emim][Br], [emim][I] to study the effect of changing the anion. In the S_N2 mechanism, the specificity for attack at methyl rather than ethyl decreases with decrease in size of the nucleophile. Smaller anions show a lower preference for methyl to ethyl group. Our measurements confirm that as we detect ethylimidazole and methylimidazole evolving at the same time from the chloride and bromide salt unlike described above in the case of the iodide salt.

Nucleophilicity order according to Chan et al. [110] is $I^- > Br^- > Cl^-$, however this order is $I^- > Cl^- > Br^-$, where Cl^- is slightly more nucleophilic than Br^- according to Lancaster et al. [125]. In our experiments, the bromide salt proved to be similar stable like followed by the iodide (slight difference in the onset temperatures) and the most vulnerable is the chloride salt (*Table 5*). Consequently, it indicates also that the decomposition and the stability cannot be described only by the S_N2 reaction. Elimination should be considered also as a possible decomposition pathway parallel to the S_N2 reaction. Hofmann elimination of a quaternary amine occurs by the leave of an ethyl group as ethene. (*Fig. 34 c*) As the ionization energy of ethene is 10.50 eV it cannot be detected by the applied photoionization. We operated the Skimmer device with 70 eV electron ionization. *Fig 35* depicts the mass traces of an [emim][Cl] measurement with EI. The increase in the signal m/z=28 during the decomposition parallel with the signals of the decomposition products and the change in mass spectrum confirms the formation of ethene. Furthermore, the formation of HCl stands also for the Hofmann elimination. The basicity order is $Cl^- > Br^- > I^-$ which makes chloride salts more vulnerable to elimination. The detected imidazole indicates further decomposition of 1-ethylimidazole due to C-N bond cleavage. Besides imidazole, ethene should be as well as a dissociation product of 1-ethylimidazole. In addition, ethene and ethyl halide can be formed also by elimination of ethyl iodide. *Fig. 34 d* and *e* illustrate these possible pathways.

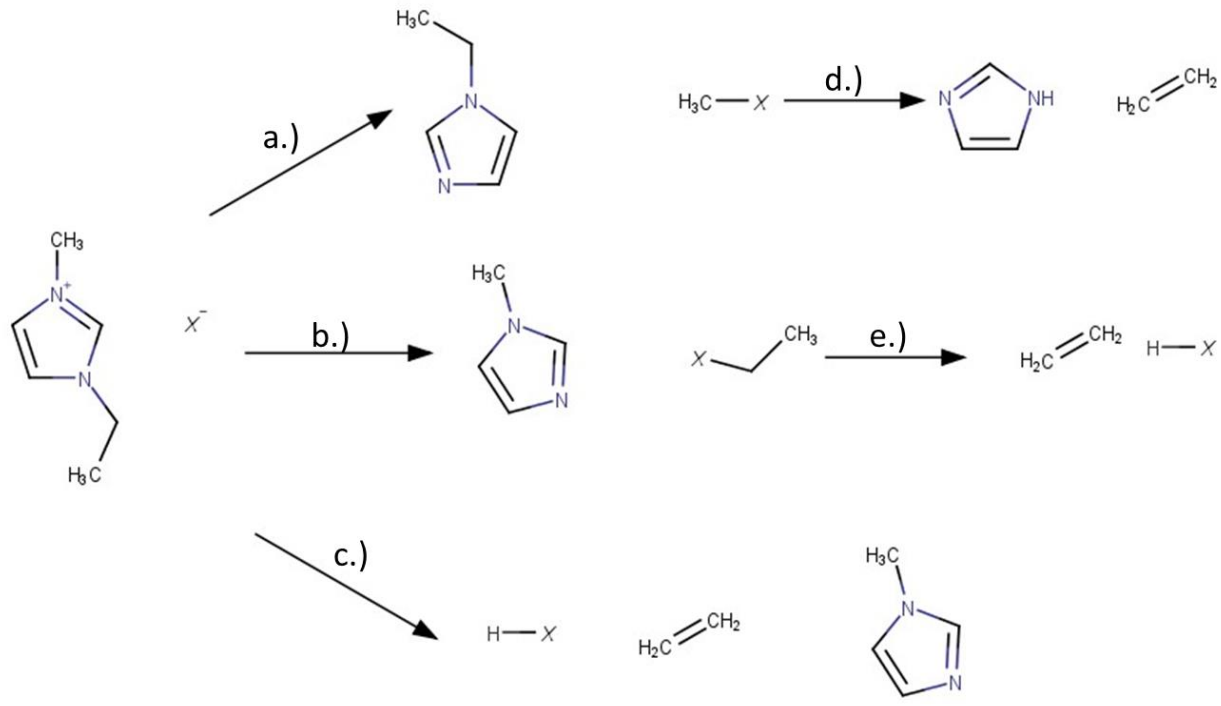

Fig. 34: Proposed thermal decomposition pathways of 1-ethyl-3-methylimidazolium halides (X = Cl, Br, I)

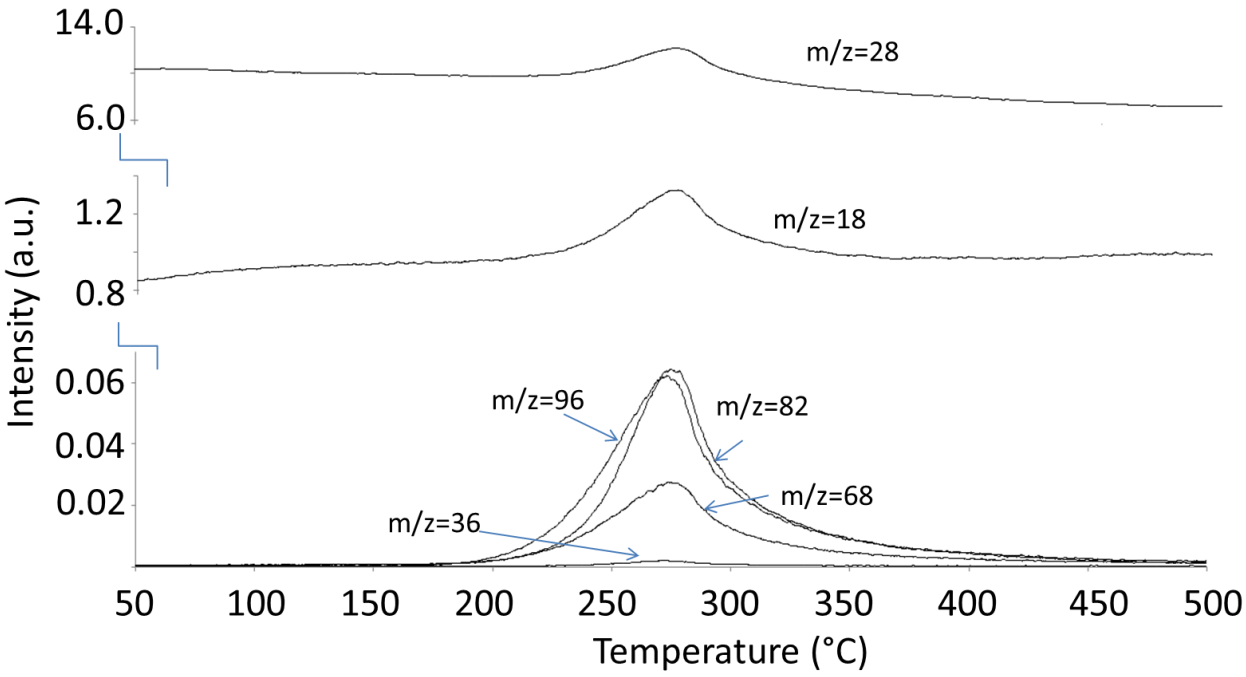

Fig. 35: EI (70 eV) mass traces of [emim][Cl] in nitrogen

The $emim^+$ cation (m/z=111) was not detected. That would suggest the formation of gaseous ion pairs [108]. Under our experimental conditions, we did not detect the intact gaseous ion pairs, either. The degradation of imidazole ring was not observed in the studied temperature range.

Fig. 36 depicts the mass traces from [emim][I] under synthetic air atmosphere, we detected additional degradation products at m/z=127 and m/z=254. TG-DSC curves show that decomposition occurs exothermically (*Fig. 29*).

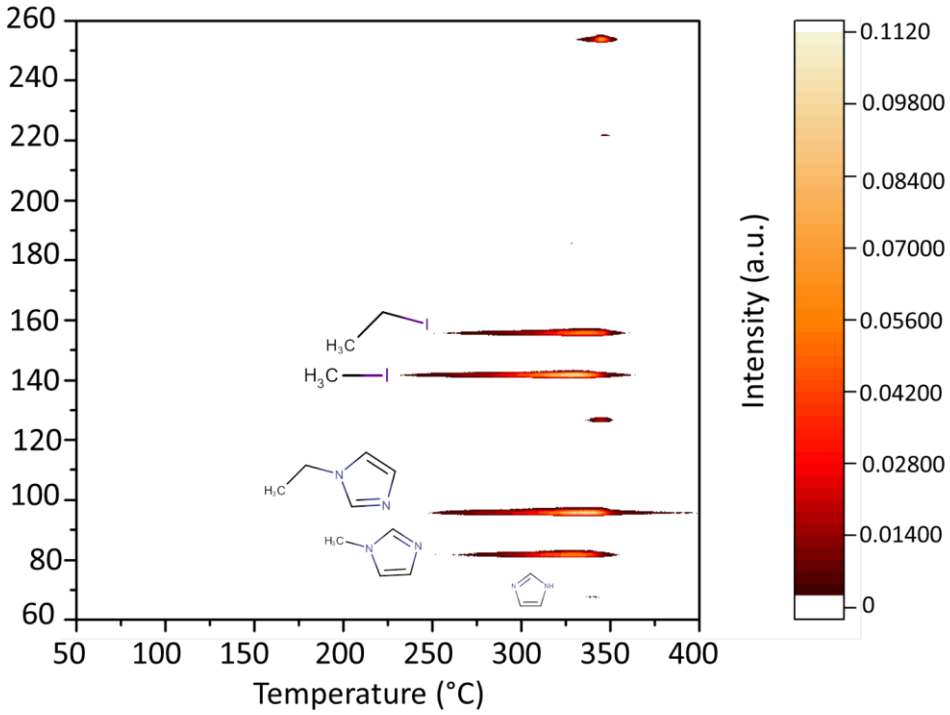

Fig. 36: TA-Skimmer-SPI-TOFMS results of 1-ethyl-3-methylimidazolium iodide in synthetic air

The decomposition of the 1-butyl-3-methylimidazolium halides occurs similarly to the way described for the ethyl salts. *Fig. 37* depicts the mass traces gained during the measurement of 1-butyl-3-methylimidazolium iodide (nitrogen atmosphere), the degradation products observed are: butyl idodide (m/z=184), methyl iodide (m/z=142), 1-butylimidazole (m/z=124), 1-ethylimidazole (m/z=96), 1-methylimidazole (m/z=82), imidazole (m/z=68) and butene (m/z=56). The decomposition of ([bmim][I] via the reverse Menshutkin reaction (*Fig. 38 a-b*) proceeds on both the N-substituents; the nucleophilic attack is slightly more preferred on the methyl substituent as a result of the higher steric hindrance of the longer butyl chain. However, this preference is only slight. The butyl halide and 1-butylimidazole have not yet been detected by MS [96,107]; they were only assumed. Photoionization enables the direct detection of butyl iodide and 1-butylimidazole unlike described in the TA-EI-MS method by Hao et al. [107]. The detected butene can originate from the Hofmann elimination (*Fig. 38 c*) but also the elimination of HI from butyl iodide (*Fig. 38 f*). Further decomposition of butyl iodide is not evident; the detected butene can be formed by elimination from butyl iodide (Fig. 38 f) or by C-N cleavage of butylimidazole (*Fig. 38 e*).

1-ethylimidazole is formed by the C-C cleavage of 1-butylimidazole (*Fig. 38 d*), imidazole was detected like in the ethyl salt measurements at higher temperatures (*Fig. 28 e, h*).

As basicity decreases in the order $F^- > Cl^- > Br^- > I^-$, the chloride salts will show greater vulnerability to elimination as well. By increasing the alkyl chain length, this preference will increase.

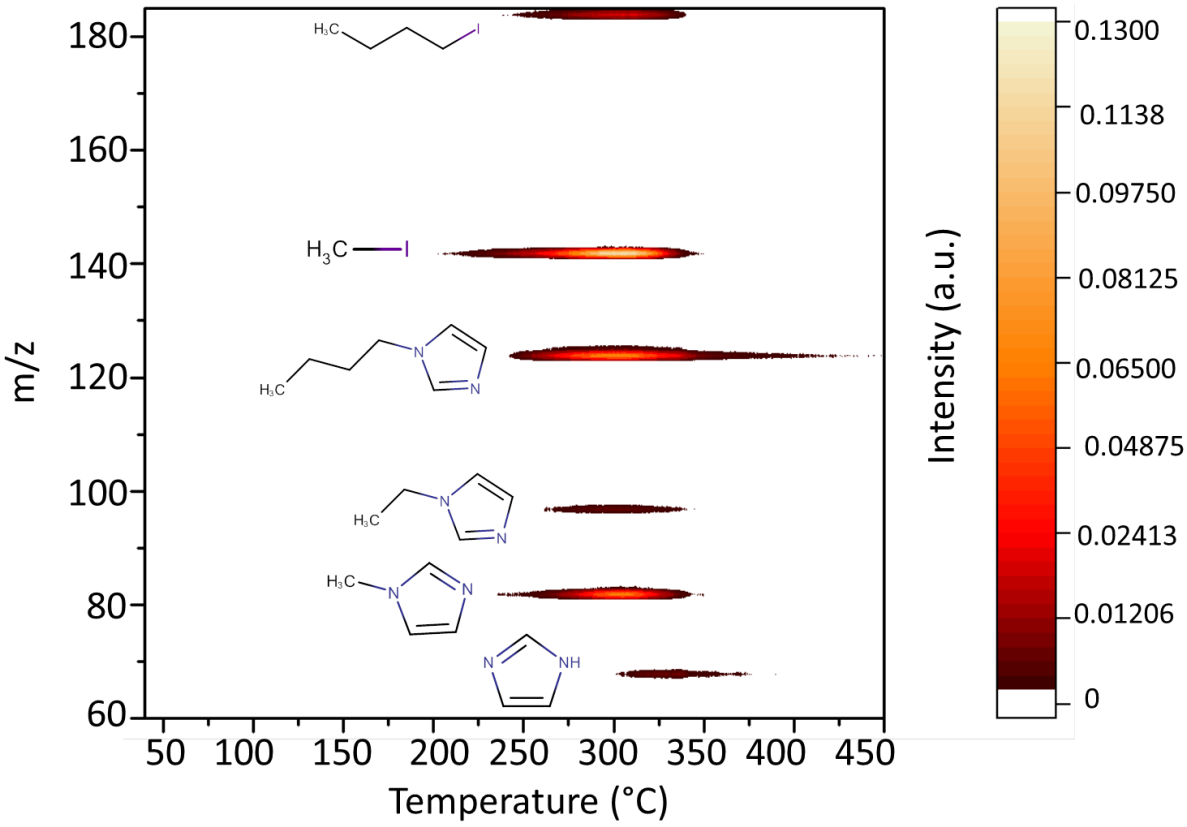

Fig. 37: TA-Skimmer-SPI-TOFMS results of 1-butyl-3-methylimidazolium iodide in inert atmosphere (nitrogen)

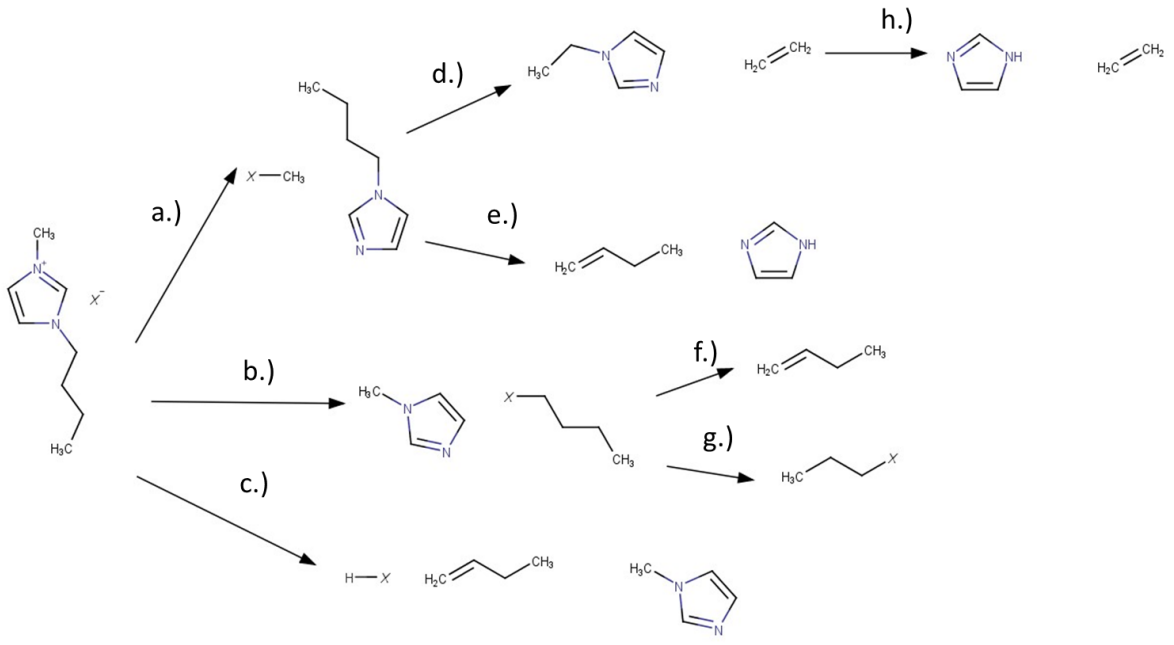

Fig. 38: Proposed thermal decomposition pathways of 1-butyl-3-methylimidazolium halides (X = Cl, Br, I)

Hexyl salts

The decomposition products of 1-hexyl-3-methylimidazolium iodide (nitrogen atmosphere) are (*Fig. 39*): hexyl iodide (m/z=212), 1-hexylimidazole (m/z=152), methyl iodide (m/z=142), 1-buthylimidazole (m/z=124), 1-ethylimidazole (m/z=96), hexene (m/z= 84), methylimidazole (m/z=82), imidazole (m/z=68), and butene (m/z=56, low signal intensity, not shown in the contour plot). The decomposition of ([hmim][I] is similar to that observed [bmim][I]. The reverse Menshutkin reaction occurs obviously on both the N-substituents (*Fig. 40 a-b*); the methyl substituent is slightly more preferred than the hexyl chain and the formation of hexene suggests Hofmann elimination (*Fig. 40 c*). The formation of 1-buthylimidazole, 1-ethlyimidazole (*Fig. 40 d-e*), imidazole, hexene, and butene confirm C-C and C-N cleavages.

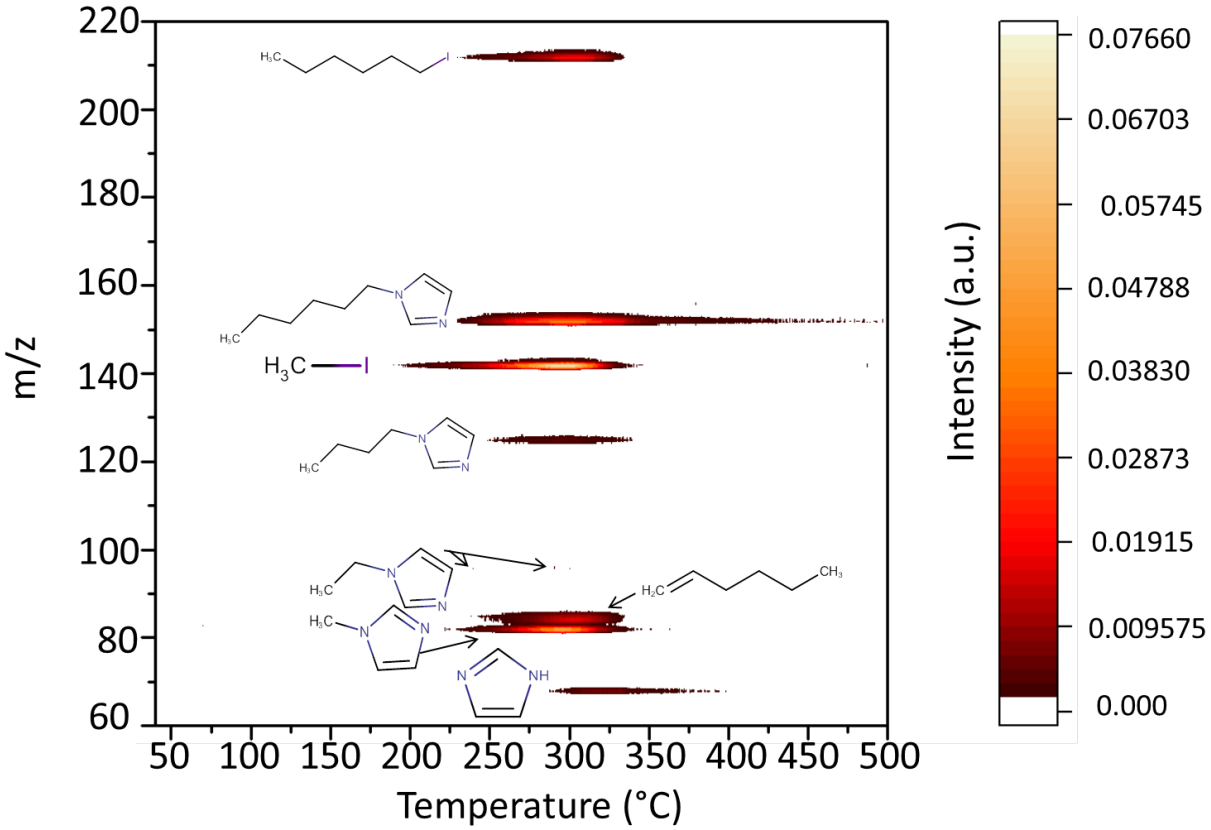

Fig. 39: TA-Skimmer-SPI-TOFMS results of 1-hexyl-3-methylimidazolium iodide

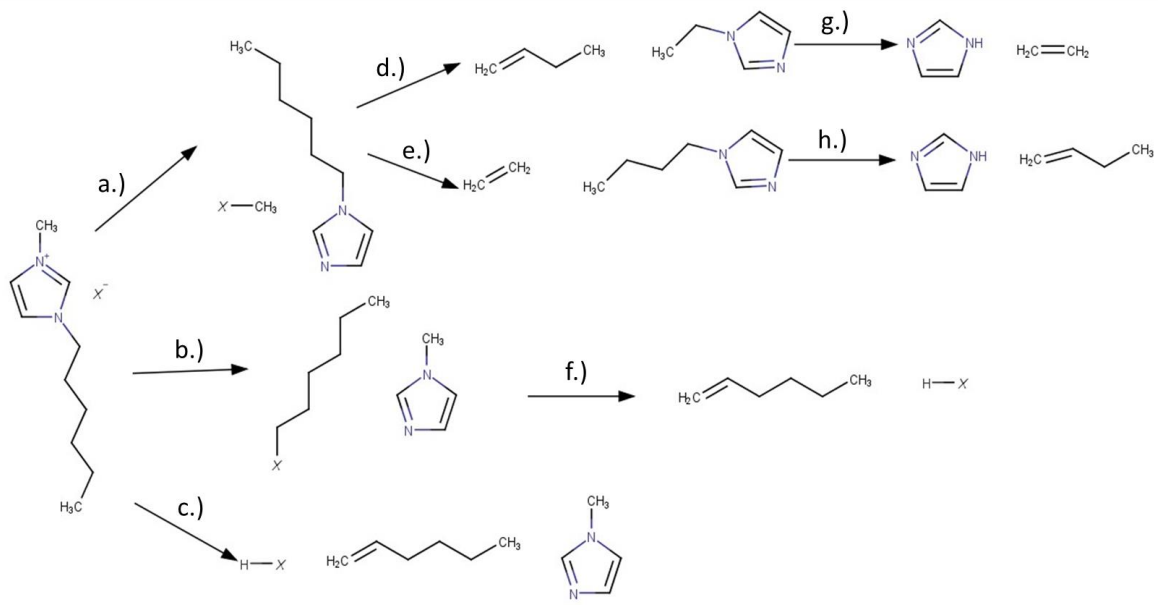

Fig. 40: Proposed thermal decomposition pathways of 1-hexyl-3-methylimidazolium halides (X= Cl, Br, I)

Conclusions

We developed a thermal analysis based method for the characterization of elemental sulfur and selenium, especially for the speciation of their vapors. The skimmer coupling enables the online characterization of low volatile compounds in the vapor phase. It is an alternative method to KEMS, which is rarely available. Moreover, KEMS is hardly available with soft ionization.

The described method applies an easy-to-handle, commercially available deuterium lamp to produce ionizing photons; there is no need for synchrotron or monochromator in contrast to older KEMS devices. Photoionization enables the fragment-free characterization of the evolving species. The direction of further development is to use more intense photon sources, since enhanced photon densities will lead to even smaller limits of detections.

We detected the species S_n (n=2,5-8) in sulfur vapor and Se_n (n=2,5-8) in selenium vapor. The high potential of the approach implies further elucidation of allotrope forming elements such as phosphorus, arsenic, tellurium etc.

ILs, including the investigated 1-alkyl-3-methylimidazolium halides, are increasingly applied in large (industrial) scale also at elevated temperatures e.g. as synthesis media. Thus, it is relevant to describe their high temperature behavior and determine their safe operational temperatures.

The reported data suggests that the TA-Skimmer-SPI-TOFMS technique is well applicable for the online identification of decomposition products of ILs because of the non-fragmenting character of photoionization. The extent of the applied technology was elucidated, in terms of the additional benefits to those described in the literature. It was possible to unambiguously detect decomposition products whose formation was only assumed from EI data or predicted by quantum chemical calculations.

From the detected decomposition products, the decomposition patterns of the investigated 1-alkyl-3-methylimidazolium halides were deduced: their decomposition via the reverse Menshutkin reaction and different elimination reactions leads to alkyl halides, alkyl imidazoles, hydrogen halides, and alkenes. The increased vulnerability of the chloride salts is due to Hofmann elimination competing with the reverse Menshutkin reaction. Hofmann elimination cannot be excluded also in the bromide and iodide salts but it is present to a less extent. The structure-decomposition relationship was evaluated, depending on the alkyl-chains and the halide anion. Amongst the detected decomposition products, alkyl halides are critical compounds from an environmental perspective (e. g. alkyl bromides can be photolyzed in the atmosphere to release elemental bromine, which is far more destructive to stratospheric ozone than chlorine) as well as a medical perspective (potential occupational carcinogens).

List of abbreviations

DSC	differential scanning calorimetry
DTA	differential thermal analysis
EG	evolved gas
EGA	evolved gas analysis
EI	electron ionization
FTIR	Fourier transform infrared
GC	gas chromatography
IE	ionization energy
IR	infrared
KEMS	Knudsen effusion mass spectrometry
MALDI	matrix assisted laser desorption/ionization
MPI	multiphoton ionization
oa-TOFMS	orthogonal acceleration time-of-flight mass spectrometry
PI	photo ionization
QMS	quadrupole mass spectrometers
REMPI	resonance-enhanced multi photon ionization
RT	retention time
SPI	single photon ionization
STA	simultaneous thermal analysis
TA	thermal analysis
TG	thermogravimetry
TOFMS	time of flight mass spectrometry

Appendix

[emim]Cl in N_2, Ar and synth. air (TG/DSC)

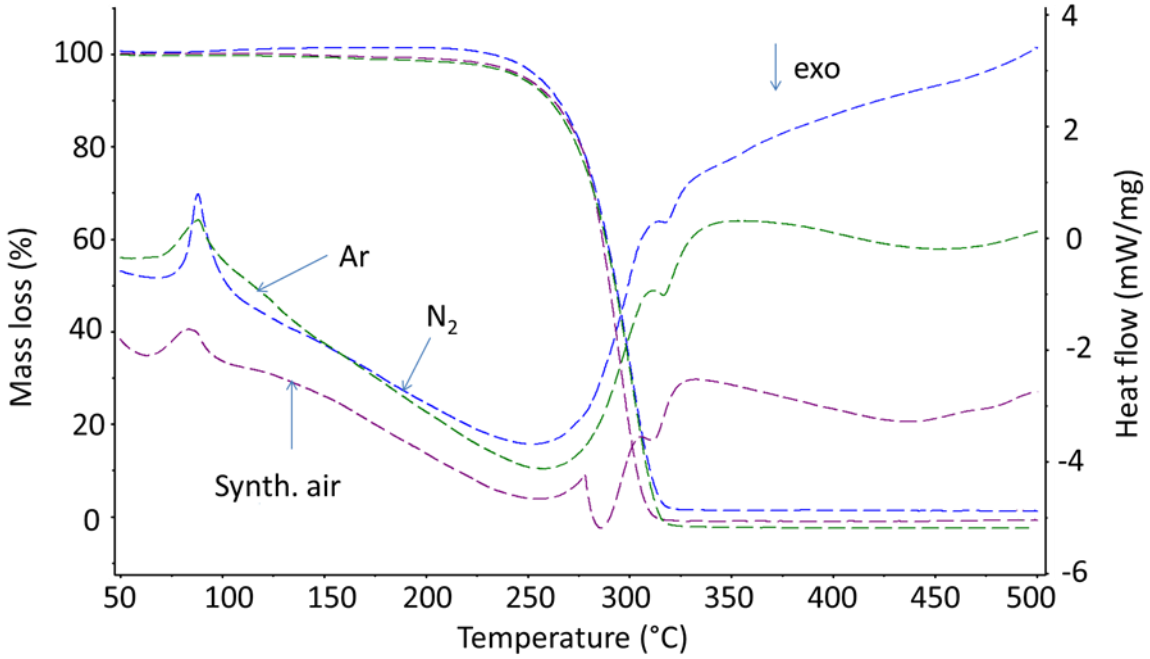

[emim]Br in N_2, He and synth. air (TG/DSC)

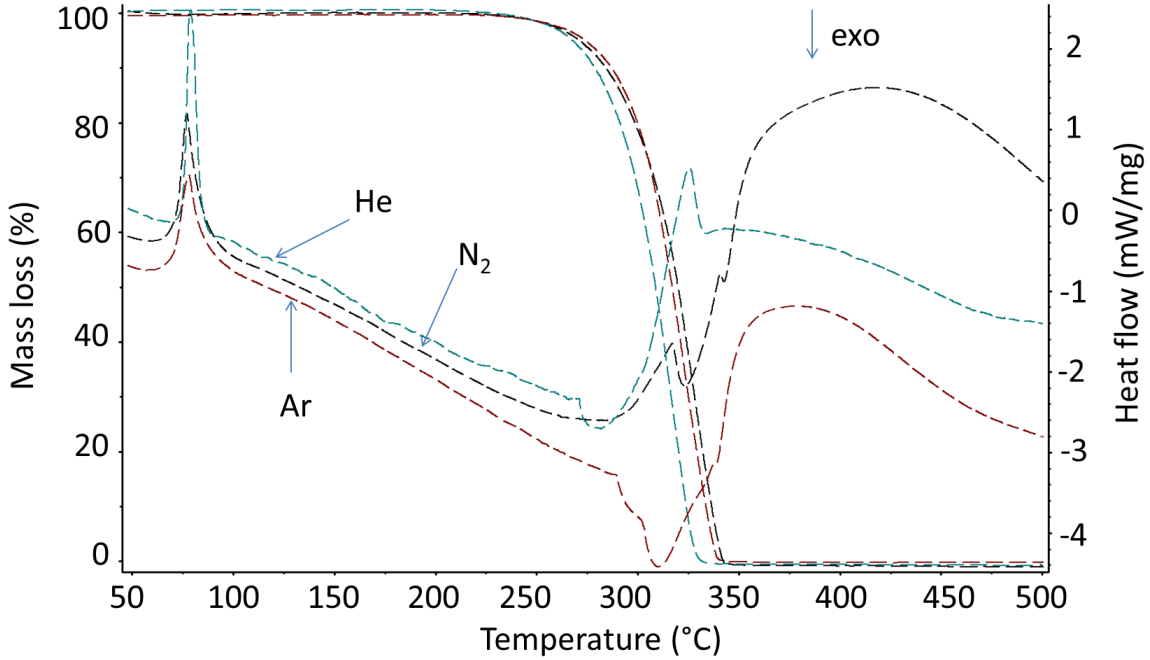

[bmim]Cl in N_2 and synth. air (TG/DSC)

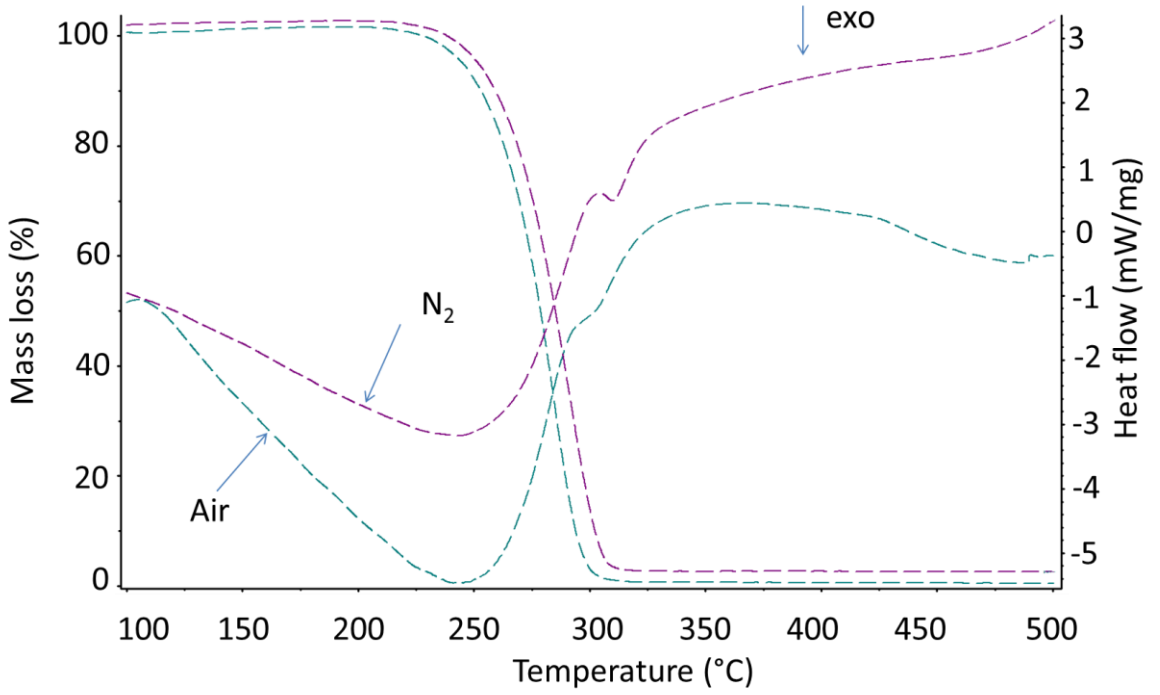

[bmim]Br in in N_2 and synth. air (TG/DSC)

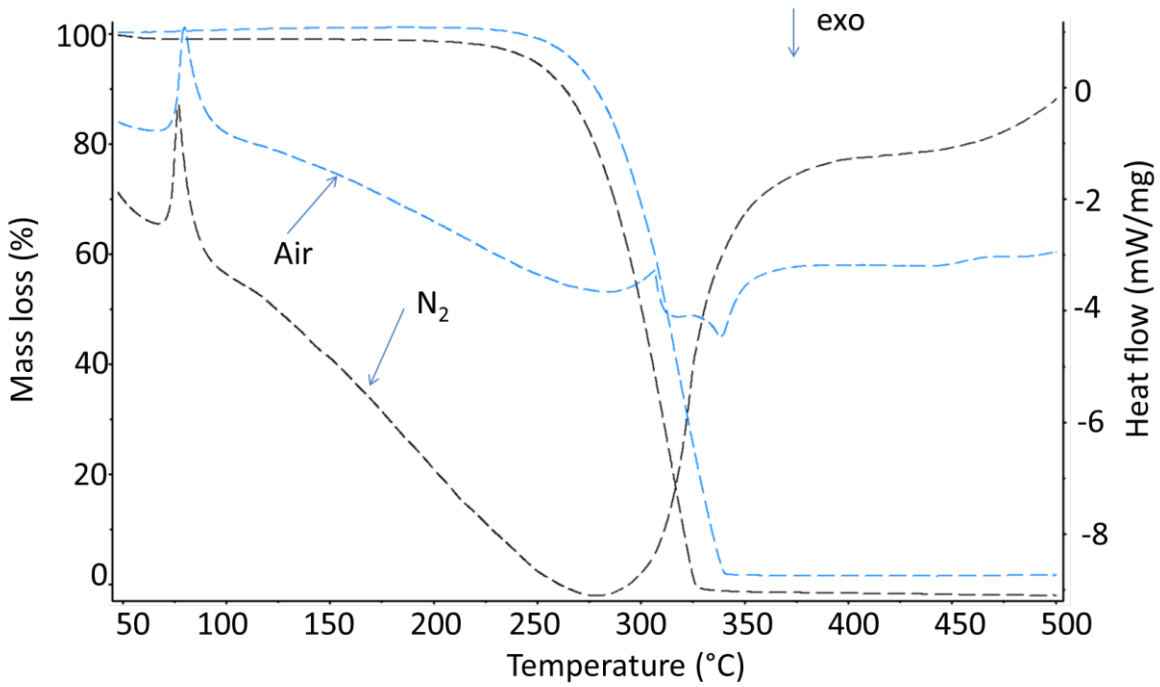

[bmim]I in in N_2, and synth. air (TG/DSC)

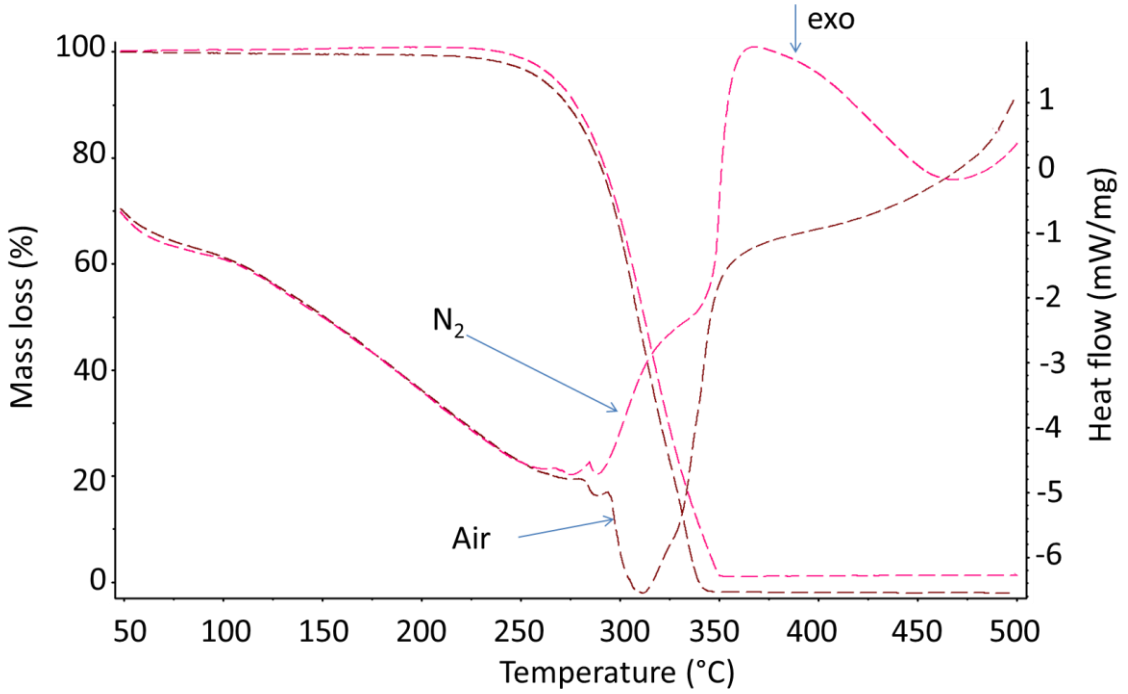

[hmim]X in N_2 (TG/DSC)

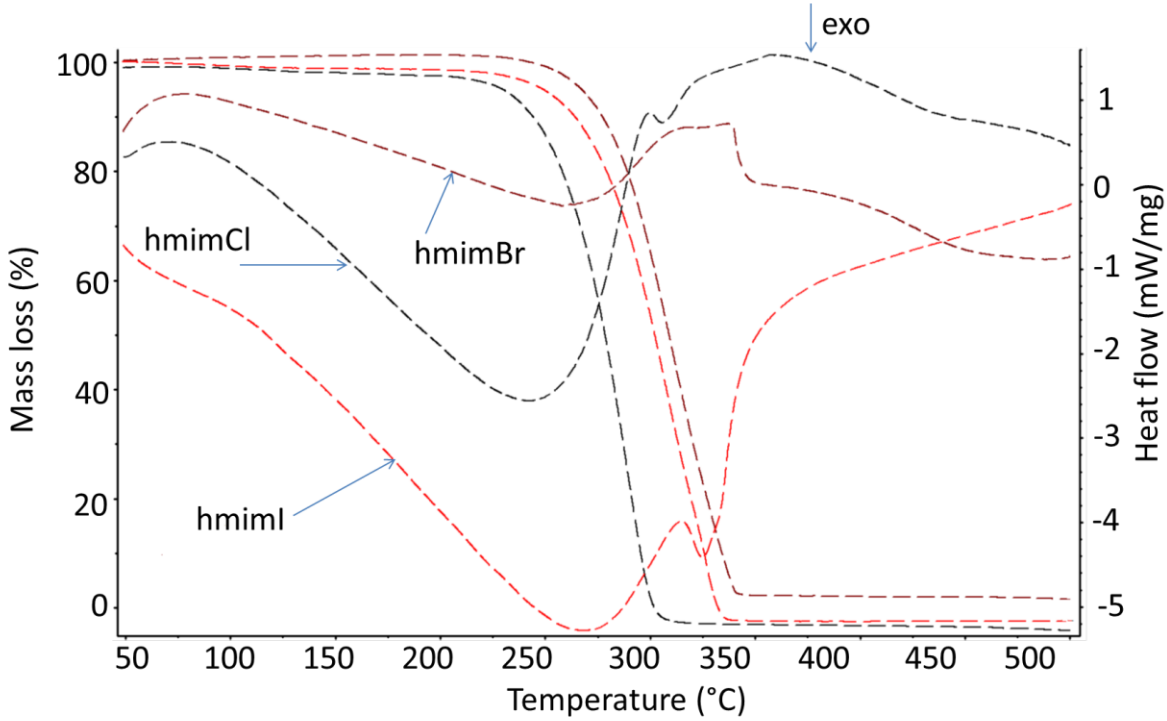

[emim]Cl in air (MS data)

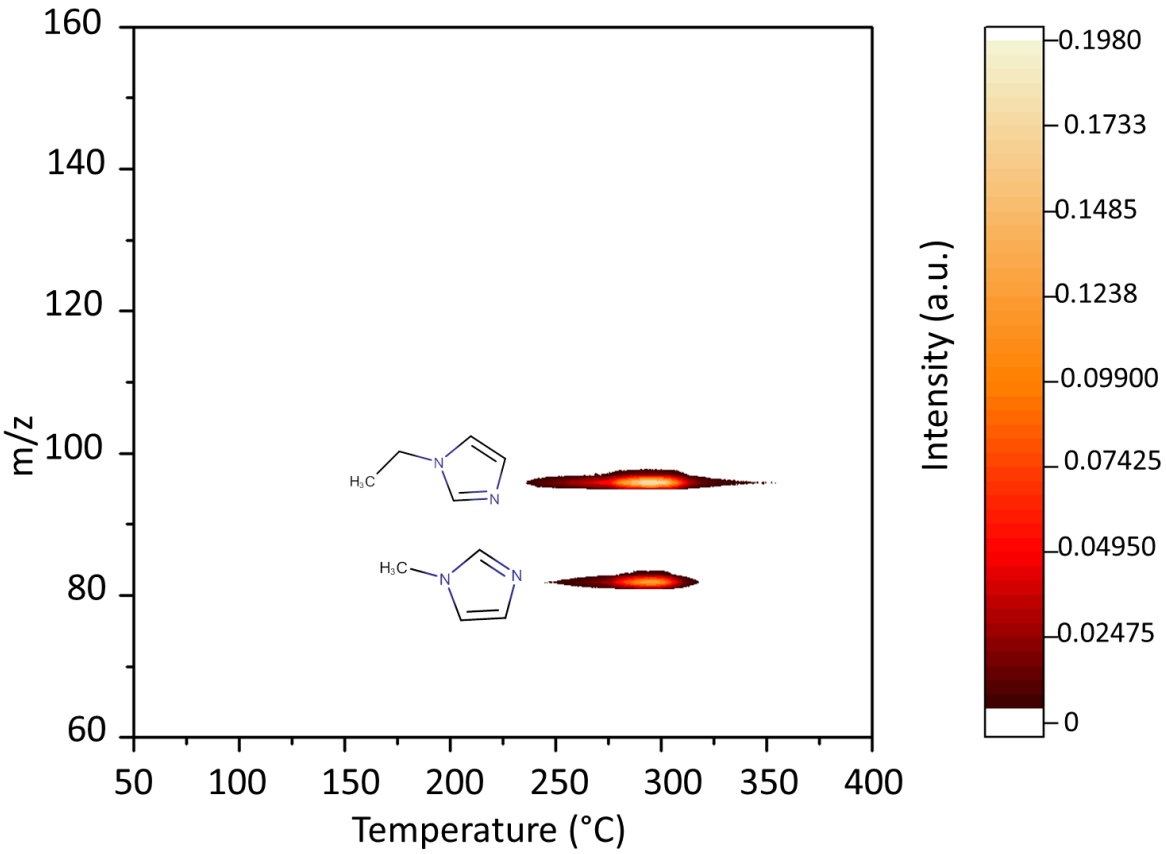

[emim]Br air (MS data)

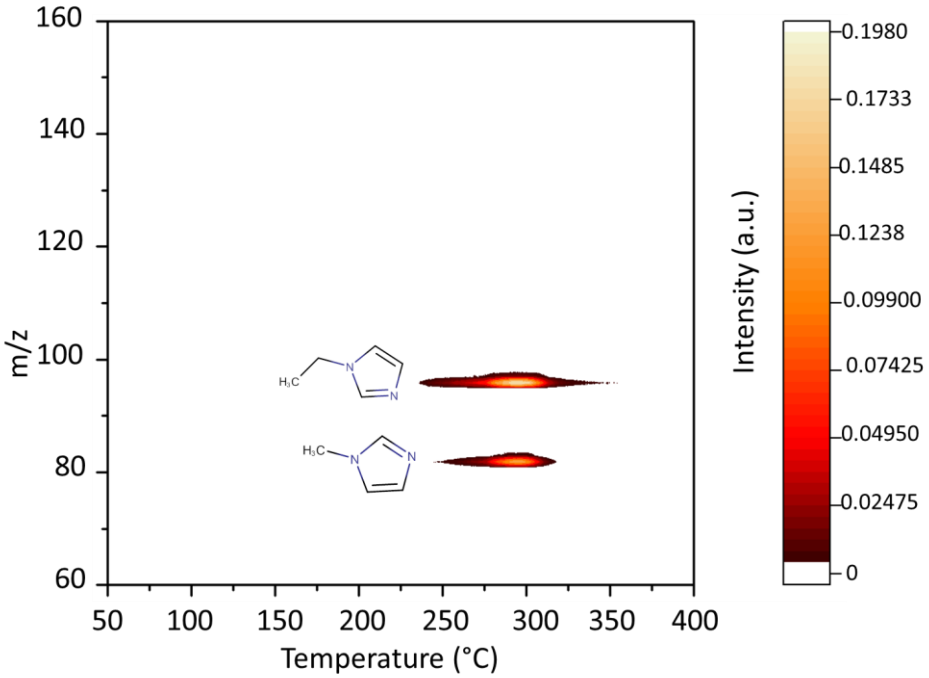

[bmim]Cl in N_2 (MS data)

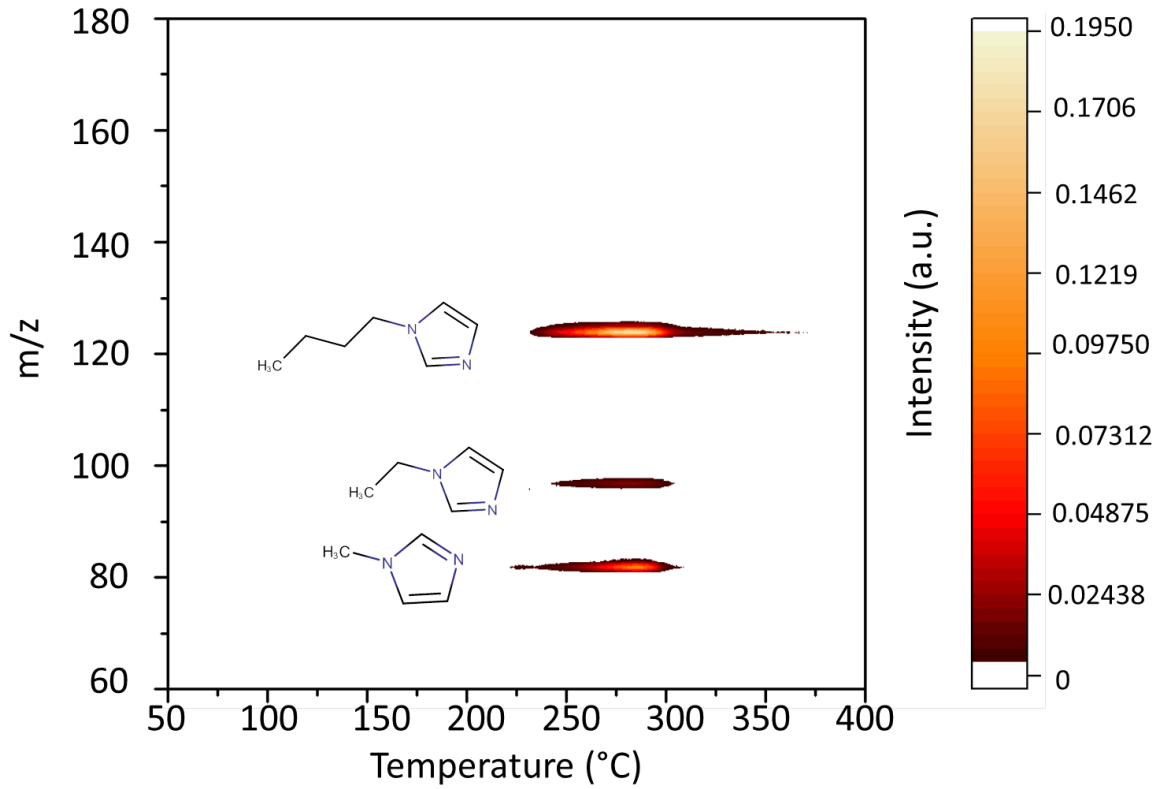

[bmim][Cl] air (MS data)

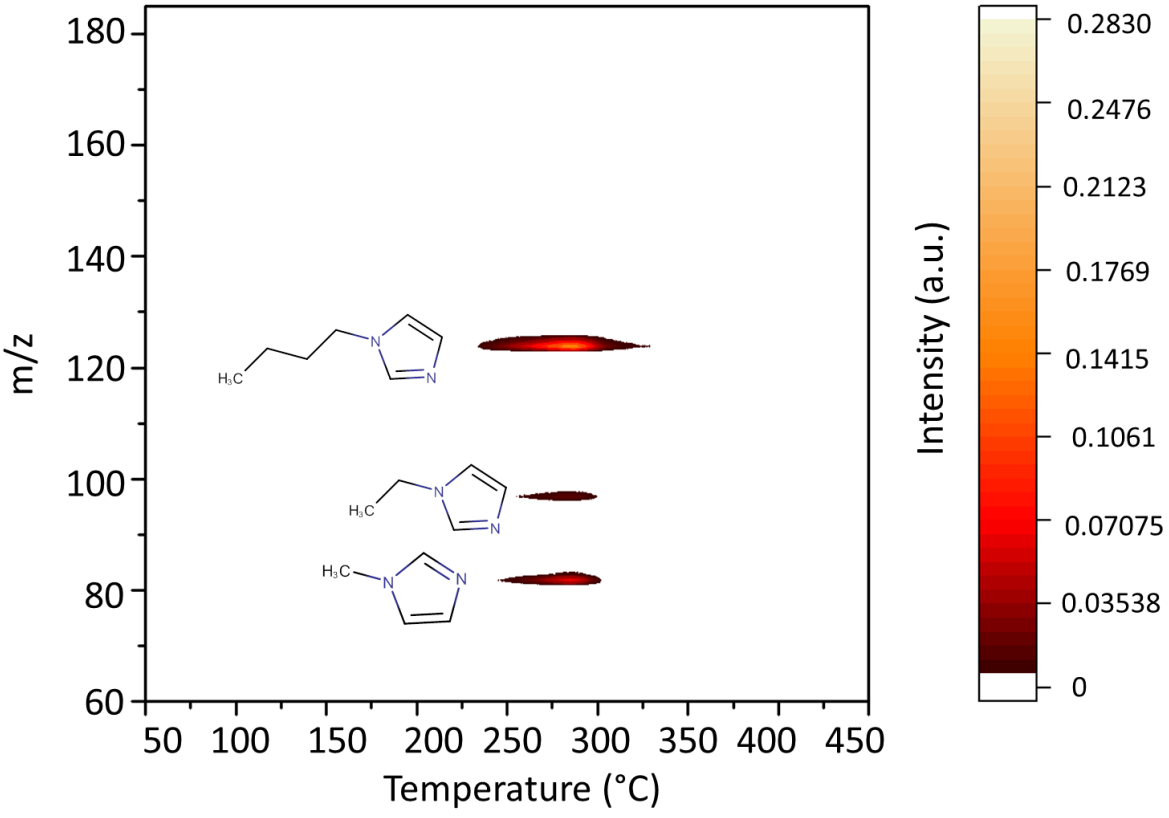

[bmim]Br in N_2 (MS data)

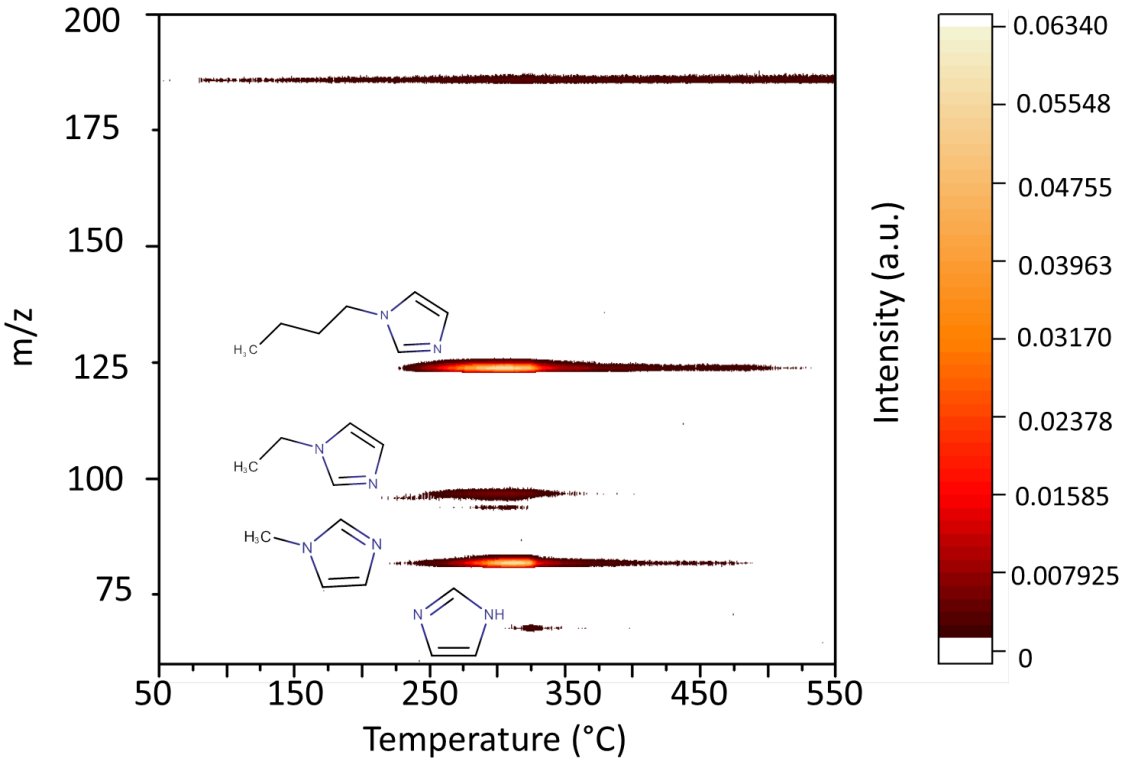

[bmim]Br in synthetic air (MS data)

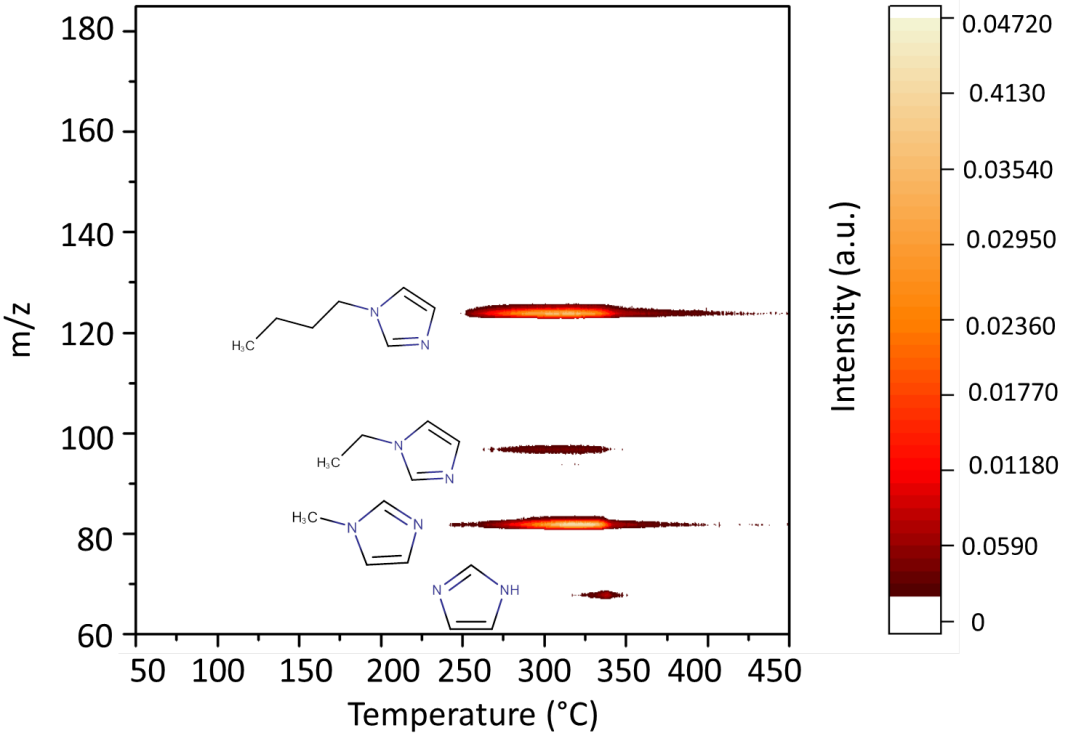

[hmim]Cl in N_2 (MS data)

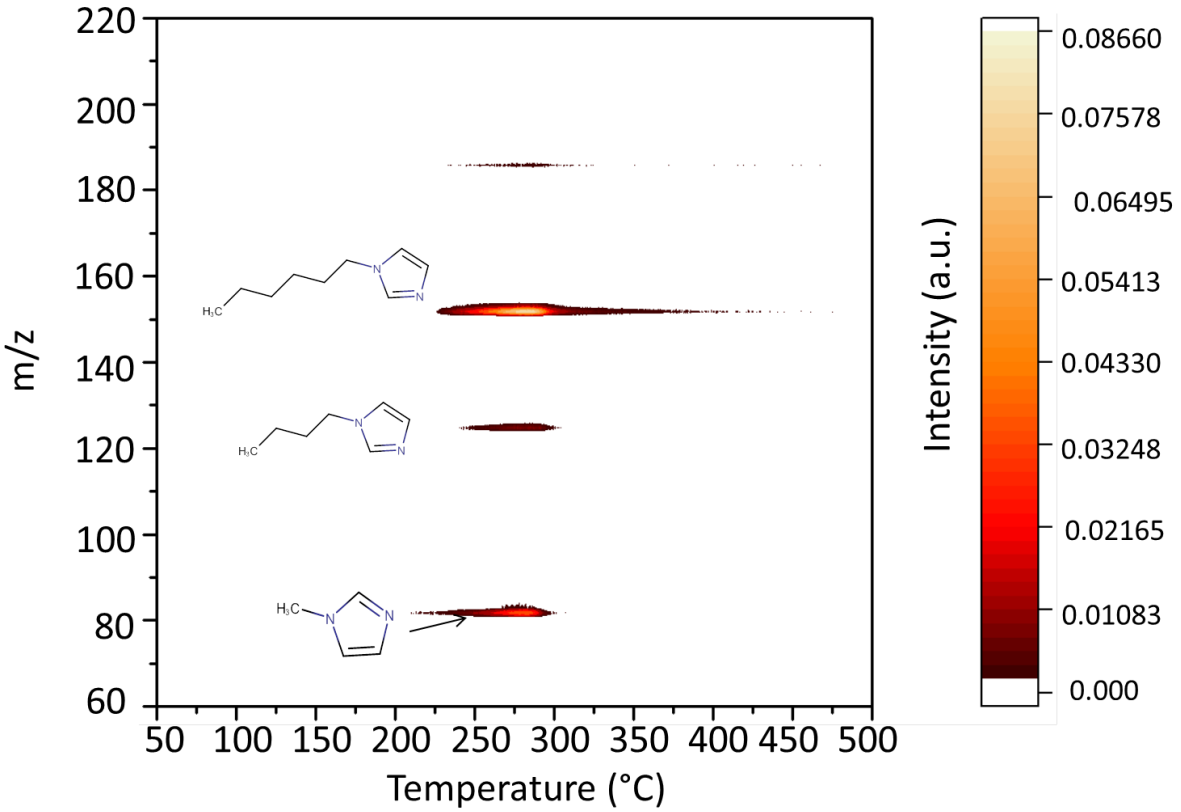

[hmim]Br in N_2 (MS data)

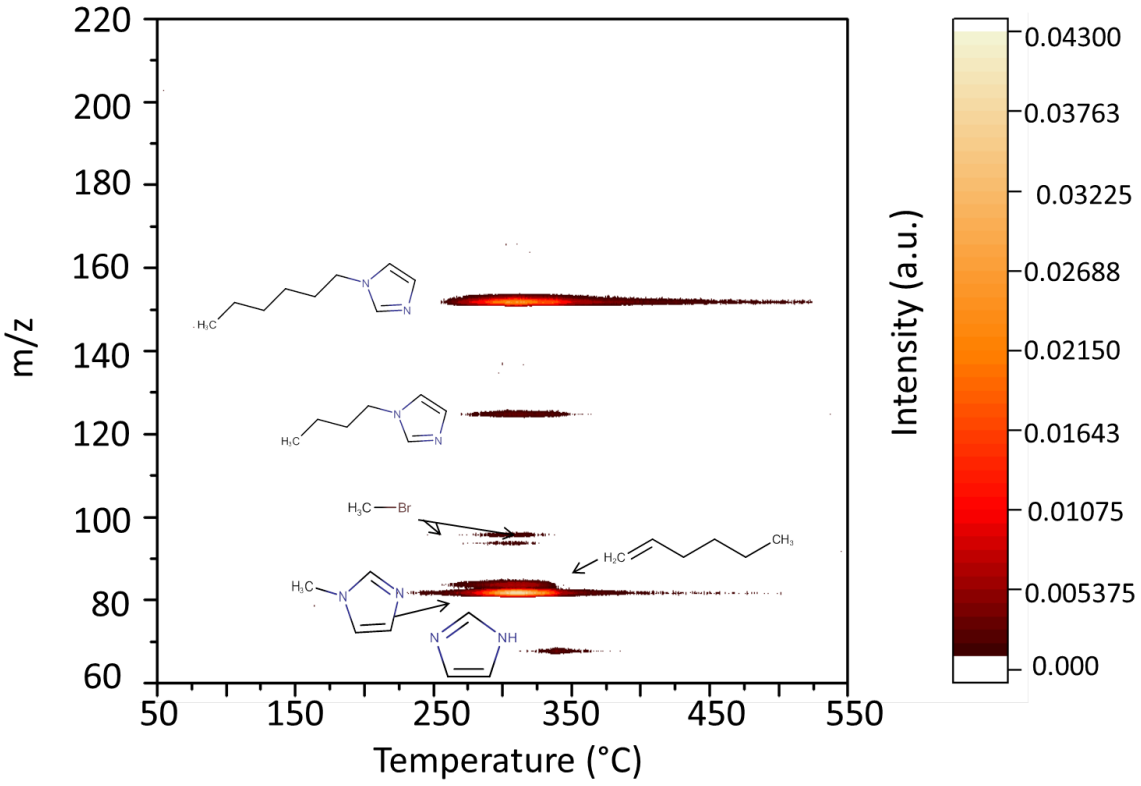

References

1. Brown ME. Introduction to Thermal Analysis. 2. Kluwer Academic Publishers; 2001.

2. Lever T, Haines P, Rouquerol J, Charsley EL, Van Eckeren P, Burlett DJ. ICTAC nomenclature of thermal analysis (IUPAC Recommendations 2014). Pure Appl. Chem. 2014;86:545–53.

3. Morse D, Baer DM. Laboratory Balances: How They Work, Checking Their Accuracy. Lab. Med. 2004;35:48–51.

4. Haines PJ. Thermal methods of analysis. First Edit. Dordrecht: Springer Science+Business Media; 1995.

5. Guilhaus M. Principles and instrumentation in time-of-flight mass spectrometry: Physical and instrumental concepts. J. Mass Spectrom. 1995;30:1519–32.

6. Murray KK, Boyd RK, Eberlin MN, Langley GJ, Li L, Naito Y. Definitions of terms relating to mass spectrometry (IUPAC Recommendations 2013). Pure Appl. Chem. 2013;85:1515–609.

7. Guilhaus M, Mlynski V, Selby D. Perfect Timing: Time-of-flight Mass Spectrometry. Rapid Commun. Mass Spectrom. 1997;11:951–62.

8. Guilhaus M, Selby D, Mlynski V. Orthogonal acceleration time-of-flight mass spectrometry. Mass Spectrom. Rev. 2000;19:65–107.

9. Dawson JHJ, Guilhaus M. Orthogonal-acceleration time-of-flight mass spectrometer. Rapid Commun. Mass Spectrom. 1989;3:155–9.

10. Mamyrin BA, Karataev VI, Shmikk D V., Zagulin VA. The mass-reflectron, a new nonmagnetic time-of-flight mass spectrometer with high resolution. Sov Phys JETP. 1973;37:45–8.

11. Cotter RJ. The New Time-of-flight Mass Spectrometry. Anal. Chem. News Featur. 1999;445–51.

12. Mamyrin BA. Time-of-flight mass spectrometry (concepts , achievements , and prospects). 2001;206:251–66.

13. Hoffmann E De, Stroobant V. Mass Spectrometry - Priniples and Applications. Mass Spectrom. Rev. 2007.

14. Andrews DL. Applied Laser Spectroscopy: Techniques, Instrumentation, and Applications. Wiley; 1992.

15. Ledingham KWD, Singhal RP. High intensity laser mass spectrometry - A review. Int. J. Mass Spectrom. Ion Process. 1997;163:149–68.

16. Hanley L, Zimmermann R. Light and molecular ions: The emergence of vacuum UV single-photon ionization in MS. Anal. Chem. 2009;81:4174–82.

17. Bente M, Sklorz M, Streibel T, Zimmermann R. Thermal Desorption - Multiphoton Ionization Time-of-Flight Mass Spectrometry of Individual Aerosol Particles : A Simplified Approach for Online Single-Particle Analysis of Polycyclic Aromatic Hydrocarbons and Their Derivatives. 2009;81:2525–36.

18. King B, Pellin MJ, Moore JF, Veryovkin IV, Savina MR, Tripa CE. Estimation of useful yield in surface analysis using single photon ionization. Appl. Surf. Sci. 2003;203/204:244–7.

19. Wieser J, Murnick DE, Ulrich A, Huggins H a., Liddle A, Brown WL. Vacuum ultraviolet rare gas excimer light source. Rev. Sci. Instrum. 1997;68:1360.

20. Trevor JL, Mencer DE, Lykke KR, Pellin MJ, Hanley L. Surface mass spectrometry of biotinylated self-assembled monolayers. Anal. Chem. 1997;69:4331–8.

21. Hatano Y. Spectroscopy and dynamics of molecular superexcited states. Aspects of primary processes of radiation chemistry. Radiat. Phys. Chem. 2003;67:187–98.

22. Hatano Y. Interaction of VUV photons with molecules - Spectroscopy and dynamics of molecular superexcited states. J. Electron Spectros. Relat. Phenomena. 2001;119:107–25.

23. Adam T, Zimmermann R. Determination of single photon ionization cross sections for quantitative analysis of complex organic mixtures. Anal. Bioanal. Chem. 2007;389:1941–51.

24. Cool TA, Wang J, Nakajima K, Taatjes CA, Mcllroy A. Photoionization cross sections for reaction intermediates in hydrocarbon combustion. Int. J. Mass Spectrom. 2005;247:18–27.

25. Eschner MS, Zimmermann R. Determination of photoionization cross-sections of different organic molecules using gas chromatography coupled to single-photon ionization (SPI) time-of-flight mass spectrometry (TOF-MS) with an electron-beam-pumped rare gas excimer light source (EBEL): . Appl. Spectrosc. 2011;65:806–16.

26. Bartle KD, Myers P. History of gas chromatography. TrAC - Trends Anal. Chem. 2002;21:547–57.

27. A. T. James. The Invention of gas-liquid chromatography. Trends Biochem. Sci. 1977;2:244–6.

28. Settle FA. Handbook of Instrumental Techniques for Analytical Chemistry. 1997.

29. Schindler A, Neumann G, Rager A, Füglein E, Blumm J, Denner T. A novel direct coupling of simultaneous thermal analysis (STA) and Fourier transform-infrared (FT-IR) spectroscopy. J. Therm. Anal. Calorim. 2013;113:1091–102.

30. Fischer M, Wohlfahrt S, Varga J, Saraji-Bozorgzad M, Matuschek G, Denner T, et al. Evolved gas analysis by single photon ionization-mass spectrometry. J. Therm. Anal. Calorim. 2014;116:1461–9.

31. Fischer M, Wohlfahrt S, Matuschek G, Post E, Denner T, Streibel T, et al. Thermal analysis / evolved gas analysis using single photon ionization Mass spectrometry for the investigation of tobacco. 2013;1667–73.

32. Wohlfahrt S, Fischer M, Saraji-Bozorgzad M, Matuschek G, Streibel T, Post E, et al. Rapid

comprehensive characterization of crude oils by thermogravimetry coupled to fast modulated gas chromatography-single photon ionization time-of-flight mass spectrometry. Anal. Bioanal. Chem. 2013;405:7107–16.

33. Fischer M, Wohlfahrt S, Varga J, Matuschek G, Saraji-Bozorgzad MR, Denner T, et al. Optically Heated Ultra-Fast-Cycling Gas Chromatography Module for Rapid Separation of Direct Sampling and Online Monitoring Applications. Anal. Chem. 2015;87:8634–9.

34. Kaisersberger E, Post E. Applications for skimmer coupling systems , combining simultaneous thermal analysers with mass spectrometers. Thermochim. Acta. 1998;324:197–201.

35. Kaisersberger, E, Emmerich W-D, Pfaffenberger H. New TA-MS coupling system with increased sensitivity for low v olatile materials. Thermochim. Acta. 1985;88:319–22.

36. Steudel, R; Steudel, Y, Wong M. Speciation and Thermodynamics of Sulfur Vapor. Top. Curr. Chem. 2003;117–34.

37. Rühl E, Flesch R, Tappe W. Sulfur 1 s excitation of S2 and S8: Core – valence- and valence – valence – exchange interaction and geometry-specific transitions. J. Chem. Phys. 2002;116:3316.

38. Durand JM, Olivier-Fourcade J, Jumas JC, Womes M, Teodorescu CM, Elafif A, et al. K edge absorption spectra of sulphur in vapour, molecular and polymerized solid phases. J. Phys. B At. Mol. Opt. Phys. 1996;29:5773–84.

39. Engel AS, Bovenkamp GL, Prange A. In situ speciation of sulfur vapors by X-ray absorption near edge structure spectroscopy. Chem. Geol. Elsevier B.V.; 2014;380:1–6.

40. Berkowitz J, Lifshitz C. Photoionization of high-temperature vapors. II. Sulfur molecular species. J. Chem. Phys. 1968;48:4346–50.

41. Berkowitz J, Marquart JR. Equilibrium composition of sulfur vapor. J. Chem. Phys. 1963;39:275.

42. Berkowitz J, Chupka WA. Photoionization of high-temperature vapours. I. The iodides of sodium, magnesium and thallium. J. Chem. Phys. 1966;45:1287.

43. H. Fujisaki, J. B. Westmore WT. Mass spectrometric study of subliming selenium. Can. J. Chem. 1966;14:3063.

44. Berkowitz, J., Chupka WA. Equilibrium Composition of Selenium Vapor; the Thermodynamics of the Vaporization of HgSe, CdSe, and SrSe. J. Chem. Phys. 1966;45:4289.

45. Berkowitz J, Chupka W a. Photoionization of High-Temperature Vapors. VI. S2, Se2, and Te2. J. Chem. Phys. 1969;50:4245.

46. Grimley RT, Grindstaff QG, DeMercurio T a., Forsman J a. A study of the selenium vapor system by angular distribution mass spectrometry. J. Phys. Chem. 1982;86:976–82.

47. Yamdagni R, Porter RF. Mass Spectrometric and Torsion Effusion Studies of the Evaporation of Liquid Selenium. J. Electrochem. Soc. 1968;115:601.

48. Viswanathan R, Balasubramanian R, Darwin Albert Raj D, Sai Baba M, Lakshmi Narasimhan TS. Vaporization studies on elemental tellurium and selenium by Knudsen effusion mass spectrometry. J. Alloys Compd. Elsevier B.V.; 2014;603:75–85.

49. Richard J, Vick R, Junk G. Determination of elemental sulfur by gas chromatography. Environ. Sci. …. 1977;1084–6.

50. Chen Y-W, Joly HA, Belzile N. Determination of elemental sulfur in environmental samples by gas chromatography-mass spectrometry. Chem. Geol. 1997. p. 195–200.

51. Toniazzo V, Mustin C, Portal JM, Humbert B, Benoit R, Erre R. Elemental sulfur at the pyrite surfaces: speciation and quantification. Appl. Surf. Sci. 1999;143:229–37.

52. Gryglewicz G, Gryglewicz S. Determination of elemental sulfur in coal by gas chromatography-mass spectrometry. Fresenius. J. Anal. Chem. 2001;370:60–3.

53. Burger B V., Visser R, Moses A, Le Roux M. Elemental sulfur identified in urine of cheetah, Acinonyx jubatus. J. Chem. Ecol. 2006;32:1347–52.

54. Kornprobst JM, Wielgosz-Collin G, Barnathan G, Ganachaud R, Carriou Y, Masek F, et al. Identification des allotropes S6 et S7 du soufre dans le trophosome du vestimentifère Riftia pachyptila. Comptes Rendus Chim. 2002;5:513–6.

55. Zhao H. Determination of elemental sulfur in naphtha and gasoline by gas chromatography/mass spectrometry. Chinese J. Chromatogr. (Se Pu). 2003;21:210–3.

56. Yin C, Li H, Liu H, Zhao L, Bai Z, Wang Y, et al. Study on the formation, determination, and removal of elemental sulfur in ultra-low sulfur gas oil. Fuel Process. Technol. 2014;120:16–21.

57. Welton T. Room-temperature ionic liquids: Solvents for synthesis and catalysis. Chem. Rev. 1999;99:2071–83.

58. Hallett JP, Welton T. Room-temperature ionic liquids: solvents for synthesis and catalysis. 2. Chem. Rev. 2011;111:3508–76.

59. Branco LC, Carrera GVSM, Aires-de-Sousa J, Lopez Martin I, Frade R, Afonso AMC. Physico-Chemical Properties of Task-Specific. Ion. Liq. Theory, Prop. New Approaches. 2011. p. 61–95.

60. Rogers RD, Seddon KR. Ionic Liquids - Solvents of the Future? Science (80-.). 2003;302:792–3.

61. Ludwig R, Maginn E, Balasubramanian S. Editorial: Ionic Liquids: The Fundamentals and Forces Driving Their Rise. ChemPhysChem. 2012;13:1603–1603.

62. Sowmiah S, Srinivasadesikan V, Tseng M-C, Chu Y-H. On the Chemical Stabilities of Ionic Liquids [Internet]. Molecules. 2009. Available from: http://www.mdpi.com/1420-3049/14/9/3780/

63. Domańska U, Okuniewska P, Markowska A. Phase equilibrium in binary systems of ionic liquids, or deep eutectic solvents with 2-phenylethanol (PEA), or water. Fluid Phase Equilib.

2015;

64. Cunha E, Pinto PCAG, Saraiva MLMFS. Evaluation of ionic liquids as alternative solvents for aldolase activity: Use of a new automated SIA methodology. Talanta. Elsevier; 2015;141:293–9.

65. Pires PAR, Malek NI, Teixeira TC, Bioni TA, Nawaz H, Seoud OA El. Imidazole-catalyzed esterification of cellulose in ionic liquid/molecular solvents: A multi-technique approach to probe effects of the medium. Ind. Crops Prod. Elsevier B.V.; 2015;77:180–9.

66. Jogunola O, Eta V, Hedenström M, Sundman O, Salmi T, Mikkola J-P. Ionic liquid mediated technology for synthesis of cellulose acetates using different co-solvents. Carbohydr. Polym. Elsevier Ltd.; 2016;135:341–8.

67. Wendler F, Todi LN, Meister F. Thermostability of imidazolium ionic liquids as direct solvents for cellulose. Thermochim. Acta. Elsevier B.V.; 2012;528:76–84.

68. Mahrova M, Pagano F, Pejakovic V, Valea A, Kalin M, Igartua A, et al. Pyridinium based dicationic ionic liquids as base lubricants or lubricant additives. Tribol. Int. Elsevier; 2015;82:245–54.

69. Anand M, Hadfield M, Viesca JL, Thomas B, Hernández Battez A, Austen S. Ionic liquids as tribological performance improving additive for in-service and used fully-formulated diesel engine lubricants. Wear. 2015;334–335:67–74.

70. Hernández Battez A, Bartolomé M, Blanco D, Viesca JL, Fernández-González A, González R. Phosphonium cation-based ionic liquids as neat lubricants: Physicochemical and tribological performance. Tribol. Int. Elsevier; 2016;95:118–31.

71. Itoga M, Aoki S, Suzuki A, Yoshida Y, Fujinami Y, Masuko M. Toward resolving anxiety about the accelerated corrosive wear of steel lubricated with the fluorine-containing ionic liquids at elevated temperature. Tribol. Int. Elsevier; 2015;93:640–50.

72. Ide Y, Takahashi T, Iwai K, Nozoe K, Habu H, Tokudome S. Potential of ADN-based Ionic Liquid Propellant for Spacecraft Propulsion. Procedia Eng. Elsevier B.V.; 2015;99:332–7.

73. Reeder ZK, Adler AM, Miller KM. 1-Alkyl-3-methyl-1,2,3-triazolium [NTf2] ionic liquids: synthesis and properties. Tetrahedron Lett. Elsevier Ltd; 2016;57:206–9.

74. Chakrabarti MH, Mjalli FS, AlNashef IM, Hashim MA, Hussain MA, Bahadori L, et al. Prospects of applying ionic liquids and deep eutectic solvents for renewable energy storage by means of redox flow batteries. Renew. Sustain. Energy Rev. Elsevier; 2014;30:254–70.

75. Kiszkiel I, Starczewska B, Leśniewska B, Późniak P. Extraction of ranitidine and nizatidine with using imidazolium ionic liquids prior spectrophotometric and chromatographic detection. J. Pharm. Biomed. Anal. 2015;106:85–91.

76. Martinis EM, Berton P, Monasterio RP, Wuilloud RG. Emerging ionic liquid-based techniques for total-metal and metal-speciation analysis. TrAC - Trends Anal. Chem. 2010;29:1184–201.

77. Grabda M, Oleszek S, Panigrahi M, Kozak D, Eckert F, Shibata E, et al. Theoretical

selection of most effective ionic liquids for liquid–liquid extraction of NdF3. Comput. Theor. Chem. 2015;1061:72–9.

78. Zhang P, Hu L, Lu R, Zhou W, Gao H. Application of ionic liquids for liquid–liquid microextraction. Anal. Methods. 2013;5:5376–85.

79. Huang K, Han X, Zhang X, Armstrong DW. PEG-linked geminal dicationic ionic liquids as selective, high-stability gas chromatographic stationary phases. Anal. Bioanal. Chem. 2007;389:2265–75.

80. Breitbach, Zachary S.Armstrong DW. Characterization of phosphonium ionic liquids through a linear solvation energy relationship and their use as GLC stationary phases. Anal. Bioanal. Chem. 2008;390:1605–17.

81. Berthod a., Ruiz-Ángel MJ, Carda-Broch S. Ionic liquids in separation techniques. J. Chromatogr. A. 2008;1184:6–18.

82. Baltazar QQ, Leininger SK, Anderson JL. Binary ionic liquid mixtures as gas chromatography stationary phases for improving the separation selectivity of alcohols and aromatic compounds. J. Chromatogr. A. 2008;1182:119–27.

83. Liu H, Dai J, Zhou J, Huang H, Chen F, Liu Z. A hybrid ionic liquid–matrix material, [TiO2–Si–NH3+][CHC−], as a novel matrix for the analysis of small molecules by MALDI-TOF MS. Int. J. Mass Spectrom. Elsevier B.V.; 2015;376:85–9.

84. Shah JK, Maginn EJ. Monte Carlo simulations of gas solubility in the ionic liquid 1-n-butyl-3-methylimidazolium hexafluorophosphate. J. Phys. Chem. B. 2005;109:10395–405.

85. Swatlowski RP, Holbrey JD, Rogers RD. Ionic liquids are not always green: hydrolysis of 1-butyl-3-methylimidazolium hexaflurophosphate. Green Chem. 2003;5:361–3.

86. Castro MC, Arce A, Soto A, Rodríguez H. Liquid-liquid equilibria of mutually immiscible ionic liquids with a common anion of basic character. J. Chem. Thermodyn. 2016;102:12–21.

87. Keating MY, Gao F, Ramsey JB. TGA-MS study of the decomposition of phosphorus-containing ionic liquids trihexyl(tetradecyl)phosphonium decanoate and trihexyltetradecylphosphonium bis[(trifluoromethyl)sulfonyl] amide. J. Therm. Anal. Calorim. 2011;106:207–11.

88. Wu B, Reddy RG, Rogers RD. Novel ionic liquid thermal storage for solar thermal electric power systems. Proc. Sol. Forum. 2001;445–52.

89. Weyershausen B, Lehmann K. Industrial application of ionic liquids as performance additives. Green Chem. 2005;7:15.

90. Jiménez AE, Bermúdez MD, Iglesias P. Lubrication of Inconel 600 with ionic liquids at high temperature. Tribol. Int. 2009;42:1744–51.

91. Phillips BS, John G, Zabinski JS. Surface chemistry of fluorine containing ionic liquids on steel substrates at elevated temperature using Mössbauer spectroscopy. Tribol. Lett. 2007;26:85–91.

92. Jin C-M, Ye C, Phillips BS, Zabinski JS, Liu X, Liu W, et al. Polyethylene glycol functionalized dicationic ionic liquids with alkyl or polyfluoroalkyl substituents as high temperature lubricants. J. Mater. Chem. 2006;16:1529–35.

93. Zeng Z, Phillips BS, Xiao JC, Shreeve JM. Polyfluoroalkyl, polyethylene glycol, 1,4-bismethylenebenzene, or 1,4-bismethylene-2,3,5,6-tetrafluorobenzene bridged functionalized dicationic ionic liquids: Synthesis and properties as high temperature lubricants. Chem. Mater. 2008;20:2719–26.

94. Groh MF, Breternitz J, Ahmed E, Isaeva A, Efimova A, Schmidt P, et al. Ionothermal Synthesis, Structure, and Bonding of the Catena -Heteropolycation 1 ∞ [Sb 2 Se 2] +. Zeitschrift für Anorg. und Allg. Chemie. 2015;641:388–93.

95. Tan Z, Welz-biermann U, Yan P-F, Liu Q-S, Fang D-W. Thermodynamic Properties of Ionic Liquids. Ion. Liq. Prop. New Approaches. 2011. p. 3–36.

96. Maton C, De Vos N, Stevens C V. Ionic liquid thermal stabilities: decomposition mechanisms and analysis tools. Chem. Soc. Rev. 2013;42:5963–77.

97. Smiglak M, Reichert WM, Holbrey JD, Wilkes JS, Sun L, Thrasher JS, et al. Combustible ionic liquids by design: is laboratory safety another ionic liquid myth? Chem. Commun. 2006;2554.

98. Liaw HJ, Chen KY, Chen HY, Liu SN. Effect of heating temperature on the flash point of ionic liquids. Procedia Eng. Elsevier B.V.; 2014;84:293–6.

99. Earle MJ, Esperança JMSS, Gilea MA, Canongia Lopes JN, Rebelo LPN, Magee JW, et al. The distillation and volatility of ionic liquids. Nature. 2006;439:831–4.

100. Fox DM, Awad WH, Gilman JW, Maupin PH, De Long HC, Trulove PC. Flammability, thermal stability, and phase change characteristics of several trialkylimidazolium saltsThe authors wish to thank the scientists at the Occupational Safety and Health Administration ? Salt Lake Technical Center for their measurement of the i. Green Chem. 2003;5:724.

101. Deyko a, Lovelock KRJ, Licence P, Jones RG. The vapour of imidazolium-based ionic liquids: a mass spectrometry study. Phys. Chem. Chem. Phys. 2011;13:16841–50.

102. Ohtani H, Ishimura S, Kumai M. Thermal decomposition behaviors of imidazolium-type ionic liquids studied by pyrolysis-gas chromatography. Anal. Sci. 2008;24:1335–40.

103. Wooster TJ, Johanson KM, Fraser KJ, MacFarlane DR, Scott JL. Thermal degradation of cyano containing ionic liquids. Green Chem. 2006;8:691.

104. Sawicka M, Storoniak P, Skurski P, Blazejowski J, Rak J. TG-FTIR, DSC and quantum chemical studies of the thermal decomposition of quaternary methylammonium halides. Chem. Phys. 2006;324:425–37.

105. Awad WH, Gilman JW, Nyden M, Harris RH, Sutto TE, Callahan J, et al. Thermal degradation studies of alkyl-imidazolium salts and their application in nanocomposites. Thermochim. Acta. 2004;409:3–11.

106. Efimova A, Pfützner L, Schmidt P. Thermal stability and decomposition mechanism of 1-

ethyl-3-methylimidazolium halides. Thermochim. Acta. 2015;604:129–36.

107. Hao Y, Peng J, Hu S, Li J, Zhai M. Thermal decomposition of allyl-imidazolium-based ionic liquid studied by TGA-MS analysis and DFT calculations. Thermochim. Acta. Elsevier B.V.; 2010;501:78–83.

108. Chambreau SD, Boatz J a., Vaghjiani GL, Koh C, Kostko O, Golan A, et al. Thermal decomposition mechanism of 1-ethyl-3-methylimidazolium bromide ionic liquid. J. Phys. Chem. A. 2012;116:5867–76.

109. Xue Z, Zhang Y, Zhou X, Cao Y, Mu T. Thermal stabilities and decomposition mechanism of amino- and hydroxyl-functionalized ionic liquids. Thermochim. Acta. Elsevier B.V.; 2014;578:59–67.

110. Chan BKM, Chang N-H, Grimmett MR. The Synthesis and Thermolysis of Imidazole Quaternary Salts. Aust. J. Chem. 1977;30:2005–13.

111. Meine N, Benedito F, Rinaldi R. Thermal stability of ionic liquids assessed by potentiometric titration. Green Chem. 2010;12:1711.

112. Del Sesto RE, McCleskey TM, Macomber C, Ott KC, Koppisch AT, Baker G a., et al. Limited thermal stability of imidazolium and pyrrolidinium ionic liquids. Thermochim. Acta. 2009;491:118–20.

113. Kroon MC, Buijs W, Peters CJ, Witkamp GJ. Quantum chemical aided prediction of the thermal decomposition mechanisms and temperatures of ionic liquids. Thermochim. Acta. 2007;465:40–7.

114. Efimova A, Hubrig G, Schmidt P. Thermal stability and crystallization behavior of imidazolium halide ionic liquids. Thermochim. Acta. Elsevier B.V.; 2013;573:162–9.

115. Keil P, Kick M, König A. Long-term stability, regeneration and recycling of imidazolium-based ionic liquids. Chemie-Ingenieur-Technik. 2012;84:859–66.

116. Scammells PJ, Scott JL, Singer RD. Ionic Liquids: The Neglected Issues. Aust. J. Chem. 2005;58:155–69.

117. Seeberger A, Andresen A-K, Jess A. Prediction of long-term stability of ionic liquids at elevated temperatures by means of non-isothermal thermogravimetrical analysis. Phys. Chem. Chem. Phys. 2009;11:9375–81.

118. Navarro P, Larriba M, Garc??a J, Rodr??guez F. Thermal stability and specific heats of {[emim][DCA] + [emim][TCM]} mixed ionic liquids. Thermochim. Acta. Elsevier B.V.; 2014;588:22–7.

119. Heym F, Korth W, Thiessen J, Kern C, Jess A. Evaporation and decomposition behavior of pure and supported ionic liquids under thermal stress. Chemie-Ingenieur-Technik. 2015;87:791–802.

120. Saraji-Bozorgzad MR, Streibel T, Kaisersberger E, Denner T, Zimmermann R. Detection of organic products of polymer pyrolysis by thermogravimetry-supersonic jet-skimmer time-of-flight mass spectrometry (TG-Skimmer-SPI-TOFMS) using an electron beam pumped rare

gas excimer VUV-light source (EBEL) for soft photo ionisation. J. Therm. Anal. Calorim. 2011;105:691–7.

121. Varga J, Wohlfahrt S, Fischer M, Saraji-Bozorgzad MR, Matuschek G, Denner T, et al. An evolved gas analysis method for the characterization of sulfur vapor. J. Therm. Anal. Calorim. Springer Netherlands; 2017;127:955–60.

122. Currell BR, Williams AJ. Thermal analysis of elemental sulphur. Thermochim. Acta. 1974;9:255–9.

123. Wiberg N. Lehrbuch der anorganischen Chemie. de Gruyter; 2007.

124. Guthrie, G B, Scott, D W, Waddington G. Thermodynamic Functions and Heat of Formation of S8 (Gas). J. Am. Chem. Soc. 1954;76:1488–93.

125. Lancaster NL, Welton T, Young GB. A study of halide nucleophilicity in ionic liquids. J. Chem. Soc. Perkin Trans. 2. 2001;2267–70.